THE CHEMISTRY OF CERAMIC GLAZES

A THESIS SUBMITTED FOR THE DEGREE OF DOCTOR OF PHILOSOPHY

BY

NASEEF · J · ALI

University of Aston In Birmingham

Gosta Green

Birmingham B4 7ET

March 1983

In the Name of Allāh,
The All-compassionate, The All-merciful

Praise belongs to Allāh, the Lord of all being;
the All-compassionate, the All-merciful;
the Master of the Day of Judgement:
Thee only we serve, and to Thee alone we pray
for succour;
Guide us in the straight path;
the path of those whom Thou hast blessed,
not of those against whom Thou art wrathful,
nor of those who are astray.

* * * * *

TO MY PARENTS

The work described in this thesis was carried out between 1979 and 1983 in the Chemistry Department, University of Aston in Birmingham. It has been carried out independently and has not been submitted for any other degree.

Naseef J. Ali

THE UNIVERSITY OF ASTON IN BIRMINGHAM

THE CHEMISTRY OF CERAMIC GLAZES

by

NASEEF J ALI

A thesis submitted for the degree of
Doctor of Philosophy, March 1983.

SUMMARY

The development of ideas and theories concerning the structure of glazes, as one of the glassy materials, are reviewed in the general introduction. The raw materials and the manufacturing process for glazes are described (Chapter One).

A number of new vanadyl(IV) dipyridylamine and tri-pyridylamine complexes have been prepared, various spectroscopic techniques are used in the investigation of the vanadyl ion in a weak ligand field, the situation of those found in a glaze environment (Chapter Three).

In glaze recipes containing silica, potash feldspar, china clay, MO(M= Ca, Sr, Ba, Ti and Zn) and NiO, the ligand field theory is used in the elucidation of the effect of M (in MO) on the absorption spectra and co-ordination behaviour of Ni(II) in glazes. The magnetic and visible spectral results are reviewed in terms of Dietzel's idea of field strength of M and also in terms of Shteinberg's theory of glaze structure. X-ray diffraction is used for the identification of various species that formed after the firing process of glazes (Chapter Four).

In Chapter Five, ^{57}Fe Mössbauer spectroscopy, supplemented by E.S.R., X-ray and visible spectral measurements are used in the investigation of iron in a glaze composition similar to that used in Chapter Four. The Mössbauer results are used in following the influence of; M in MO (M= Sr, Ca and Ba), oxides of titanium(IV) and vanadium(V), and firing conditions on the chemistry of iron. Generally the iron(II) and iron(III) in the fired glazes are in octahedral sites although there are a range of similar, though not identical environments. A quite noticable influence of M (in MO) on the resonance line width is seen. In one case evidence is found for iron(IV) in an iron/vanadium glaze. E.S.R. of vanadium containing glazes indicate that vanadium is present as VO^{2+} in a highly distorted tetragonal environment.

MÖSSBAUER
NICKEL
VANADIUM
IRON
ESR

ACKNOWLEDGEMENTS

I would like to sincerely thank Professor W.R.McWhinnie for his supervision, assistance, encouragement and enthusiasm throughout the course of this research.

Thanks are also due to Dr.D.Vaughan and Mr.K.Murthy (Geology Department, University of Aston in Birmingham) for assistance in obtaining Mossbauer spectra, and all members of the Department of Chemistry at UAB who have helped during the course of this work.

My thanks are also due to the University of Baghdad for a study leave.

Finally, I would like to express my greatest thanks to my wife for her patience and understanding during the course of this work.

LIST OF CONTENTS

LIST OF TABLES

LIST OF FIGURES

CHAPTER ONE

GENERAL INTRODUCTION

1.1 Preamble

Glazes are vitreous substances formed as a film of glass on a ceramic base by supercooling of high viscosity mixtures of complex silicates and/or borates. The raw material for glazes and those for pottery to which they are applied are common for glass and ceramics, and may be broadly divided on the basis of the so-called molecular formula into:

a) material supplying the basic oxides which will flux with SiO_2 and B_2O_3 to form glassy materials containing complex silicates and borate

b) materials supplying Al_2O_3

c) materials supplying B_2O_3 and SiO_2

In addition there are special additives such as opacifiers, crystallising agents and colouring agents.

Before the application of the glaze slip on the ware a preparative operation is done which comprises weighing out, mixing, grinding and the adjusting of the pint weight (the weight in ounces of one pint of the slip) and viscosity so that a coating of sufficient thickness is taken up on the articles when they are dipped. After these operations the articles are dried and then placed for firing.

There are some properties which must be fulfilled for any glaze to be used in covering ceramic bodies;

i) insoluble in water and the usual acids and alkalis
ii) resistance to damaging, crazing and peeling
iii) an aesthetic appearance
iv) fusible within a predetermined temperature range
v) has no toxic effect if it is applied on household ware.

1.2.1 Structure of Glazes and Glasses[1,2]

Having defined a glaze as a film of glass on a ceramic body, it is of interest to know what glass is. At the beginning it is of importance to mention that the answer to this question is not yet complete and that there are several hypotheses developed which approach the answer from different angles, and this is due to the extreme complexity of glasses.

For many years a simplified view was to look at glass as a complicated liquid in the supercooled state. The American Society for Testing Materials (A.S.T.M) proposed a definition for the glass which is widely accepted; "Glass is an inorganic product of fusion which has cooled to a rigid condition without crystallising". This definition is restrictive for two reasons; firstly, there are certain organic materials e.g., glucose, glycerol and

some organic polymers, which can be supercooled to a rigid condition without crystallising and which in this form would have a glassy state. Secondly, the non-crystalline substances can be prepared by methods other than cooling a melt e.g., by deposition from vapour phase.

So how is this solid and rigid glass described as liquid. Such a relationship between the glassy state and normal solid and liquid states can be understood on the basis of what happens during the cooling melts, as shown in the volume-temperature diagrams (Figure 1.1).

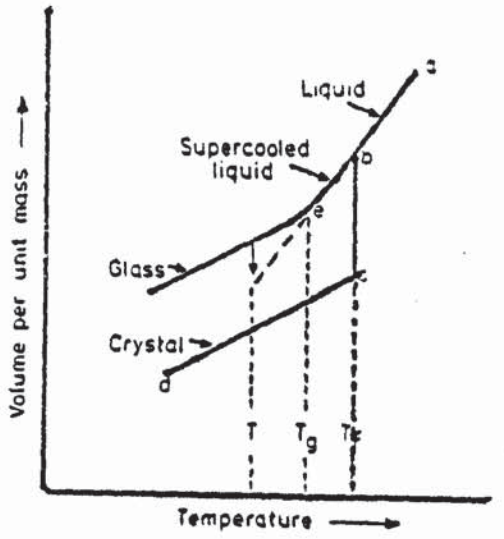

Figure 1.1 Relation between the glassy, liquid and solid states.

If the melt crystallises on cooling it is observed that there is a closely defined temperature (T_f in Fig 1.1) at which solidification occurs and at this temperature a discontinuous volume change takes place. For a material which can be cooled to the glass state, no such changes occur. Instead a volume decrease takes place along the line be. There are two sources for such contraction in volume, firstly the decreasing amplitude of atomic vibrations, and secondly, the changes in the structure of the melt. As the viscosity increases with falling temperature, the structural changes occur increasingly slowly until eventually the viscosity becomes so high that no further changes are possible. The temperature at which the change in slope occurs is called the transformation temperature or glass transition temperature, T_g. The temperature T, a little below T_g (Fig 1.1) is a temperature at which the volume of the glass decreases slowly until it reaches a point on the dotted line, which is an extrapolation of the contraction curve of the supercooled liquid. The rate of change of volume decreases as the dotted line is approached i.e., as the structure of the glass approaches the equilibrium "Configuration" which is characteristic of the supercooled melt at the temperature T.

The temperature variation of the heat content of glassy materials can be used in the elucidation of the transformation range. Heat is evolved on the solidification of

substances which crystallise, while there is no exothermic effect corresponding with the change of glassy substances from liquid to the solid state.

1.2.2 Theories of Glass Formation

The elucidation of glass formation is not an easy task, since it consists of various chemical and physical processes which are continuously changing during the synthesis of the glass. Glass researches have studied these processes from different views and many ideas have been developed, e.g., Bezborodov[3] mentioned seven theories of glass structure. The most popular and the more apposite of these theories to the ceramic glazes are presented in this section i.e., the crystallite and the random network theories.

The crystallite theory suggests that when glass melts are cooling, crystallites are formed which then make up the main body of the glass. These crystallite models[4], where very small crystalline regions are connected by disordered material, were examined by Warren and Biscoe[5]. They showed that the breadth of the first diffraction peak in vitreous silica required a crystallite size of no larger than 8Å. At this size the term crystal loses any meaning. Furthermore, vitreous silica showed little low angle scattering of X-rays; any appreciable amount of fine non-uniformities would lead to such scattering.

Goldschmidt[9] demonstrated that to represent an approximate order in glasses, the same rules as those applied to crystals can be used. He suggested that the ability of an oxide to form a glass might be related to the way in which the oxygen ions were arranged around the cation to form the unit cell of the crystal structure. He noticed that for simple oxides a relationship exists between the glass forming tendency and the ratio of the size of cation to the size of the oxygen. As a consequence, for an oxide M_xO_y, the co-ordination number of the M cation will be four if the radius ratios R_m/R_o lies between 0.225 and 0.414, and these oxides were termed a glass former. In this case, the oxygens are arranged at the corners of a tetrahedron with the cation occupying a central position.

Goldschmidt's ideas were used and developed by Zachariasen[12] who pointed out (1932) that the ability of an oxide to form a tetrahedral configuration could not be an absolute criterion of glass-forming ability since the radius ratio for BeO, for example, will permit oxygen ions to form tetrahedral grouping around the beryllium ion and yet this oxide cannot be obtained in the glassy state. Zachariasen started from the basis that the interatomic forces in an oxide glass must be similar to those in a crystal of the same composition. The disordered character of the glass structure (the lack of long-range order) lends it an internal energy surplus over that of the corresponding crystal structure. This difference

in internal energy cannot be too high, or else it would induce quick crystallisation. In order to fulfil this condition glass must be assumed to possess the same co-ordination polyhedra as those in crystals, and the bonds between the polyhedra may be similar. Disorder without any important increase in internal energy can develop only if the relative orientation of polyhedra in glass is different from that in the crystal. Not every structure allows such a disorder without the cations coming too close to one another, resulting, on account of the repulsive forces which develop, in a considerable increase in internal energy. Figure 1.2 shows the difference between the regular crystalline lattices and the random network for an oxide having the formula M_2O_3:

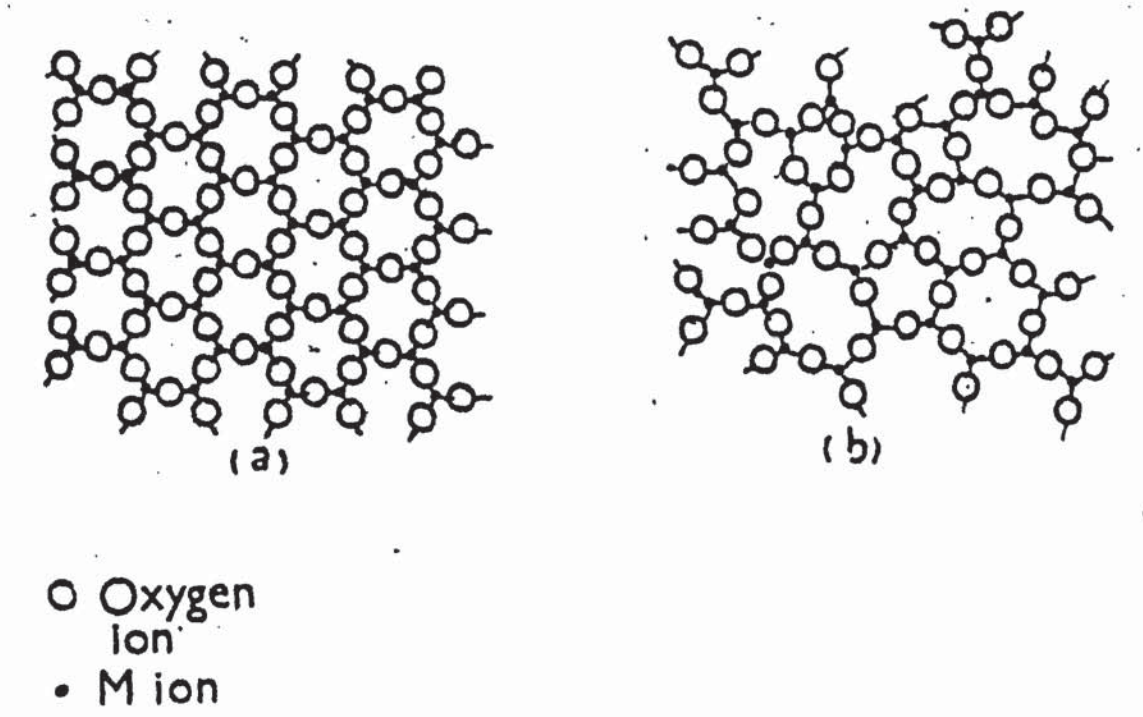

Figure 1.2 Two-dimensional representation of an a) crystalline form b) glassy form.

Thus, Zachariasen succeeded in proposing certain conditions for glass formation:

a) An oxygen atom must be linked to no more than two cation ions.

b) The number of oxygen atoms surrounding the cation must be small.

c) The oxygen polyhedra must share corners only and not edges or faces.

d) Three at least of the polyhedron vertices must be bonded to other polyhedra.

The oxides which comply with these rules can form space networks and were termed network formers. There are two other types of oxides which are included in glass composition, but which cannot participate in the building up of the space network. These are network-modifying oxides and intermediate oxides. The cations introduced by the modifying oxides induce the breaking of some of the bonds between the tetrahedron vertices, so that the lattice develops several holes in which they settle scattered at random. These structural changes are shown in Figure 1.3.

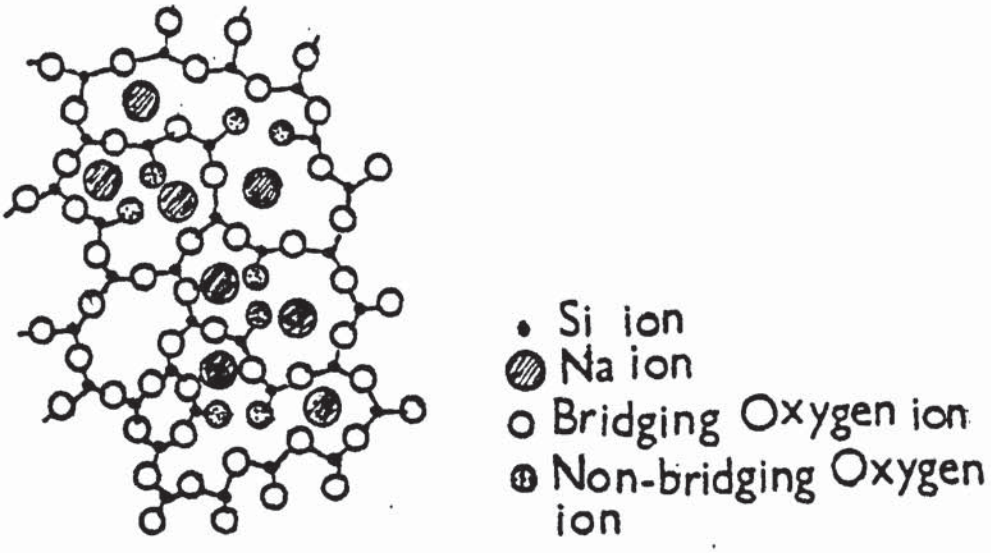

Figure 1.3 Structure of Na_2O - SiO_2 glass.

The tetrahedral groups introduced by the intermediate oxides, like AlO_4, can replace SiO_4 tetrahedra in silicate lattices to give the arrangement shown in Figure 1.4.

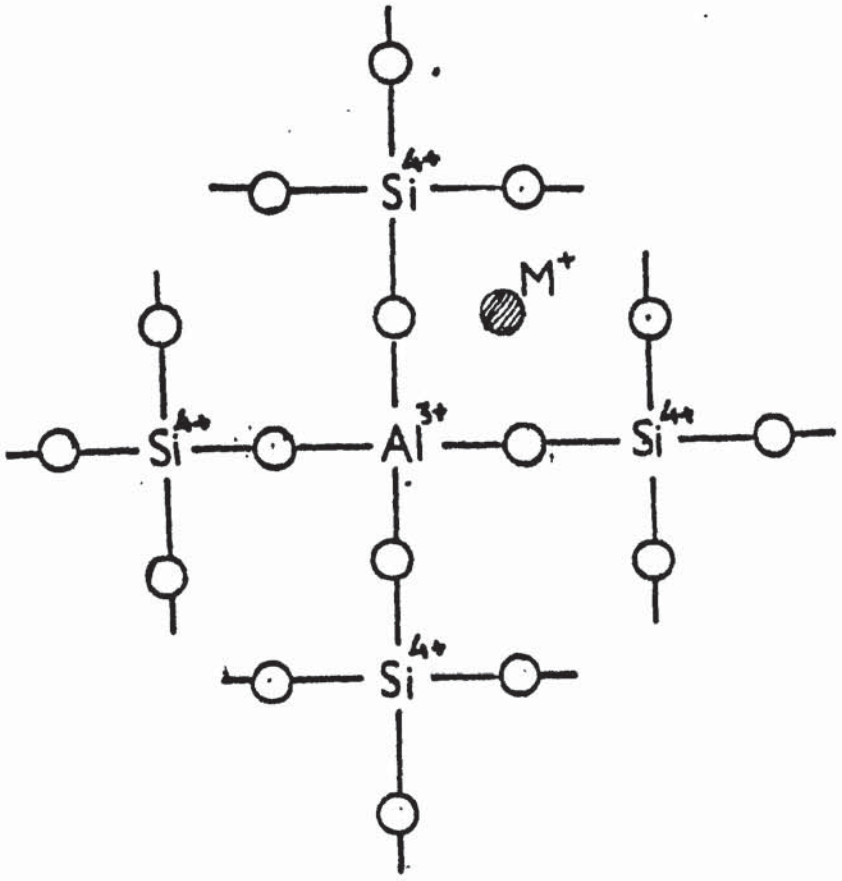

Figure 1.4 Aluminium in silicate glasses.

Since each aluminium ion has a charge of +3 as compared with a charge of +4 for each silicon ion, an additional unit positive charge must be present to ensure electroneutrality. One alkali metal ion per AlO_4 tetrahedron would satisfy this requirement and the alkali metal ion could be accommodated in the interstices between tetrahedral groups. This type of structural arrangement is found for many aluminosilicates such as feldspars and zeolites, where the crystals are built up of linked SiO_4 and AlO_4 groups.

The Zachariasen theory was well acknowledged by glass technologists,but, within academic science, alternative theories exist and it is less completely acceptable. The good reception of the network theory by glass and glaze-ceramic specialists is due to the fact that it explains in a working manner why glass melts at lower temperature when certain oxides are incorporated. It explains the connection between the physical properties of glass and composition. Thus, inserting oxygen ions by means of alkaline oxides weakens the glass structure, the network then breaks up, viscosity falls, chemical resistance is impaired and the coefficient of thermal expansion rises. The theory also explains the role played by boric oxide, fluorine and other compounds used in glazes. Boric oxide, for instance, alters the properties of alkaline silicate glasses in different ways, depending on content.

Plotting various properties such as refractive index and density against the boric oxide content of a glaze, produces certain peaks and depressions. This effect is due to the change in co-ordination number of boron with different oxide contents. The effect of fluorine on the chemical resistance and viscosity of alkaline silicate glazes and glasses can be explained by the fact that fluoride ions, in small amounts, penetrate the silicon network, replacing the oxygen ions. This weakens the structure and causes the glass or glaze to melt at lower temperatures.

On the side of structural researches, Zachariasen's theory received confirmation and criticism at the same time. B.E.Warren and his colleague confirmed Zachariasen's model by X-ray diffraction studies in a series of papers published in the 1930's and early 1940's.

Shteinberg[6,8](1967) challenged the random network theory by suggesting that the idea of Belov[7] on glass structure positively explained that it is not silicon, nor the silicon-oxygen group that is the chief building unit of the structure of glass (formers), but the cations. In Shteinberg's book, she demonstrated the effect of bivalent cations on the structure and properties of strontium glazes. The conclusions, it is claimed, are applicable to commercial silicate glasses, especially leadless, boron-free and alkaline-free compositions. Belov[7] shares

Zachariasen's views in his ideas on the similarity of the structure of silicate glasses and the crystalline phases that separate out of them, but the main difference was that in addition to the crystal-chemical aspect, he emphasised the leading role of cations in the formation of the structure and properties of glass. This factor Belov ascribed to the large cation, to which in general the form of the strong, but not rigid, silicon-oxygen group adopts itself because of the spatial geometric factors involved. According to these ideas, the small cations insert themselves into the structure of the glass which is thus dictated by the large cations. On this basis, Shteinberg set out to develop commercial strontium glazes which she claims are equal to lead glazes for durability, brilliance and other properties. She synthesised strontium leadless, boron-free glazes which do not readily crystallise, and which contained a second small Me^{2+} (Mg, Zn, Be). In her opinion it is not sufficient to consider the structure of glass to be affected by the geometric differences in sizes of the cation alone.

Dietzel[9] (1942) derived a similar idea, but on the basis of the Zachariasen-Warren theory. He correlated the intensity of the electrostatic ion field with the glass forming tendency and with some properties of glasses. Thus both the geometric and the electric properties of ions are

taken into account simultaneously. One measure of the power of a cation to attract electrons, and therefore of ability to form covalent bonds, which was chosen by Dietzel, is the ionic field strength given by:

$$F = \frac{z}{\bar{r}^2}$$

where z is the valency and

$\bar{r}$ is the ionic radius.

The values computed for the ions which occur more frequently in glass are given in Table 1.1.

The values of F allow a classification of oxides according to their roles in glass structure, though this criterion might place Be in the category of network forming ions. The concept of field strength represents a simplified viewpoint since it considers ions to behave as rigid spheres. This is not strictly true because large ions of low charge and non-noble gas ions are deformable. Nevertheless, this idea is a useful aid to understanding the roles of various ions in glass structure.

There have been other attempts to characterise oxides with regards to their ability to form glasses. One of these involved the calculation of electronegativity difference between the cation and oxygen to give a measurement of

Table 1.1 Properties of some of the elements which occur in glasses.

1	2	3	4	5	6	7	8
Ion	Ionic Radius* A (r)	Field Strength $Z/r^2 \times 10^8 cm^{-1}$	Electro-negativity	Dissociation Energy MO_x KJmole^{-1}	Single Bond KJmole^{-1}	$\frac{B_{m-o}}{T_m^{\Theta}}$ KJmole^{-1}K^{-1}	Structural role in glass
B^{3+}	0.23	56.71	2.0	1464.4	497.89	0.686	Network
P^{5+}	0.35	40.81	2.1	1849.3	368-464	0.435-0.548	
Si^{4+}	0.42	22.67	1.8	1774.01	443.50	0.221	forming
As^{5+}	0.46	23.62	2.0	1460.2	296.52		
Ge^{4+}	0.53	14.23	1.8	1803.3	451.87	0.326	ions
Te^{4+}	0.70	8.16	2.1				
Be^{2+}	0.31	20.81	1.5	1046	263.59		Inter-
Al^{3+}	0.51	11.53	1.5	1681.9	442.58		
Ti^{4+}	0.68	8.65	1.6	1820.04	305.43	0.142	mediate
Zr^{4+}	0.80	6.25					
V^{5+}	0.59	14.36	1.6	1878.6	376-468	0.062-0.497	ions
Mg^{2+}	0.66	4.59	1.2	928.84	154.80	0.054	Network
Li^{+}	0.68	2.16	1.0	602.49	150.62		
Ca^{2+}	0.99	2.04	1.0	1075.2	133.88	0.046	modifying
Na^{+}	0.97	1.06	0.9	502.08	83.68		
Ba^{2+}	1.34	1.11	0.9	1087.84	138.07	0.062	ions
K^{+}	1.33	0.56	0.8	481.16	54.39		
Sr^{2+}	1.13	1.56	1.0	1071.1	92.04		

* Pauling ionic radii $^{\Theta}$ T_m = Melting temperature

the covalent-ionic nature of the bond[11]. The electronegativities of the elements more frequently occurring in glasses are included in column (4) of Table 1.1. The oxygen electronegativity being 3.5, a difference of 1.7, corresponding to 50% ionic character, is obtained for the Si-O bond. The increase in the difference between electronegativities, results in an increase in ionic character. B-O is found to possess 44% ionic character, while that of Al-O amounts to 60%. Table 1.1 shows that the elements considered to be network formers have, in general, high electronegativity (more than 1.8), while those assumed to act as modifiers display values lower than 1.2. There are many examples which show that the correlation between electronegativity and glass forming tendency is weak, e.g., the electronegativity of Sn and Sb are equal or close to that of Si, yet their oxides in the pure state do not form glasses by melt supercooling. Another example is that of BeF_2, which yields a stable glass, the bond has 80% ionic character. One benefit of this approach is the discovery of TeO_2 glass by Stanworth[11]. The fact that tellurium has the same electronegativity value as phosphorus opened the way to a research which showed that TeO_2 can form binary stable glasses with Al_2O_3, BaO and PbO.

Sun[13] pointed out an idea for correlating the glass-forming tendency to the energy required to dissociate the

oxide into gaseous constituent atoms. Table 1.1 presents both the dissociation energy (column 5) and the bond energy computed by dividing the dissociation energy by the co-ordination number (column 6) for the oxides which enter more often in glass. According to these values, the energy of bonding to oxygen in network-forming oxides is higher than 376 KJ, while in modifier oxides it does not go beyond 251.04 KJ. Although Sun noticed certain disagreements, he succeeded in proposing some interesting ideas; (a) he mentioned the importance of polymeric structure in glass formation, (b) to keep the bonds stable at high temperature inside the polymeric structural elements, they have to be very strong, and (c) he relied on the importance of cyclisation for glass formation.

Rawson[14] extended Sun's concept to calculate the ratio between single bond energies and melting point (column 7, Table 1.1). For network formers the ratio has values higher than 0.209 KJ $mole^{-1}K^{-1}$, while in the case of modifiers it is lower than 0.062 KJ $mole^{-1}K^{-1}$.

Although it is possible by using the previous approaches to differentiate between the oxides according to their glass forming tendency, none of them have a perfect and complete explanation of glass formation.

Recently a bitter criticism of the random network theory came from Rawson in his book[2](page 28) , where he stated

that "Zachariasen's views on the reasons for glass formation have not proved helpful - rather the reverse". Rawson described the picture presented by Zachariasen as likely to be correct in broad outline. He mentioned that in reality the situation is not likely to be simple. For example, it is well known that most samples of silica glass are oxygen-deficient. This gives rise to defects in the structure. Similar defects may exist in binary and ternary oxide glasses. Rawson emphasised that Zachariasen's hypothesis cannot be applied to all inorganic glass forming materials, e.g., it is of no value when considering the structure of vitreous selenium, and it is very unlikely that it has very much to say about the chalcogenide glasses and the metallic glasses. However, for the commercially important silica glasses, it has provided a very useful mental picture for structural ideas.

1.3 Classification of Glazes

There are many ways of classifying the glazes, and these depend on the point of view of the worker, whether he is a glass technologist, a craft potter or a chemist.

a) Classification by technologists
   (i) Lead containing glazes
   (ii) Leadless glazes

This is because of the effect of lead on the physical properties of the clay bodies.

b) Classification based on the ware to which it is applied:

(i) Majolica glaze
(ii) Earthenware glaze
(iii) Sanitary glaze

c) Classification according to the effects produced on the finished articles:

(i) Matt glaze
(ii) Semi-matt glaze
(iii) Satin Nellum glaze
(iv) Opaque glaze

d) Classification based on the maturing or firing temperature of the glaze:

(i) Majolica glaze (900 - 1050^{o}C)
(ii) Earthen type (1000 - 1150^{o}C)
(iii) Fire clay sanitary type (1200 - 1250^{o}C)
(iv) Porcelain type (1300^{o}C and above)

1.4 Raw Materials

The basic materials that compose the glaze can be expressed in terms of oxides, even though these will not be introduced as oxides, but as complex silicate or borates, so the oxides present in the glaze are classified as:

a) Acidic oxides
b) Amphoteric oxides
c) Basic oxides

a) Acidic oxides

These may be silica or silica and boric acid. Boric acid has the effect of decreasing the maturing temperature of the glaze, and promoting craze resistance. Boric oxide is usually added as borax or boric acid.

b) Amphoteric oxides

This is mainly aluminium which is not introduced as oxide, but in the combined form as clay, feldspar or Cornish stone. The main function of the alumina is to prevent crystal formation, leading to a milky appearance, this action is called devitrification. Using high quantities of alumina in glaze formation will increase the viscosity of the glaze at its maturing temperature.

c) Basic oxides

These are the fluxing oxides which react with the acidic oxides during firing to form silicates or borates.

Examples of oxides which are usually used in glaze recipes are listed below:

1) Lead oxide

The incorporation of lead oxide in the ceramic glazes leads to a low melting temperature and low viscosity in the molten glaze, and gives a brilliant smooth glaze, with high refractive index. On the other hand, lead has a poisoning effect. Since the oxide and basic carbonate of lead are soluble in the hydrochloric acid contained in gastric juices, they are a potential source of poisoning. Lead usually enters through the mouth and nose and accumulates in the body until a dangerous level is reached and signs of anaemia, partial paralysis and malfunctioning of the kidneys appear. These troubles can be reduced by firstly applying strict safety regulations in the working area and secondly by using an insoluble frit of lead oxide.

2) Soda and Potash

This is introduced as feldspar, stone or as the carbonate, and in addition Na_2O may be introduced as borax. They are used in relatively small proportion, since high quantities of alkali oxides cause:

(i) Reduction in stability of glaze, because they are reactive.

(ii) Resulting in high thermal expansion in glaze which makes the glaze easily damaged.

3) Calcium

Calcium is introduced as carbonate (limestone) which acts as a flux in the glass if added up to a certain amount. Extra quantities will cause devitrification.

The glaze formula is likely to contain other additives which have different effects on the glaze, some of them act as opacifying agents, which remain undissolved in the glaze after firing e.g., SnO_2, ZnO and TiO_2. Other additives have special decorative effects, specially in production of malt glazes - which have a rough textured surface. This is achieved by adding oxides like CaO, ZnO, BaO or MgO.

The colouring materials form one of the most important additives. The effect of such materials on structure of glaze is one of the main objectives of this work. Some

of these materials are listed below,

Antimony oxide, gives yellow colouration
Chromium oxide, green or red (when used as lead chromate) yellow (when used as barium chromate), pink (when used with tin).
Cobalt oxide, blue (gives such colour as a result of formation of cobalt alumina silicate).
Copper oxide, green, blue (in presence of high alkali), red (in reducing atmosphere).
Gold oxide, pink, purple (in presence of tin).
Iron oxide, yellow and brown, green (in reducing atmosphere).
Manganese Dioxide, brown, violet or pink (in glaze of high alkalies).
Platinum, like gold
Titanium dioxide, yellow and brown (with iron)
Uranium oxide, introduced either as oxide or as sodium-uranate to give yellow, orange.

There are also other additives which are introduced to improve the electrical insulating, magnetic and heat transfer properties of ceramic glazes.

1.5 The Glazing Processes

The glazing of ceramic articles involves three main stages:

(i) Preparation of the glaze

(ii) Application of slip glaze to the ware

(iii) Firing of the glaze

(i) Preparation of the glaze

These operations comprise, choosing the glaze ingredients, weighing out, mixing, grinding and then adjusting the pint weight and viscosity. The oxides necessary to arrive at the molecular formula of the glaze recipe can be added either as separate oxides (e.g., Al_2O_3, SiO_2,...), or in a combined form like feldspar, clay,... etc. Since the glazes produced in both cases may not behave identically, the choosing of glaze ingredients must often be done empirically.

The grinding of the glaze mixture is usually done in a medium which keeps it away from contamination with foreign materials. This can be achieved by using porcelain mills, fused alumina or rubber mills. The grinding must be neither coarse nor too fine. This is because coarse grinding makes it difficult to work the slip glaze at a high enough pint weight and makes the coating of glaze uneven, while overgrinding of the glaze mixture to a fine powder makes the glaze more dusty when dried and easily knocked off, besides being wasteful of power.

Adjusting the pint weight and viscosity is very important in glaze preparation, because the amount of glaze taken up on dipping depends on these two factors besides the porosity of the articles and the time of immersion.

If the amount of glaze is too much, the ware is likely to craze, and the molten glaze may run, giving stuck ware. The colloidal materials such as china clay, bentonite and various gums and starch are usually used to adjust the viscosity of the slip glaze.

(ii) Application of the slip glaze

Application of glaze is usually done either by dipping or spraying. Spraying is a technique which is indispensable for some pieces which are too heavy to handle, for example, some articles of sanitary and electrical ware. It is also used increasingly for coloured glazes when it is important to get an even coating of glaze to avoid shading. The main disadvantage of spraying is that 25% of the glaze will not fall on the articles and this must be recovered.

(iii) Firing of the glaze

Before placing the glazed ware for firing, it must be dried. The aim of firing is not only to melt the glaze, but also to allow it to flow evenly over the surface

of the articles and all gas bubbles must be released. This stage is called the maturing stage of the glaze. Incomplete maturing means poor brilliance and the glaze may be disfigured by pinholes where gas has escaped but the firing conditions have not allowed the molten glaze to fill up the craters left. The viscosity of the glaze at the melting temperature has a remarkable effect on the glazing operation, because low viscosity of the glaze (too fluid) tends to stick the ware to the supports or bats, while insufficient fluidity can lead to crawling and similar troubles. The amount of alkali oxides (Na_2O, K_2O and Li_2O) and the acidic oxides, have a distinctive effect on the melting temperature of the slip glaze. Increased alkali lowers the firing temperature, while the reverse is true for the increase in acidic oxides.

1.6 Reactions Occurring on Firing[23]

It is possible to outline the reactions which occur on firing as follows:

1) Expelling the moisture left in the ware after drying or gained from the atmosphere. This takes place at $100^{o}C$.

2) Dehydroxylation

Dehydroxylation is the removal of OH groups as H_2O from clay structures e.g.,

$$Al_2O_3 \cdot 2SiO_2 \cdot 2H_2O \xrightarrow{450^{\circ}C-500^{\circ}C} Al_2O_3.2SiO_2 + 2H_2O$$

kaolinite → metakaolin + steam

3) Burning of organic materials

This stage involves the decomposition of organic materials to carbon dioxide and water by means of oxygen. This occurs at a temperature between 300°C - 700°C or even higher.

4) Glass formation (vitrification)

Glass formation may start at any temperature above 900°C depending on the composition of the body. In this stage of firing particles of fluxing material react with particles of other body constituents with which they are in contact to form a liquid. The following factors affect the vitrification process:

(i) The maximum temperature to which the glass will fire; at too high a temperature so much liquid may be formed that the body may lose shape.

(ii) Particle size of the starting materials; this affects the porosity of the final glaze, the

finer the particle size, the greater its surface area per unit weight.

(iii) Ratio of fluxing to refractory materials in the recipe, this will alter the temperature at which vitrification occurs.

(iv) Time of firing; rapid firing to high temperature prevents sufficient heat treatment of the body.

(v) Viscosity of the liquid formed during firing.

(vi) Kiln atmosphere; firing in strong oxidizing atmosphere leads the oxidation of Iron (II) to Iron (III) and causes a colouration in the glaze.

1.7 The Present Work

This work is an attempt to use physico-chemical methods of analysis in investigating the role played by transition metal cations in ceramic glazes. Since the glaze is a supercooled liquid without a definite arrangement of atoms or ions such as is found in crystals, dependence on one or two techniques gives no definite information on glaze structure.

X-ray diffraction analysis can give some information on general structure of silicate lattices, because it can identify the species in the fired glaze mixture. This technique suffers from lack of sensitivity to small impurities and from non-validity when amorphous phases are encountered.

The application of the infra-red spectroscopic technique to the problem of ceramic glazes has grown in importance. This is because of its ability to identify specific groups of atoms within a material, and because of its optical probing which can be used for elucidation of the submicroscopic structure of crystals and glazes[16]. The studying of glaze by this method is done by comparing the spectra obtained for the new glazes with spectra obtained previously for certain well known compounds. It is thus possible to determine the presence of primary groups developed in the precrystallization period, and hence to study their behaviour as a function of melting history and chemical composition. Infra-red spectroscopy shows difficulty in identifying either impurities or slight structural modifications.

Mössbauer spectroscopy can give certain types of information which are uniquely obtainable by this technique. The most unique feature of Mössbauer spectroscopy is its specificity.

It is not only specific for a given element under study, it can differentiate between oxidation states. Mössbauer spectroscopy is useful in answering questions about certain ions in glass, such as whether or not an ion is molecularly dispersed throughout a glass, or is clustered in colloidal particles, and what is the coordination number. This technique and its application to glasses have been reviewed by Kurjian[17]. Naturally abundant iron contains 2.2% ^{57}Fe so that one possible disadvantage of the technique is that it requires large amounts of iron in order to obtain a spectrum. This problem can be surmounted either by isotopic enrichment or by low temperature measurements which increase the recoil free fraction and facilitate easier measurement over shorter periods of time. The other disadvantage of this method is that the results obtained are tentative and need confirmation with other techniques before conclusive structural information can be deduced from them.

The characterisation of glaze colour changes require the knowledge of the valence in the undisturbed bound state, so E.S.R. was used[18,19], especially with respect to the high sensitivity to transition metals (Ti, V, Cr, Mn, Cu,...etc) which are predominantly used. Recently a comprehensive review has been published, which covers the use of E.S.R. in the investigation of glasses[20].

Optical absorption spectra are valuable in determining the coordination number and configuration of high valent ions such as those of the transition metals, which have been extensively studied[21,22]. In general these studies show that the immediate surroundings of these ions in silicate glasses are much like the surroundings in a corresponding crystal or even in a solution with complexed ions. These studies also show that the transition metal ions are invariably under the influence of a relatively weak crystal field. This finding is consistent with the picture of glass structure in which the short-range environment is quite regular, and the random characteristic of the glassy state occurs only over dimensions of several structural units. In view of this, the use of optical absorption spectroscopy in conjunction with a number of other spectroscopic technique to study the vanadyl ion in weak field enviromnents is initially selected (Chapter 3).

The existence of bivalent iron in the finished glaze has a technical importance to the craft potter, and they achieved it by expensive and hazardous processes. One of the major objectives of this work is the use of Mössbauer spectroscopy in determining the chemical changes affecting the oxidation of Iron II in ceramic glazes.

Another major objective of this work is to employ other physico-chemical measurements to elucidate the structure and symmetry of iron, nickel and vanadium containing glazes. Visible spectra are mainly used in studying nickel containing glazes, whilst E.S.R. is used in the investigation of vanadium and iron containing glazes. Throughout the course of this work, X-ray diffraction analysis was used in order to identify various species that are formed at different stages of the firing process. Many of these spectroscopic results, particularly for the strontium containing glazes, are reviewed in terms of Shteinberg's theory of glass structure.

CHAPTER TWO

EXPERIMENTAL DETAIL

2.1 Analyses

Microanalyses for carbon, hydrogen, nitrogen and halogen were performed by the Chemistry Department, University of Aston in Birmingham.

2.2 Conductivity Measurements

Molar conductivities were measured with a Mullard conductivity bridge using a standard conductivity cell.

2.3 Magnetic Susceptibility Determinations

Magnetic susceptibilities were measured by the Gouy method at room temperature. A semi-micro Stanton instrument balance was used in conjunction with an electromagnet operating at a current of 10 amperes. Gouy tube constants were determined using $Hg[Co(CN)_4]$ as a standard with known gram susceptibility of 16.44×10^{-6} e.g.s. unit at $20^{\circ}C$. Susceptibilities were then calculated according to the method described in the practical book of Angelici[24].

2.4 Electronic Spectra

An SP800 spectrophotometer was used to record the electronic absorption spectra. For the insoluble solid samples

the electronic spectra were obtained by coating a Wattmann filter paper with a nujol mull of the finally powdered samples.

2.5 Infra-red Spectra

Infra-red spectra were recorded using Perkin-Elmer 225 and 237 spectrophotometers between 4000 cm^{-1} and 250 cm^{-1}. The samples were prepared either as nujol mulls or as KBr discs.

2.6 Electron Spin Resonance Spectra

Electron spin resonance spectra were obtained using a JEOL JES-PE electron spin resonance spectrometer operating in the X-band calibrated with a standard Mn^{2+} sample diluted with magnesium oxide.

2.7 X-Ray Powder Diffractogram Traces (XRD)

Some of the X-ray powder diffractogram traces were done within the Geology Department of Aston University, using Co K_α radiation, wavelength 1.791 Å.

Other X-ray powder diffractogram traces were obtained as a standard analytical service within the Chemistry Department of Aston University, using Cu K_α radiation,

wavelength 1.54 Å. Exposure times of up to four hours were necessary. The identification of chemical species was achieved through comparison with the XRD of raw materials and through reference to the powder diffraction file.

2.8 Mössbauer Spectra

Mössbauer measurements were done in collaboration with the Geology Department.

The powdered samples were mounted in a holder made of a piece of rectangular paper board with a hole in the centre as shown in the diagram:

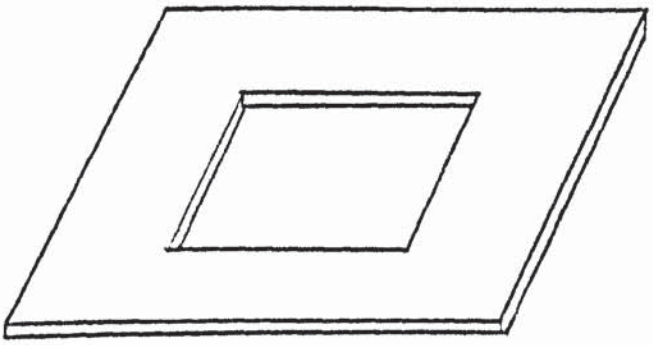

One side of the hole was covered by a thin aluminium foil. The powder was spread uniformly on the hole area, then the other side was covered by sellotape.

Mössbauer spectra of powdered samples mounted in such holders were recorded on a constant acceleration

spectrometer in 512 channels of 1024 channel multichannel analyser (Ino-tech, inc. 5200). The source was ^{57}Co in a Pd matrix and calibration was relative to the spectrum of iron foil.

A computer programme was used for the fitting of a sum of Lorentzian lines to a Mössbauer spectrum. The programme was written by Dr A J Stone and the theoretical basis of this programme was described in an appendix to a paper by Bancroft, Maddock, Org, Prince and Stone[25]. This programme assuming Lorentzian lineshapes in the Gauss non-linear method with a facility for constraining any set of parameters or linear combinations of parameters. The appendix of this thesis shows an example of input and output data.

2.9 Glaze Firing

The samples were fired in either platinum or porcelain crucibles in a Carbolyte MFHT Furnace with a gas inlet facility. The firing under inert atmosphere was initially done by using a quartz beaker fitted with a quartz inlet tube as described by Gillespie[26]. This was found not to be a completely practical method as cracking of the quartz beaker, which is expensive, takes place after

using it for two firings. Therefore, a fire resistant asbestos brick was shaped as in the diagram, and inverted over the crucible and connected to the gas inlet pipe by a quartz inlet tube.

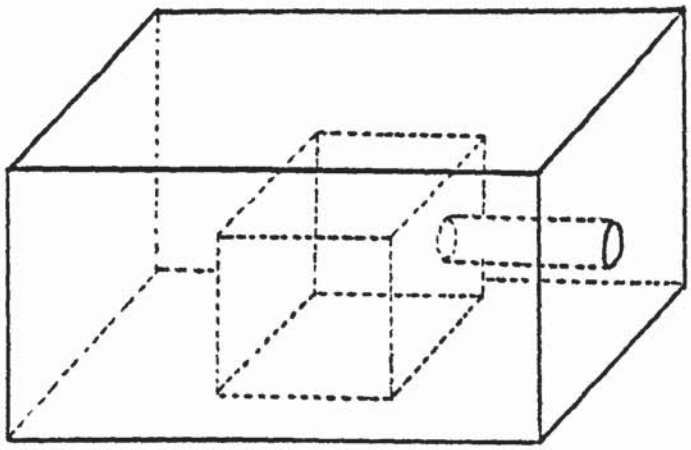

CHAPTER THREE

COORDINATION CHEMISTRY OF DIPYRIDYLAMINE AND TRIPYRIDYLAMINE VANADYL ION COMPLEXES

3.1 Introduction

Electronic spectra of transition metal containing glasses[21] have indicated that the transition metal ions are invariably under the influence of relatively weak crystal fields. Following this, the use of different physical methods in the study of the coordination behaviour of the vanadyl ion, a species of subsequent interest to us as a glaze constituent (Chapter 5), in weak ligand field environments is initially presented.

The ligands used for this study were di(2-pyridyl)amine and tri(2-pyridyl)amine:

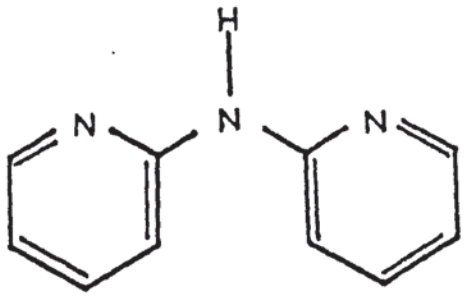

Di(2-pyridyl)amine
abbreviated to
(Dipyam)

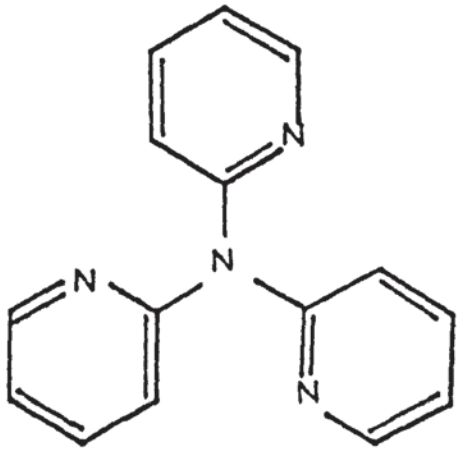

Tri(2-pyridyl)amine
abbreviated to
(Tripyam)

The coordination of these two ligands to the transition metal ions has been studied extensively, and a general review of the coordination behaviour of these ligands has been given by McWhinnie[27]. Although this review appeared in 1970, the chemistry of these ligands still receives attention by some workers[28,29] especially those working on crystal structure[30,31]. No vanadyl ion complexes with dipyam and tripyam have been reported.

There are two major factors which are responsible for the nature and strength of ligand-metal bonding, namely the stereochemistry of the ligand, and the electronic properties of the coordination moeties.

The dipyam and tripyam ligands differ sterically from other pyridine derivatives, like 2,2'-bipyridyl and 1,10-orthophenanthroline. The latter is planar or very nearly in its complexes, and it forms five-membered chelate rings, whereas the former is not planar and forms six-membered chelate. The introduction of >NH bridging group between the two pyridine rings of these ligands leads to the chelate rings being sufficiently flexible to fulfill the two important requirements; δ-bonding involving overlap of the lone pair on the ring nitrogen with vacant low energy orbitals of correct symmetry on the metal and π-bonding involving overlap of the filled

d-orbitals on the metal with the delocalized π-cloud above and below the aromatic ring. The basicities of the ring nitrogen in these ligands has been compared with the basicity of 2-aminopyridine[32], and found in the order of basic strength dipyam > 2 ampy > tripyam.

It was found that dipyam and tripyam[27,33], coordinate to transition metals through the ring nitrogens rather than via the amine nitrogen.

The base tripyam was found to coordinate either bidentate or terdentate, there being as yet no evidence of unidentate coordination.

In contrast to nearly 60 other known oxometal cations, vanadium IV and uranium VI give rise to a large number of stable complexes. This is due to the stability of V=O bond toward the chemical reactions which involve other ligands with the coordination sphere[34]. The vanadium-oxygen stretching frequency in the infra-red spectra is highly sensitive to the ligands coordinated to the vanadyl group[35]. A comprehensive review of the oxovanadium (IV) complexes has been published by Selbin[36,37].

3.2 Experimental

3.2.1 Chemicals

The ligand di(2-pyridyl)amine was obtained from Aldrich Co. The ligand tri(2-pyridyl)amine was prepared by the method of Wibaut and La Bastide[38], which was modified by Lancaster and McWhinnie[39]. Aminopyridine (Koch-light Laboratories Ltd) and 2-bromopyridine (Aldrich Chemical Co Ltd) were used in the preparation of tripyridylamine. The salts $VOCl_2$ (50% aqueous solution) and $VOSO_4.5H_2O$ were obtained from B.D.H. Co.

3.2.2 Preparation of the Complexes

Preparation of sulfatoaquodimethylformamide-di(2,2' pyridylamine oxovanadium IV

A solution of di(2,2' pyridyl) amine (0.05 mole, 8.55 gm) in 30 ml of DMF was added to a solution of $VOSO_4.5H_2O$ (0.025 mole, 4.07 gm) dissolved in 30 ml of DMF. The mixture was refluxed for about ½ hr. A bluish-violet precipitate formed and was collected by filtration. The powder was washed with 50 ml of acetone and 30 ml of diethylether. Yield 4 gm.

Preparation of dichlorodiaquobis(di-2,2' pyridyl-amine)oxovanadium IV

An aqueous solution of $VOCl_2$ (0.025 mole, 7 ml of 50% by weight solution) was added to a melted di-(2,2' pyridyl)amine (0.05 mole, 8.55 gm). The mixture refluxed with ethanol for about ½ hr, a green precipitate settled and was removed by filtration. This precipitate has an unknown structure. The filtrate was left overnight for gradual evaporation. Long green crystals were formed, which were washed with acetone and diethylether and dried over calcium chloride under vacuum.

Preparation of dichlorotetraquobis (di-2,2' pyridyl-amine)oxovanadium IV

An aqueous solution of $VOCl_2$ (7 ml of 50% aqueous solution, 0.025 mole) was mixed with 20 ml of ethanol. The solution was added dropwise to an acetone solution of di(2,2' pyridyl)amine (0.05 mole, 8.55 gm in 100 ml acetone). A brownish-green precipitate appeared, which was filtered, washed with 50 ml of acetone, and dried over calcium chloride, under vacuum. Yield, 10.5 gm.

Preparation of dibromoaquo (di-2,2' pyridylamine) oxovanadium IV

The above procedure was carried out by using aqueous $VOBr_2$ instead of $VOCl_2$. A green precipitate settled down. Yield, 8.8 gm.

Preparation of dichloroaquo(tri-2,2' pyridylamine) oxovanadium IV

The above procedure was repeated using the appropriate salt ($VOCl_2$) and ligand (tri-2,2' pyridylamine). A blue precipitate formed. Yield, 8.65 gm.

3.3 Results and Discussion

3.3.1 General Discussion

Analysis of the vanadyl complexes (Table 3.1) shows that the empirical formulae of only two complexes (those with $VOCl_2$) are in accord with two molecules of ligand being coordinated with one of VO^{2+} and all are hydrated.

The dipyam and tripyam free ligands contain a pair of bands assigned to in plane C-N stretching (Table 3.2)

Table 3.1 Analytical Data for Complexes

No	Complexes	Colour	Solubility	Found				Required			
				C	H	N	Other	C	H	N	Other
I	$VOCl_2(dipyam)_2.H_2O$	green	slightly soluble in methanol, DMSO, and DMF	47.2	5.4	17.0	14.1	48.19	4.01	16.86	14.01
II	$VOCl_2(dipyam)_2.4H_2O$	greenish brown	slightly soluble in ethanol, DMSO and DMF	41.1	4.4	15.3	13.3	43.47	4.75	15.21	12.8
III	$VOSO_4(dipyam).H_2ODMF$	bluish violet	sparingly soluble in DMSO	36.6	3.9	13.4	8.1	36.70	4.23	13.17	7.52
IV	$VOBr_2(dipyam).H_2O$	green	sparingly soluble in DMSO	28.3	2.8	10.2	34.8	28.84	2.64	10.09	38.2
V	$VO(tripyam).Cl_2.H_2O$	bluish green	slightly soluble in methanol and DMSO	44.5	3.3	14.8	17.0	44.55	3.46	13.8	17.57

Table 3.2 The Infra-red Spectra of the Complexes (Frequency in cm^{-1}) (KBr disc)

Complexes					dipyam	tripyam	Assignments
I	II	III	IV	V			
3400 br	3400 br	3260 m 3320 s 3440 br	3400 br	3400 br			H_2O stretching
3080 vw	3080 w 3130 w	3025 m 3080 m 3140 m 3200 m	3080 vw	3100 m 3080 sh	3100 m 3185 m 3240		N-H stretching
1660 vs	1655 vs	1650 vs	1650 vs		1605		N-H bending
1603 vs 1590 sh	1605 vs 1590 v	1602 s 1590 vs 1570 s	1606 s 1588 s	1600 1618 1566 1570	1585 s 1568 s	1568 s 1592 s	In plane C-N
		1230 s 1145 s 1010 s 970 s 650,660					SO_4^{2-}
		840					H_2O rocking
900 vs	900 vs	930 vs	900 vs	940 vs			V-O stretching
320 m	320 m	320 s 350 s 370	330 m 300 w	300 s 260 m 320 m			V-N
375	380		370	355			V-X

which are shifted to higher frequency in the infra-red spectrum of all complexes including those reported here. This indicates that coordination of the pyridyl nitrogen to the vanadyl species has taken place[40].

The strong N-H bending mode is present between 1650-1660 cm^{-1} in the spectra of all dipyam complexes (Table 3.2), while it is observed at 1605 cm^{-1} for the free dipyam. This cannot be regarded as evidence for the coordination of >NH group with the metal, because the X-ray crystallographic study of Johnson and Jacobson[41] proved that the free dipyam ligand is dimeric in the solid state, the N-H being hydrogen bonded to a ring nitrogen, so it is observed at 1605 cm^{-1}. There is a possibility for the tripam ligand to behave as a terdentate ligand, i.e., coordination through three ring nitrogen atoms;

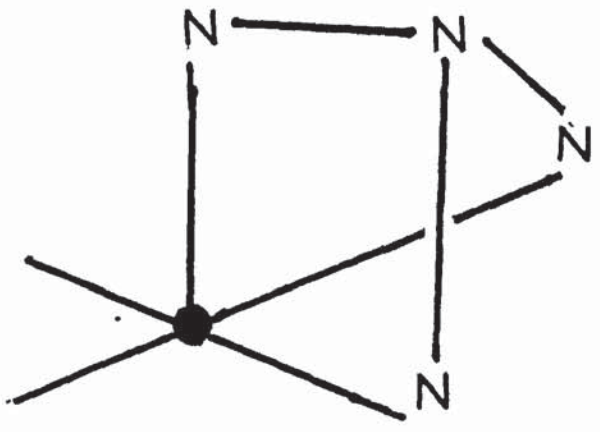

This can be ruled out in tripam complex of vanadyl-chloride due to the appearance of two groups of C-N stretching bands in the infra-red spectrum of the complex, which are attributed to the presence of both coordinated and uncoordinated rings (Table 3.2).

The metal-nitrogen stretching vibration was assigned by McWhinnie[42,43] to be around 300 cm^{-1}, but the assignment is difficult due to the presence of other bands. In the vanadyl complexes of dipyam and tripyam, the V-N stretching vibrations appears at 300 - 320 cm^{-1}.

The vanadium-oxygen frequencies in the five complexes are located at 900, 930 and 940 cm^{-1}. The bands are very strong and sharp and in the region expected for metal-double bond-oxygen stretching frequencies[44], e.g., this band occurs at 1020 cm^{-1} for $VOSO_4.5H_2O$ and at 1035 cm^{-1} for the monomeric vanadyl dichloride. The appearance of V=O stretching frequency in this range indicates a monomeric V=O unit and rules out the possibility of V-O-V-O polymer chaining[44].

The donation of electrons from the ligands to the metal ion would affect the donation ability of oxygen to vacant d-orbitals in VO^{2+} resulting in changing the ν(V=O). It was concluded[45] that the frequency change ($\Delta\nu$) is directly related to a decrease in $P_\pi \rightarrow d_\pi$ donation

from oxygen to metal and an increased electrostatic repulsion of the vanadium and oxygen species. Their effect was written as:

$$\Delta\bar{\nu} = -\sigma(L \rightarrow M) - \pi_{11}(L \rightarrow M) - \pi_{1}(L \rightarrow M)$$

σ, π_1 and π_{11} were the group orbitals of the nearest neighbour equatorial ligand atoms. These latter group orbitals are easily visualized by reference to the following figure:

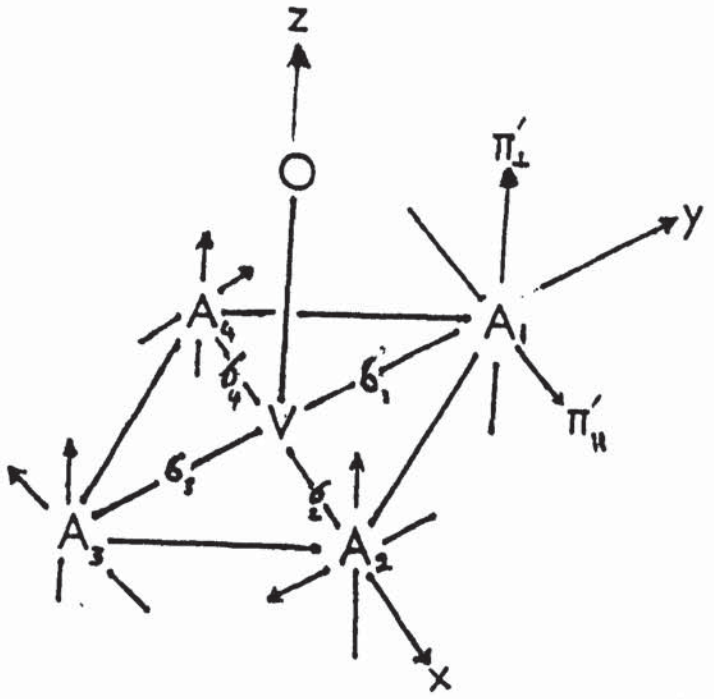

This behaviour is reflected in the lowering of ν (V=O), i.e., the greater the donation of ligand electrons to the vanadium, the greater will be the decrease expected in ν (V=O). In comparing the ability to cause this shift it was found that the coordination ability is stronger for the dipyam than for tripyam (ν(V=O) = 900 cm^{-1} for

dipyam complexes and 940 cm^{-1} for the tripyam complex), and this is in accord with the crude comparison of basicities done[32] for these two ligands. The comparison of the shift in $\nu(V=O)$ for the 2,2'-dipyridyl (979) and 1,10-phenanthroline complexes (973 - 978 cm^{-1})[45] with that for dipyam and tripyam put these ligands in the following order of σ-donation ability;
dipyam > tripyam > dipy > ophen

3.3.2 The Dipyridylamine Complexes of $VOCl_2$

The following conclusions can be drawn from the tabulated results of these two complexes:

1) The elemental analysis shows that dipyam coordinated to the metal in the ratio of 2:1 (Table 3.1).

2) The appearance of a broad band in the region of 3420-3350 cm^{-1} of the infra-red spectra of the complexes indicates the presence of water in the lattice structure of the complexes[46] (Figure 3.1).

3) the bands at 375 cm^{-1} and 385 cm^{-1} for these two complexes were assigned to be $\nu(M-Cl)$[47].

4) Investigation of the magnetic susceptibility of these two complexes in the solid state at room temperature shows that they all have effective magnetic

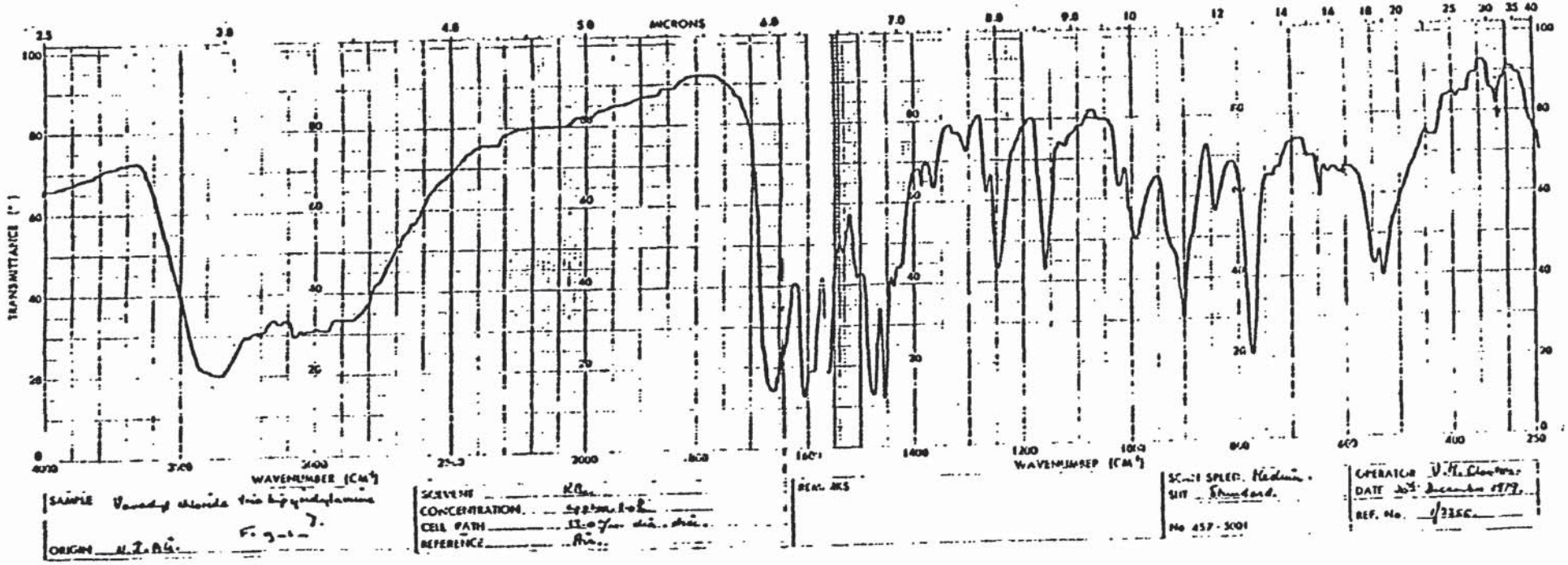

Figure 3.1 I.R. Spectrum of $VOCl_2(dipyam)_2.nH_2O$

moments less than 1.73 B.M. (0.946 B.M. and 1.242 B.M. Table 3.3). This may be explained by a considerable exchange interaction between the paramagnetic ions in the complex molecules which may have a dimeric bridge structure[48].

5) The conductivity data in DMSO characterise these complexes as 1:1 electrolyte[49], Figure 3.2. The visible spectra of these complexes in DMSO are different from the nujol mull spectra of the original solids, it seems probable that the bridge structure, which was proposed in the previous paragraph, is broken on dissolution.

From the above observations it is possible to propose two types of structure, one in solution (I) and the other in solid state (II):

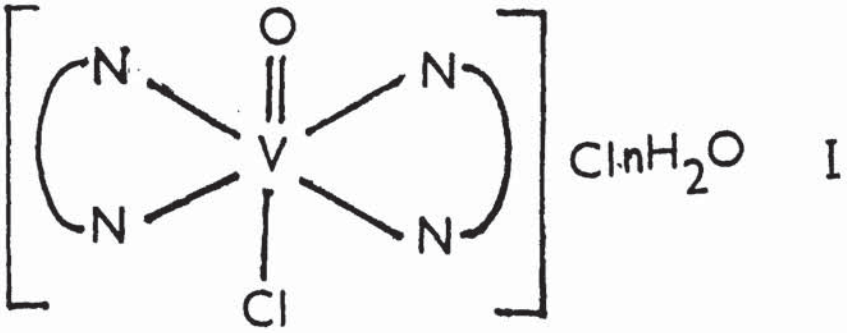

I

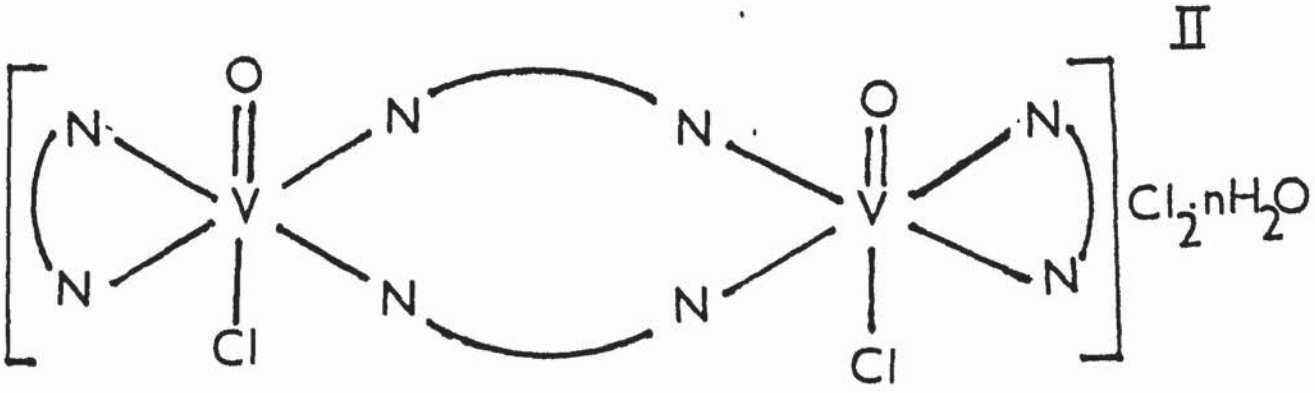

II

Table 3.3 E.S.R. and Magnetic Data for the Complexes

Complex	In DMSO solution		In solid state		
	Average g-value (g_o)	Average A-value (Gauss)	g_1	g_{11}	μ_{eff} B.M.
$VOCl_2(dipyam)_2.H_2O$	1.980	104.28			0.946
$VOCl_2(dipyam)_2.4H_2O$	1.971	104.28	1.993	1.940	1.243
$VOSO_4(dipyam)DMF.H_2O$	1.964	104.28	1.964	1.893	1.81
$VOBr_2(dipyam).H_2O$	1.977	104.1			1.18
$VOCl_2(tripyam).H_2O$	1.966	104.28			1.80

Figure 3.2 Conductivity of vanadyl complexes in DMSO

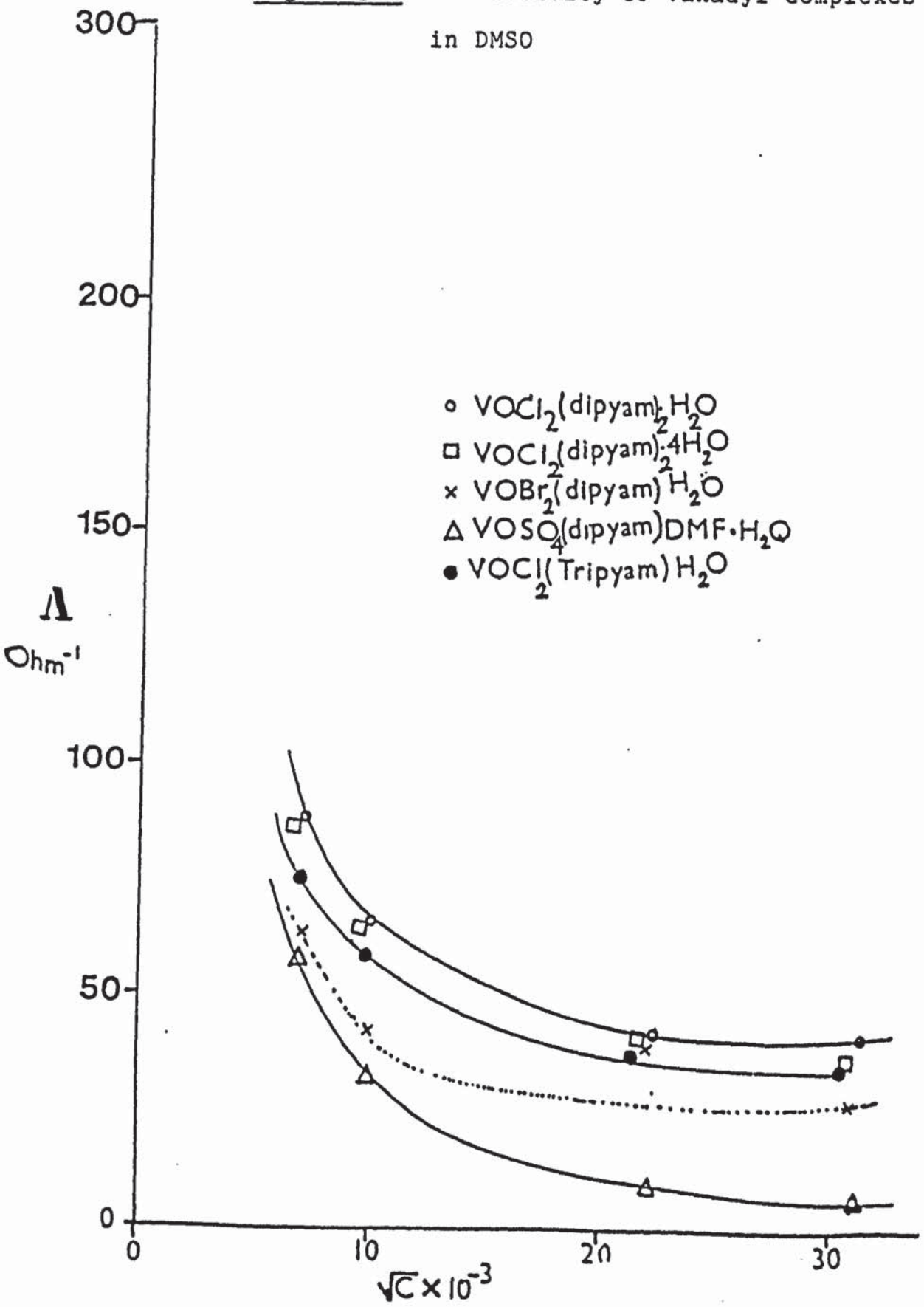

Structure I is in accord with the conductivity data, which characterise it as 1:1 electrolyte, but it is in contrast with the magnetic data. Structure II has the reverse features i.e., it obeys the magnetic data and it is against the conductivity data.

3.3.3 The Dipyridylamine Complex of $VOBr_2$

The elemental analysis of the complex is in accord with a 1:1 ratio of the ligand to metal. Conductivity data shows that the complex is a weak electrolyte. The infra-red spectrum of the complex gives evidence for the presence of M-Br vibrations and for the location of H_2O molecules in the lattice structure of the complex as mentioned above. The effective magnetic moment of the complex at room temperature (1.18 B.M.) is less than that expected for the spin only value (1.73 B.M.) and this indicates that the complex might have a polymeric structure. The two metal atoms of the dimer might be bridged by bromine atoms or by the heterocyclic ligand, so the possible structures of this complex are as follows:

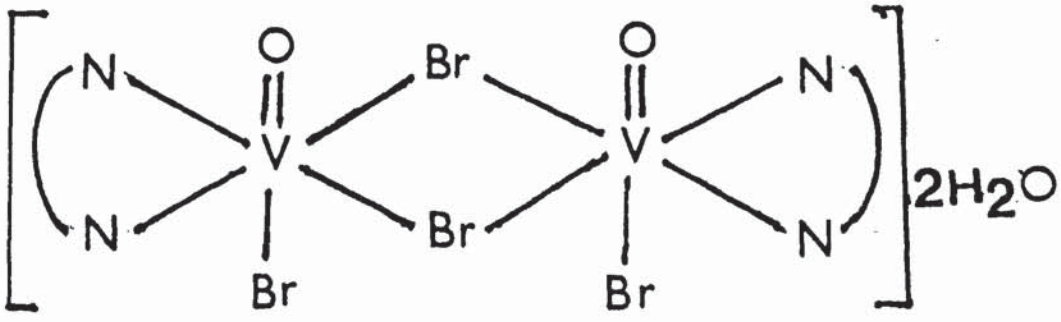

OR:

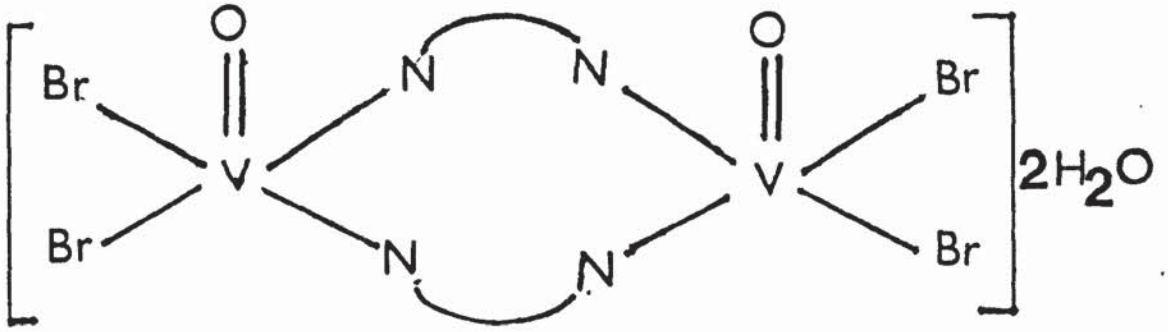

3.3.4 The Dipyam Complex with $VOSO_4$

An analysis of the infra-red spectrum of this complex gave much information about its structural features. The ν_1 and ν_2 of the sulphate ion appears at 970 cm^{-1}, and 450 cm^{-1} respectively, ν_3 splits into three bands (1010 s cm^{-1}, 1145 s cm^{-1} and 1230 cm^{-1}) while ν_4 splits into 650 and 660 cm^{-1}. These results suggest that the symmetry of SO_4^{2-} ion is lowered and probably reduced to C_{2v} (50) i.e., the sulphate might be coordinated to the metal ion as a bidentate ligand.

The complex appeared after ½ hr reflux of the starting materials in DMF, the precipitate analysed as $VOSO_4$ (dipyam).H_2O.DMF. The coordination of DMF to the metal is usually revealed by the shift of ν(CO), but the complexity of the infra-red spectra of the complex in that region (1640-1650 cm^{-1}), makes this assignment unreliable. The considerable differences between this

complex and other complexes in the ν_{m-x}, ν_{m-n} (300 - 400 cm^{-1}) and ν(>NH) (3000 - 3300 cm^{-1}) regions of the spectrum give reasonable evidence for the co-ordination of DMF (Figure 3.3).

The effective magnetic moment of the complex (1.81 B.M.) which is near to that of the free-ion value (1.73 B.M.), is an indication of a monomeric structure. The low conductivity of the complex indicates that the complex is non-electrolyte.

From the above remarks it is possible to propose the following structural formula for this complex:

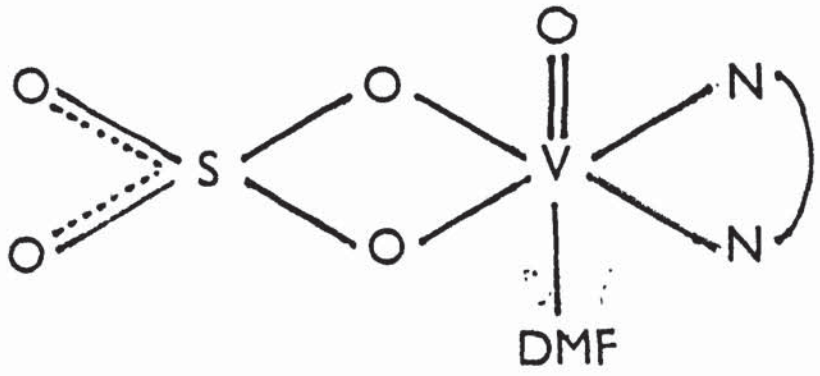

3.3.5 The Tripyam Complex of $VOCl_2$

The tabulated analytical data and physical measurements of the complex were analysed in the same way applied for the previous complexes. This study yields the

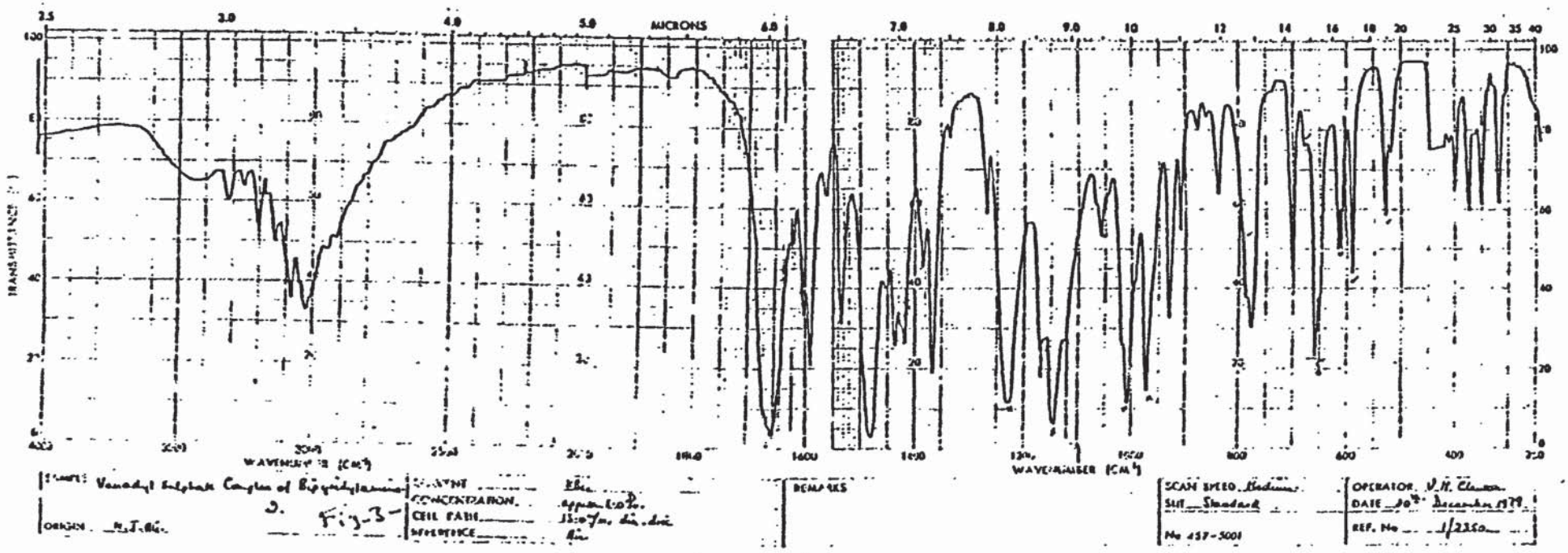

Figure 3.3 I.R. Spectrum of $VOSO_4(dipyam).H_2O.DMF$

following information:

(i) The complex is a non-electrolyte (Fig 3.2)

(ii) The complex is monomeric (μ_{eff} = 1.80 B.M.)

(iii) The complex has ν_{V-Cl} at 355 cm^{-1}

(iv) Tripyam functions as a bidentate (Pg 48)

Accordingly the following structure can be proposed for this complex:

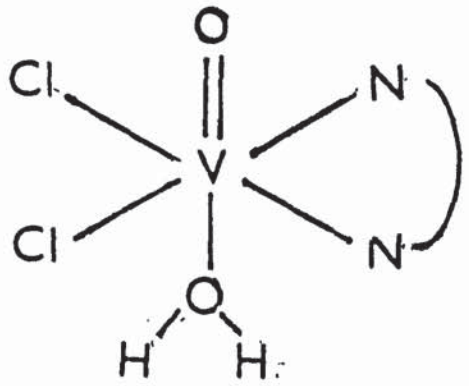

3.3.6 Visible Spectra of the Complexes

Generally the visible spectra of the vanadyl complexes show three low intensity d-d or ligand field absorption bands. These bands commonly fall in the following regions[11]:

Band I	falls	11 - 16 kK
Band II	falls	14.5- 19 kK
Band III	falls	20 - 30 kK

Band III, usually at higher energy, is often obscured by an intense charge-transfer band.

The semi-empirical molecular orbital approach of Ballhausen and Gray[51] for the hydrated vanadyl ion produces an energy level scheme which gives good agreement with the optical spectral data, Figure 3.4.

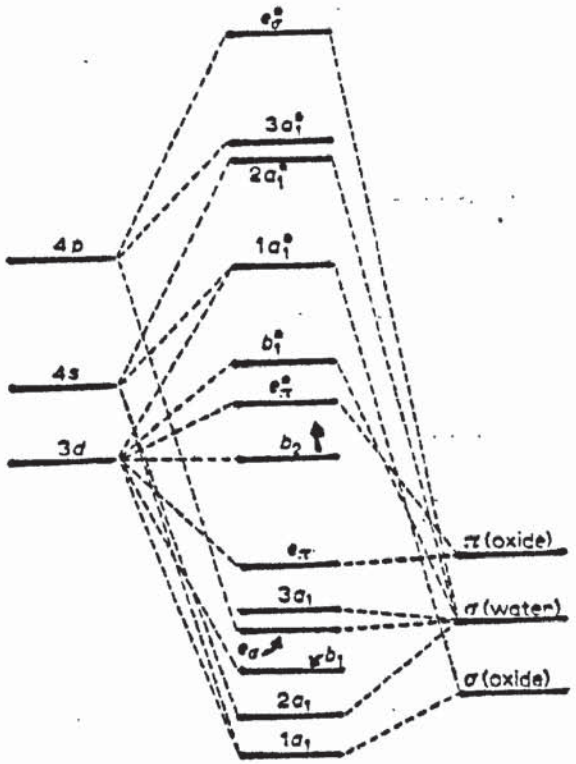

Figure 3.4 Energy level diagram for $VO(H_2O)_5^{2+}$

From the energy-level scheme, the $d_{x^2-y^2}$ level is considered a σ-antibonding orbital interacting with the in-plane ligands, the d_{z^2} level is considered to be σ-antibonding with the axial oxygen atom, the d_{xz}, d_{yz} level is considered to be π-antibonding with the

axial oxygen atom, and finally the d_{xy} orbital is non-bonding or π-antibonding with the in-plane ligands.

The solution and Nujol mull spectra of the dipyam and tripyam complexes of vanadyl ion have been assigned and listed in Table 3.4.

Band II is interpreted as $^2B_2 \rightarrow {}^2B_1$ transition which gives a direct estimate of the value of 10 Dq, and this is because its position should be dependent on the σ-donor strength of the in-plane ligands as well as on the π-donor strength of the same ligands. If the latter quantity does not vary to a large extent, then band II should be directly related to the in-plane ligand field strength. Using the values given in Table 3.4, the order of ligand strength of the two ligands is that dipyam > tripyam, which is in accord with the previous order derived from infra-red study (Pg 51).

The spectral data for the nujol mull of the dipyam and tripyam complexes spread on filter paper (Table 3.4) reveals a definite splitting of band I into three or four bands (Figure 3.5). This splitting is similar to that reported for the low-temperature ($77^{\circ}K$) spectra of some vanadyl complexes studied in the references[52,53,54]. The assignment of these split bands have been a subject of contradiction, some researchers believed that it is

Table 3.4 Visible Spectral Data of the Complexes in kK

	DMSO Solution Spectra			Nujol Mull Spread on Filter Paper		
	Band I $^2B_2 \rightarrow {}^2E$	Band II $^2B_2 \rightarrow {}^2B_1$	Band III $^2B_2 \rightarrow {}^2A$	Band I	Band II	Band III
$VOCl_2(dipyam)_2.H_2O$	11.97	15.015	22.2	12.22 12.43 12.65 12.85	15.15	21.73 25.64
$VOCl_2(dipyam)_2.4H_2O$	12.04	15.15	25.00		15.15	20.83 26.31
$VOSO_4(dipyam).H_2O.DMF$	12.15	15.503	26.66	12.04 12.34 12.65	17.24	23.52 25.00
$VOBr_2(dipyam).H_2O$	11.76	15.037	23.52	12.45 12.57 12.82	15.037	25.00 27.02
$VOCl_2(tripam).H_2O$	12.5	14.814	26.66	12.19 12.34 12.57 12.82	14.705	25.00 26.66

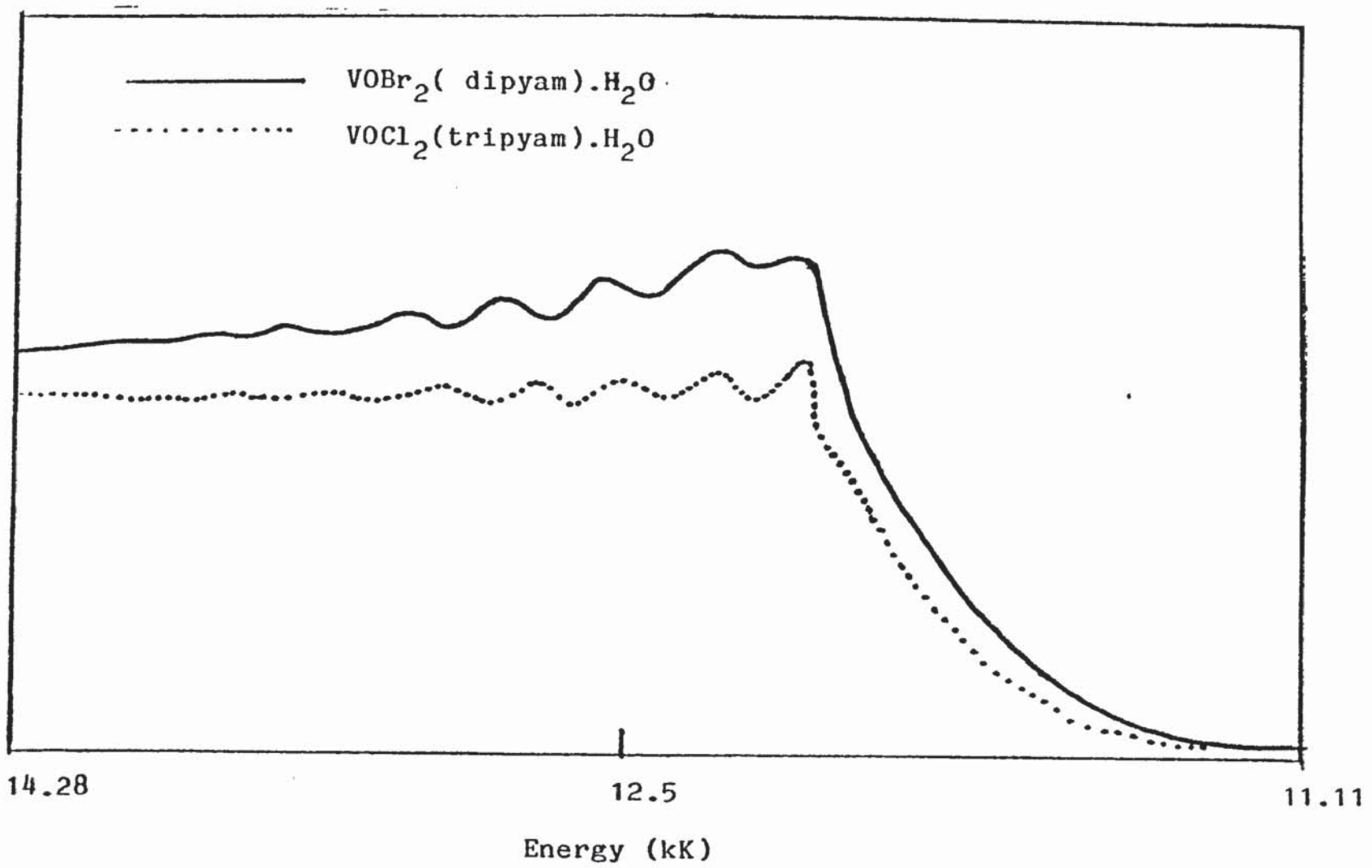

Figure 3.5 Visible spectra of vanadyl ion complexes with dipyam and tripyam

due to the vibrational transition[53,54], while others[52] assigned it as electronic transition. The latter idea (Ortolano, Selbin and McGlynn) put all d-d transition below 20,000 cm^{-1} and the first three excited levels (counting 2 for e^*_π and 1 for b^*_1) very close together i.e. clustered, and only slightly removed from the next level, thus they believed that the transitions are in the following order:

$b_2 \longrightarrow e^*_\pi$)		
) $\sim$ 13000 cm^{-1}	d-d-	
$b_2 \longrightarrow b^*_1$)		
	transition	
$b_2 \longrightarrow Ia^*_1$	$\sim$ 17000 cm^{-1}	
$e^b_\pi \longrightarrow b_2$	$\sim$ 25000 cm^{-1}	charge transfer

The number of components and their small separation of the splitting in band I in the spectra of the dipyam complexes of $VOCl_2$,(the first two complexes in Table 3.4), cannot rule out the vibrational origin of these splittings, but it is probable that two of them might have electronic origin. Accordingly the first three bands might belong to d-d transition and the fourth one due to the first charge transfer and in the following order:

From	12.22 - 12.85 kK	xy → xz
Table 3.4	15.15 kK	xy → $x^2 - y^2$
	20.83 - 21.73 kK	xy → z^2
	25.64 - 26.31 kK	first charge transfer

With respect to the spectra of the other three complexes in Table 3.4, in which the third band and the first charge transfer band appear close to each other at high energy, it is difficult to apply the above assignment because in order to use the above procedure, we have to accept a rather large splitting of the e_{π}^{*} level which is very improbable, especially for such low symmetry complexes.

It is seen from a comparison of the position of band I in the spectra of $VO(H_2O)_5^{2+}$(13.00kK), with its position in the spectra of dipyam and tripyam complexes that the tetragonal component to the ligand field is less in the latter complexes than in $VO(H_2O)_5^{2+}$ ion. The infra-red spectra are consistent with this result,for ν(V=O), for the dipyam and tripyam complexes (900-940 cm^{-1}) is lower than that found for $VOSO_4.5H_2O$ (1035 cm^{-1}) and it is the V=O bond which is primarily responsible for the tetragonal component to the ligand field. The spectral data in Table 3.4 show differences between the solution spectra and the Nujol mull spectra of the complexes. This is probably because DMSO is almost the only solvent for these complexes, and it might displace one of the ligands in the monomeric complexes or break the bridges in the dimeric complexes and consequently change the spectra.

3.3.7 E.S.R. Spectra of the Complexes

Usually the E.S.R. solution spectra of oxovanadium IV complexes consist of eight lines, similar to those obtained for the dipyam and tripyam complexes (Fig 3.6). But in the frozen solid state the axial d^1 case shows two types of resonance component; one due to the parallel feature and the other set due to the perpendicular feature. The parameters of those isotropic and anisotropic spectra are related by the following equations;

$$A_o = \tfrac{1}{3}(A_{11} + 2A_1) \qquad (1)$$

$$g_o = \tfrac{1}{3}(g_{11} + 2g_1) \qquad (2)$$

where g_o is the average g-factor and

A_o is the average hyperfine splitting

g_1 and g_{11} are related to the optical spectral data by the relations;

$$g_{11} = 2.0023 \left\{ 1 - \frac{(\epsilon_\pi^*)^2 \xi}{\Delta E_1 (^2B_2 \rightarrow {}^2E)} \right\} \qquad (3)$$

$$g_1 = 2.0023 \left\{ 1 - \frac{4(\beta_1^*)^2 \xi}{\Delta E_2 (^2B_2 \rightarrow {}^2B_1)} \right\} \qquad (4)$$

where ξ is the spin-orbit coupling constant for VO^{2+}, ϵ^* and β_1^* are the molecular-orbital bonding coef-

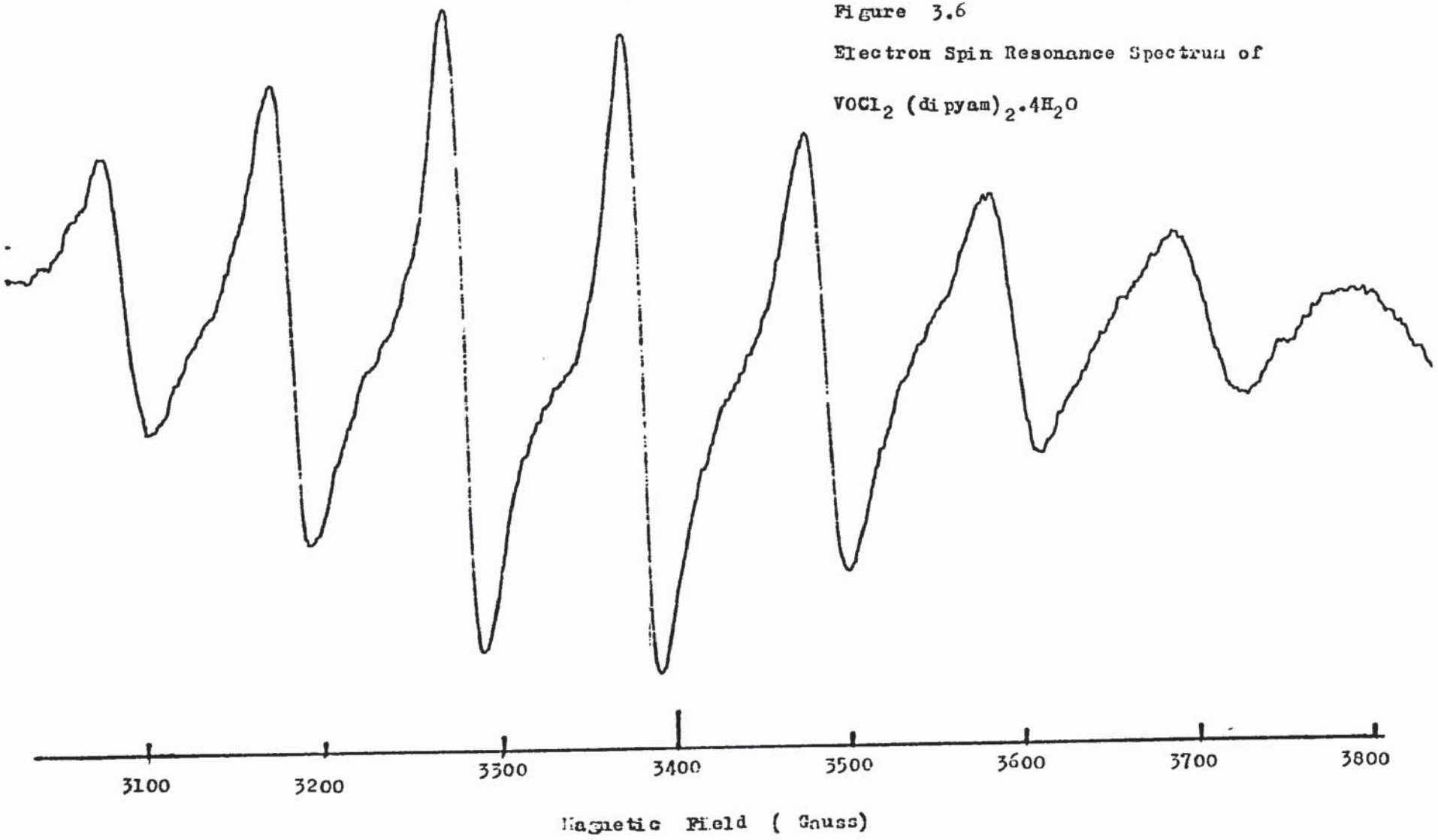

Figure 3.6

Electron Spin Resonance Spectrum of

$VOCl_2$ (dipyam)$_2$.$4H_2O$

ficients[55], ΔE_1, ΔE_2 the energies (cm^{-1}) of the first and second d-d-transition within the VO^{2+} ion, according to the Ballhausen and Gray[51] energy scheme.

Equations (3) and (4) were used to calculate $g_\perp$ and g_{11} for the dipyam. and tripyam. complexes by using the optical spectral data (Table 3.4). The values used for ξ, ϵ_π^* and β^*_1 were the same values used by Wuthrich[56] to find the g_{11} and $g_\perp$ for dipyridyl complexes;

$\xi = 170\ cm^{-1}$, $\epsilon_\pi^* = 0.78$ and $\beta^*_1 = 0.87$

The average g_o-values were found by using equation (2). The calculated g_o were compared with the experimental values in the following table;

Complexes	Experimental g_o-values	Calculated g_o-values
$VOCl_2(dipyam)_2.H_2O$	1.980	1.950
$VOCl_2(dipyam)_2.4H_2O$	1.971	1.951
$VOSO_4(dipyam)DMF.H_2O$	1.964	1.952
$VOBr_2(dipyam).H_2O$	1.977	1.951
$VOCl_2(tripyam).H_2O$	1.966	1.950

From the above comparison, it is clear that there is no agreement between the experimental and calculated values. Values for g_o were also calculated by using

several values for ξ, e.g., 135, 150, 160 cm^{-1}, but still there is no reasonable agreement.

The experimental values for g_1 and g_{11} for the complex $VOCl_2(dipyam)_2.4H_2O$ (Table 3.3),which were obtained from its solid state E.S.R. spectra, in addition to its visible spectral data obtained in solid state, were used to calculate ϵ_π^* and β^*_1 (Equations (3) and (4)) putting ξ = 135 cm^{-1}. The results are:

ϵ_π^* = 1.666

β^*_1 = 0.415

The g_o values for the other four complexes were calculated again from equations (3), (4) and (2) by using the above new values of ϵ_π^* and β^*_1 and regarding ξ = 135 cm^{-1} in addition to their optical spectral data (Table 3.4). The results are as follows:

Complexes	Experimental g_o-values	Calculated g_o-values
$VOCl_2(dipyam)_2.H_2O$	1.980	1.973
$VOSO_4(dipyam)DMF.H_2O$	1.964	1.974
$VOBr_2(dipyam).H_2O$	1.977	1.973
$VOCl_2(tripyam).H_2O$	1.966	1.974

The reason for the less than perfect agreement between some calculated and experimental g_o-values for dipyam and tripyam complexes of vanadyl ion might be due to the low symmetry of the complexes, as seen in the latter comparison, the agreement is more reasonable for the complexes with higher symmetry. On the other hand the results of the above comparison also offer support for the work of Selbin[37] in which he concluded that the comparison between E.S.R. measured g_o-values and optical spectral calculated g_o-values does not constitute unequivocal support for the Ballhausen-Gray band assignments, as some workers believed[56,57].

From the combination of equation (2) with equation (4) it is clear that the g_o is proportional to ΔE_2, i.e., the ligands with the highest ligand field strength give the highest g_o-value. Since g_o for dipyam complexes is 1.977-1.980, while that of the tripyam complex is 1.966, the ligand order should be; dipyam > tripyam.

CHAPTER FOUR

CHEMISTRY OF NICKEL GLAZES

4.1 Introduction

Nickel-silicate glazes, with their extensive use in the production of crystalline glazes, are an interesting decoration form for art pottery; the delightful range of colours obtained with Nickel glazes can be very beautiful. The nickel crystalline glazes are used commercially for the rutile glazes used in the wall tile trade[15].

The factors affecting the colour production by nickel oxide in ceramic glazes have been reviewed by Kerstan[58]. He obtained a good criterion for the effect of alkaline earth oxides in nickel glazes, as glass network modifying oxides, in the Dietzel Field (see Pg 13) strength of cation which decreases from 0.59 - 0.24 in the order, Zn, Mg, Ca, Ba and in so doing progressively loosens the glassy structure and changes the colour from blue (NiO_4; covalent bonding) to green-yellow, red (MO_6, ionic bonding) end of the spectrum. These changes from red to blue or green, blue to gray, blue to light green and red to light blue are the result of replacing BaO by ZnO, ZnO by MgO, CaO by MgO and BaO by MgO respectively. All glazes low in SiO_2 and Al_2O_3 are red, increasing the SiO_2 content changes the colour from purple to dark brown[58].

Most of the information regarding the correlation of the absorption spectra of Ni^{2+} in ceramic glazes was obtained from the studies on the characterisation of visible spectra of Ni^{2+} in glasses. The spectral identification of Ni^{2+} in glasses differs from that of Ni^{2+} in its compounds and complexes, since the latter can be achieved by either assignment by analogy to a similar compound or the similarity of an experimental spectrum to that of a compound of known structure. The former cannot be studied by these methods. The spectral data for glasses must be self-sufficient because they can be compared only with those of substances which differ chemically. The location of the absorption assignment for Ni^{2+} coloured glasses is in general uncertain. It is agreed, however, that only high-spin Ni^{2+} need be considered[59].

Zsigmondy[60] and Fedotiev and Lebedeve[61] observed the colours of Ni^{2+}-glasses which contained, respectively, alkalis and alkaline earths, Weyl and Thuemen[62] studied colour changes with variation of glass composition. Weyl[63] concluded, by analogy to solutions of Ni^{2+} salts, that an equilibrium is established between 4- and 6-coordination which depends on glass composition, thermal history and Ni^{2+} concentration, whereas Moore and Winkelmann[64] suggested a third species which would occupy a position between two O^{-} ions.

Ligand field theory has been applied to the absorption of transition metals in glasses. Generally it is a useful tool for identifying the valency state of the transition metal, the ligand field symmetry and hence the coordination to the surrounding ligands and finally the particular electronic transitions responsible for the spectral absorption.

The assignment of the coordination and the identification of the particular electronic transitions was largely completed in the first analyses of glass spectra using ligand field theory[59,65-69]. The following data, Table 4.1, show the band positions and linear absorption coefficients of Ni^{2+} in soda-lime-silica glass[66]:

Table 4.1

Coordination	Position kK	Absorption Coefficient	Electronic Transition
Octahedral	22.22	14.8	$^3A_{2g} \rightarrow {}^3T_{1g}(P)$
	10.75	2.8	$^3A_{2g} \rightarrow {}^3T_{1g}(F)$
	5.55	2.0	$^3A_{2g} \rightarrow {}^3T_{2g}$
Tetrahedral	17.85	5.0	$^3T_1\ (F) \rightarrow {}^3T_1\ (P)$
	15.87	5.0	$^3T_1\ (F) \rightarrow {}^3T_2\ (F)$
	8.33	2.5	$^3T_1\ (F) \rightarrow {}^3A_2\ (F)$

Bamford[66] concluded, by using LFT, that in sodium silicate and borate glasses, both tetrahedral and octahedral Ni^{2+} ions are present. Kumour[68] assigned essentially the same bands in two borate glasses, and Bate[67] suggested that coordination changes from predominantly octahedral to predominantly tetrahedral in borate glasses as the alkali content increases.

Gitter and Vogel[70,71] used the ligand field theory to interpret the properties of the Ni^{2+} ion in coloured glazes. They deduced that the absorption spectra of Ni^{2+} depends on the basic glass temperature and its basicity, and they found that the Ni^{2+} ion was present in octahedral and tetrahedral coordination but dodecahedral oxygen coordination with Ni^{2+} cannot be excluded. They noticed that the oxygen coordination of Ni^{2+} changes, depending on the glass composition and transformation temperature of the glazes, from octahedral to tetrahedral.

The object of the work in this chapter is to use the visible absorption spectral data in conjunction with XRD and magnetic measurement to determine the chemical changes affecting the Ni^{2+} cation environment in ceramic glazes in order to reproduce ceramic glaze finishes under more scientifically controlled conditions.

4.2 Results and Discussion

4.2.1 X-Ray Analysis of the Nickel Glazes

X-ray diffraction analyses were performed for the starting materials, and compared with the diffraction data reported in the diffraction files. In Table 4.2 the diffraction pattern of potash feldspar was in agreement with 19-932 diffraction card, which corresponded to the microcline type of potassium aluminium silicate ($KAlSi_3O_8$). The pattern of quartz in Table 4.3 was compatible with the 5-490 diffraction card which reveals the α-quartz type in the sample. Comparison of the diffraction data obtained for whiting with that in the 24-27 diffraction card (Table 4.4) shows that it consists of only one crystallographic form (calcite), while the analysis of china clay shows that it consists of two types of kaolinite, one corresponding to the 14-164a diffraction card (i.e., $Al_2(OH)_4Si_2O_5$) and the other to 12-447 diffraction card (Table 4.5).

The Ni^{2+} glaze recipes in Table 4.6 were prepared and fired to various temperatures, slowly cooled, followed by crushing to a finely divided powder. The X-ray data of these recipes are tabulated in Table 4.7.

Table 4.2 Comparison of Potash Feldspar Sample with Powder Diffraction Data Card 19-932

K Feldspar		Card 19-932		K. Feldspar		Card 19-932	
dÅ	Intensity*	dÅ	Intensity	dÅ	Intensity	dÅ	Intensity
4.21	13	4.22	45	2.61	5	2.60	6
3.97	7	3.96	8	2.55	6	2.55	6
3.82	10	3.80	20	2.51	5	2.50	6
3.75	12	3.74	14	2.42	5	2.42	2
3.65	10	3.63	6	2.32	4	2.32	4
3.46	16	3.48	16	2.27	3	2.27	<2
3.33	23	3.33	14	2.15	12	2.16	30
3.28	15	3.29	50	1.97	5	1.97	2
3.23	100	3.24	100	1.92	4	1.92	2
3.18	70			1.81	4	1.81	2
3.02	9	3.01	10	1.80	10	1.80	25
2.94	10	2.94	<2	1.57	<3	1.57	<2
2.92	8	2.91	<2				
2.89	10	2.89	8				
2.74	4	2.76	8				

*Intensity = I/I_1

Table 4.3 Comparison of Quartz Sample with Powder Diffraction Data Card 5-490

Quartz		Card 5-490	
dÅ	Intensity I/I_i	dÅ	Intensity I/I_i
4.27	23	4.26	35
3.35	100	3.34	100
2.46	9	2.45	12
2.28	7	2.28	12
2.24	5	2.23	6
2.14	6	2.13	9
1.98	5	1.98	6
1.80	17	1.81	17
1.65	5	1.65	3
1.52	10	1.54	15

Table 4.4 Comparison of Whiting Sample with Powder Diffraction Data Card 24-27

Whiting		Card 24-27	
dÅ	Intensity I/I_i	dÅ	Intensity I/I_i
3.83	8	3.85	29
3.02	100	3.02	100
2.83	4	2.83	2
2.48	10	2.49	7
2.28	15	2.28	18
2.09	12	2.09	27
1.90	15	1.90	17
1.87	15	1.87	34
1.62	3	1.62	2
1.60	6	1.60	15
1.58	2	1.58	2
1.52	3	1.52	3
1.50	3	1.50	2
1.44	4	1.44	5
1.42	3	1.41	3
1.33	2	1.33	3
1.30	2		

Table 4.5 *Comparison of China Clay Sample with Diffraction Data Cards 12-447 ,14-164*[a]

China Clay		Card 12-447 ,14-164[a]		China Clay		Card 12-447 ,14-164[a]	
dÅ	Intensity I/I_i	dÅ	Intensity I/I_i	dÅ	Intensity I/I_i	dÅ	Intensity I/I_i
16.09	25			2.39	10	2.38	25
7.18	100	7.17	100	2.34	18	2.33	15
4.99	10			2.30	11	2.28	6
4.48	16	4.46	75	2.13	5	2.11	6
4.37	16	4.34	85	1.99	13	1.98	12
4.24	15			1.79	6	1.78	4
4.20	16	4.16	65	1.66	10	1.66	25
3.86	11	3.83	50	1.62	6	1.61	16
3.57	67	3.58 3.56	80 50	1.58	4	1.58	4
3.34	22	3.37	12	1.48	10	1.48	90-100
3.19	7	3.15	4				
2.87	6						
2.56	15	2.55	85				
2.49	15	2.48	85				

Table 4.6 Composition of Nickel Containing Glazes

Ingredients	Per cent by weight of the ingredients						
	Recipe I	Recipe II	Recipe III	Recipe IV	Recipe V	Recipe VI	Recipe VII
Potassium Feldspar	52	35	55	52	52	35	52
Whiting	5		10	5	5		5
Barium Carbonate	15	46	20	15	15	40	15
Zinc Oxide	12	15	10	12			
China Clay	6	5	5	6	6	5	6
Quartz	10	5		10	10	5	10
Nickel Oxide	2	2	2	5	2	2	2
Titanium Oxide					12	15	
Tin Oxide							12
Colour of Glaze	Grey	Videt	lt violet	Grey	Greenish-yellow	Yellowish-green	lt violet

Table 4.7 X-Ray Diffraction Results of the Nickel Containing Glaze Recipes

Temperature ^{o}C	Potassium Feldspar	Quartz	Calcite	Aragonite	Others
500	Appears in all recipes	Appears in all recipes	Appears in all recipes but II & VI	Absent in all recipes	In recipes I & II presence of $BaCO_3$, ZnO, NiO noticed
600	"	"	"	"	" "
700	"	"	"	"	" "
800	"	"	"	"	In recipes I & II presence of ZnO & NiO noticed but no $BaCO_3$
900	"	"	absent in all recipes	"	In recipes I & II presence of ZnO noticed but no $BaCO_3$ or NiO
1000	"	"	"	"	No ZnO, $BaCO_3$ or NiO in recipes I & II
1100	"	"	"	"	" "
1265	"	"	"	"	No ZnO, $BaCO_3$ or NiO in recipes I & II In recipes V & VI $CaTiO_3$ and $BaTiO_3$ species present

All X-ray diffraction patterns for these recipes show the presence of potash feldspar and quartz at all stages of firing, which indicates that some of these two components had retained their crystallographic form during firing. We could not recognise the aragonite to calcite phase transformation which might occur around 400-500°C as previously mentioned[72], and this is because of the fast rise of furnace temperature to 500°C i.e., it was difficult to keep it at 400°C.

In all the samples the calcite decomposition was shown to occur at 800-900°C. The X-ray diffraction patterns for all samples at various temperatures indicate the absence of CaO. Gillespie[26] proved that the absence of a CaO peak in X-ray diffraction is due to its interaction with other species in the glaze system.

The comparison of the diffractogram traces of recipes I and II fired to 1200°C with the powder diffraction card 19-90 leads to the recognition of the presence of barium aluminium silicate ($BaAl_2Si_2O_8$) in the celsian form, Table 4.8. Nickel glaze recipes I, II, III and IV, which contained ZnO when heated to about 1200°C gave a diffractogram trace which indicated the probable presence of barium compounds of zinc silicate oxide, like $Ba_2ZnSi_3O_8$ as compared with the powdered diffraction card 23-841, Table 4.9.

Table 4.8 Comparison of XRD Pattern of Nickel Glazes Recipes I and II with Powder Diffraction File 19-90 ($BaAl_2Si_2O_8$)

Nickel glaze system		Powder diffraction card	
dÅ	Intensity I/I_i	dÅ	Intensity I/I_i
6.53	22	6.51	60
4.64	33	4.60	25
3.80	34	3.79	35
3.62	30	3.62	25
3.55	33	3.55	40
3.47	43	3.46	65
3.35	50	3.35	100
3.24	90	3.27	40
3.02	95	3.02	50
2.91	34	2.91	30
2.77	31	2.77	35
2.58	35	2.58	75
2.32	25	2.32	10
2.27	40	2.27	16
2.16	24	2.15	10
2.14	25		
2.10	25	2.10	20
2.01	26	2.01	16
1.96	34	1.95	16
1.93	30	1.93	8
1.74	27	1.73	6
1.70	26	1.70	6
1.65	23	1.65	16

Table 4.9 Comparison of XRD Data of Nickel Glaze Recipes I and II with Powder Diffraction Card (PDC) 23-841 ($BaZnSi_3O_8$)

Nickel Glaze System		Powder diffraction card	
dÅ	Intensity I/I_i	dÅ	Intensity I/I_i
6.55	33	6.59	20
5.90	20	5.96	16
4.63	42	4.66	20
4.03	43	4.01	8
3.81	82	3.82	35
3.64	30	3.65	16
3.56	53	3.53	50
3.60	96	3.59	25
3.28	76	3.29	35
3.02	76	3.03	40
2.92	66	2.93	25
2.84	53	2.80	35
2.64	62	2.64	25
2.59	60	2.60	40
2.53	40	2.56	10
2.42	30	2.43	12
2.39	38	2.35	6
2.32	33	2.29	6
2.18	40	2.18	8
2.01	30	2.00	8
1.86	40	1.87	12
1.80	30	1.82	25

Gha and Kolar[73] investigated the system $BaO-TiO_2-Al_2O_3$, and they identified by X-ray analysis the species $BaTi_4Al_2O_{12}$ as one component of the system, the data of Gha and Kolar and the data of the mineral glaze containing TiO_2 rather than ZnO i.e., recipes V and VI, indicate the presence of the above compounds in the glaze system, Table 4.10.

The replacement of zinc oxide with TiO_2 in the nickel containing glaze, recipes V and VI, changed the colour of the glaze from grey to yellowish-green or greenish-yellow. X-ray powder diffractogram traces of recipes V and VI were analysed and compared with the similar related compounds reported in the powder diffraction file. The first compound we looked for in the diffractogram of these two recipes is $NiTiO_3$ because the X-ray study of the quasibinary $NiO-TiO_2$ phase diagram[74] shows that the only ternary phase which is stable in the range of temperature 1300-1600°C is the ilumenite type compound $NiTiO_3$. But the powder X-ray diffractograms of recipes V and VI give no indication of the presence of $NiTiO_3$ compound, as compared with powder diffraction card of $NiTiO_3$.

The comparison of the diffractogram results for recipe VI with the data reported in the diffraction file card, 5-626, Table 4.11, indicates that $BaTiO_3$ in the Perovskite

Table 4.10 Comparison of Gha and Kolar XRD Data with Our Observed X-Ray of Nickel Glaze

XRD of Nickel Glaze		Gha and Kolar	
dÅ	Intensity I/I_i	dÅ	Intensity I/I_i
3.55	54	3.54	18
3.18	94	3.19	100
2.84	33	2.83	12
2.47	55	2.46	30
2.25	35	2.23	15
2.19	46	2.19	30
2.00	15	2.01	10
1.96	15	1.96	6
1.86	26	1.86	18
1.79	12	1.77	5

Table 4.11 Comparison of XRD of Recipe VI with XRD Card 5-626 ($BaTiO_3$)

Recipe VI				XRD Card 5-626			
dÅ	Intensity	dÅ	Intensity	dÅ	Intensity	dÅ	Intensity
5.29	16	2.09	22				
4.80	13	2.06	32				
4.59	12	2.04	31			2.02	12
4.45	28	1.98	27	4.03	12	1.99	37
4.10	12	1.94	19	3.99	25		
3.96	22	1.89	13				
3.67	14	1.84	19			1.80	6
3.60	24	1.78	19			1.79	8
3.08	51	1.62	12			1.64	15
3.04	34	1.62	31			1.63	35
2.99	22	1.55	16				
2.96	31	1.53	18				
2.92	33	1.41	28			1.41	12
2.80	100			2.82	100		
2.72	13						
2.66	20						
2.63	22						
2.54	10						

form is one of the predominant species in this glaze composition.

Table 4.12 shows that $CaTiO_3$ in the Perovskite form is the most probable species in recipe V, and this was confirmed by the similarity of the X-ray powder diffraction data of glaze recipe V with that reported in the diffraction file card 22-153.

The structure of Perovskite is cubic[75], the lattice consists of cubic close packed layer of composition AO_3 with the B cation occupying the octahedral interstices. Figure 4.1 shows one complete octahedron, which illustrates clearly the octahedral coordination of the B cations and the 12-fold coordination of the large A cation.

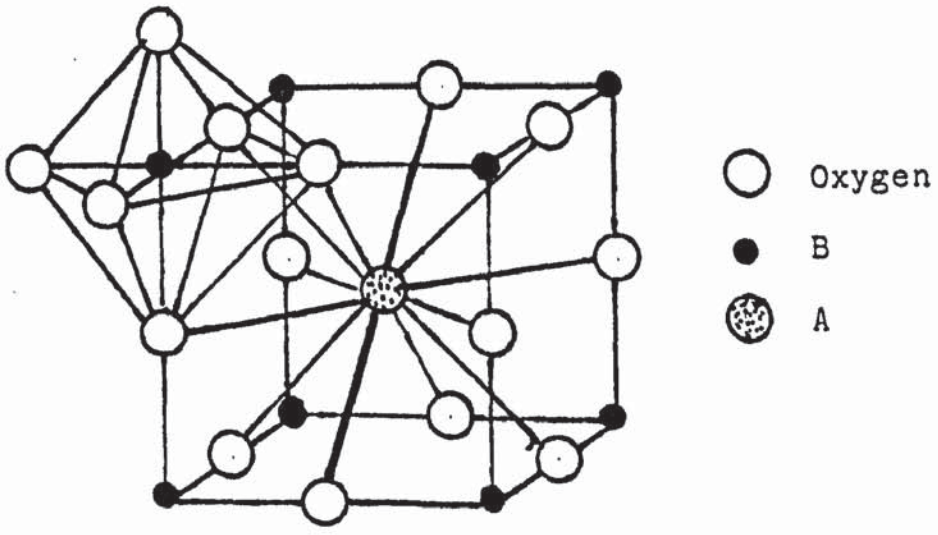

Figure 4.1 The Perovskite Structure.

Table 4.12 Comparison of XRD of Recipe V with XRD Card 22-153 ($CaTiO_3$)

Recipe V				XRD Card 22-153			
dÅ	Intensity	dÅ	Intensity	dÅ	Intensity	dÅ	Intensity
5.34	14	1.57	19			1.57	14
3.88	16	1.56	27	3.82	14	1.55	25
3.72	20	1.49	19			1.49	<1
3.44	11	1.48	18	3.42	3	1.47	<1
3.33	38	1.46	19			1.46	<1
2.69	100	1.39	9	2.70	100	1.36	3
2.53	29			2.56	1		
2.50	26	1.36	18	2.31	4	1.35	11
2.32	13	1.34	21	2.30	7	1.34	5
2.30	16	1.31	12			1.31	<1
2.22	21						
2.20	24	1.29	8	2.21	6	1.29	1
2.06	11	1.26	13	2.05	2	1.27	1
1.92	42	1.23	11	1.91	50	1.23	<1
1.85	17	1.21	14	1.85	3	1.21	2
1.70	28	1.19	13	1.71	3	1.19	1
1.69	29	1.16	12	1.77	2	1.16	4
1.63	15			1.67	3		
1.61	10			1.63	1		

The incorporation of a chromophore into the lattice of a compound or solid solution will develop a colour in the structure. The formation of such a system depends on whether the introduced chromophore fulfills the following structural parameters[75]:

1) The material must conform to correct proportions of ions on the various distinguishable lattice sites.

2) The material must conform to the fundamental principle of overall electroneutrality.

3) The ions on the various lattice sites must conform to the size relationships imposed by the geometry of the structure.

From the preceding brief discussion of the Perovskite structure, it is apparent that Ni^{2+} conforms to the basic criteria of stoichiometry, electroneutrality and ionic size (ionic radius of Ni^{2+} 0.61 Å), for the Perovskite structure.

4.2.2 The Absorption Spectra of Ni^{2+} in the Ceramic Glaze

Elucidation of the optical and magnetic properties of Ni^{2+} ion in glazes can provide information about the electronic states and the site symmetry of the metal ion in

the host glaze. To make sure that Ni^{2+} ion is the only absorbing species, spectra for all fired recipes without nickel were recorded and showed no bands in the visible region. This latter result was supplemented by the magnetic moment measurements done for the glaze recipes, Table 4.13. These results indicate that the magnetic behaviour observed for the various recipes is that which is expected for magnetically dilute paramagnetic species and that the nickel ion has the normal low oxidation state of two i.e., Ni(II).

Turner and Turner[59] deduced that the optical absorption of Ni^{2+} in the alkali tetrasilicate glasses consists of two types of spectra. Type (I) spectra may be recognised by a single strong band near 22.00 kK and a weaker band near 11.00 kK, whereas type (II) spectra show a strong multiple-peaked absorption near 20.00 kK and a weak but well resolved peak near 13.00 kK. They assigned the type (II) spectra to a tetrahedral species and the type (I) spectra to octahedral Ni^{2+}. The absorption spectra of Ni^{2+} in sodium-silicate glasses were assigned by Bamford[66] to consist of six bands 22.22 kK, 10.75 kK, 5.55 kK, 17.85 kK, 15.87 kK and 8.33 kK. The first three bands were associated with octahedral coordination and the second three bands with tetrahedral coordination. Low[76] proposed that the three bands 8.62 kK, 14.7-13.69 kK and 24.39 kK appeared in the absorption spectra

Table 4.13 Magnetic and Visible Spectral Data of Nickel in the Glaze Recipes

Recipe	Ni(%)	X_m^*(298K) x 10^{-6}	μ_{eff}(BM) Found	μ_{eff}(BM) Expected	Visible Spectral Data (kK)
I	1.450	6304.23	3.89	1.7 - 2.5 (Ni^{3+}) 2.80 - 4.0 (Ni^{2+})	22.98,17.39,18.86,15.62,12.50
II	1.58	5726.08	3.70		21.459,18.11,15.625,13.47
III	1.48	5388.73	3.59		21.64,18.181,15.57,13.69
IV	3.64	6089.17	3.82		23.64,18.181,15.479,13.88
V	1.62	5258.53	3.55		25.00,15.24
VI	3.569	5574.9	3.66		25.00,15.38,13.927
VII	1.487	6325.045	3.89		23.25,18.18,15.38

* Diamagnetic corrections of the atoms other than Ni in the recipe were made by directly measuring the diamagnetic susceptibility of the fired recipe which contained no nickel ion.

of Ni^{2+} in magnesium oxide arising from the following transitions respectively;

$$^3A_{2g} \longrightarrow {}^3T_{2g}, \quad {}^3A_{2g} \longrightarrow {}^3T_{1g}(F) \text{ and } {}^3A_{2g} \longrightarrow {}^3T_{1g}(P)$$

Thus the visible spectral data for the glaze recipes I-IV and VII (Table 4.13, Figures 4.2 and 4.3) indicate that Ni^{2+} appears to be present in both octahedral and tetrahedral coordination. The band in the region 21.459-25.00 kK for all the recipes (Table 4.13) can certainly be assigned to the $^3A_{2g} \longrightarrow {}^3T_{1g}(P)$ transition arising in an octahedral ligand field.

Recipes V and VI, in which the zinc oxide was replaced by titanium dioxide, shows an absorption spectrum which indicates that the octahedral coordination is the most predominant. This high probability is due to the disappearance of the band around 18.181 k.K which can be assigned to the $^3T_1(F) \longrightarrow {}^3T_1(P)$ transition arising in tetrahedral ligand field. The disappearance of the band around 18.181 kK was accompanied by the persistence of the band in the region of 15.50 kK. This latter result is not in accord with Bamford's[22] conclusion which assigned both of the bands at 18.18 kK and 15.50 kK as diagnostic bands for the tetrahedral coordination. So, the band around 18.181 k.K can certainly be regarded as the only diagnostic band for tetrahedral coordination

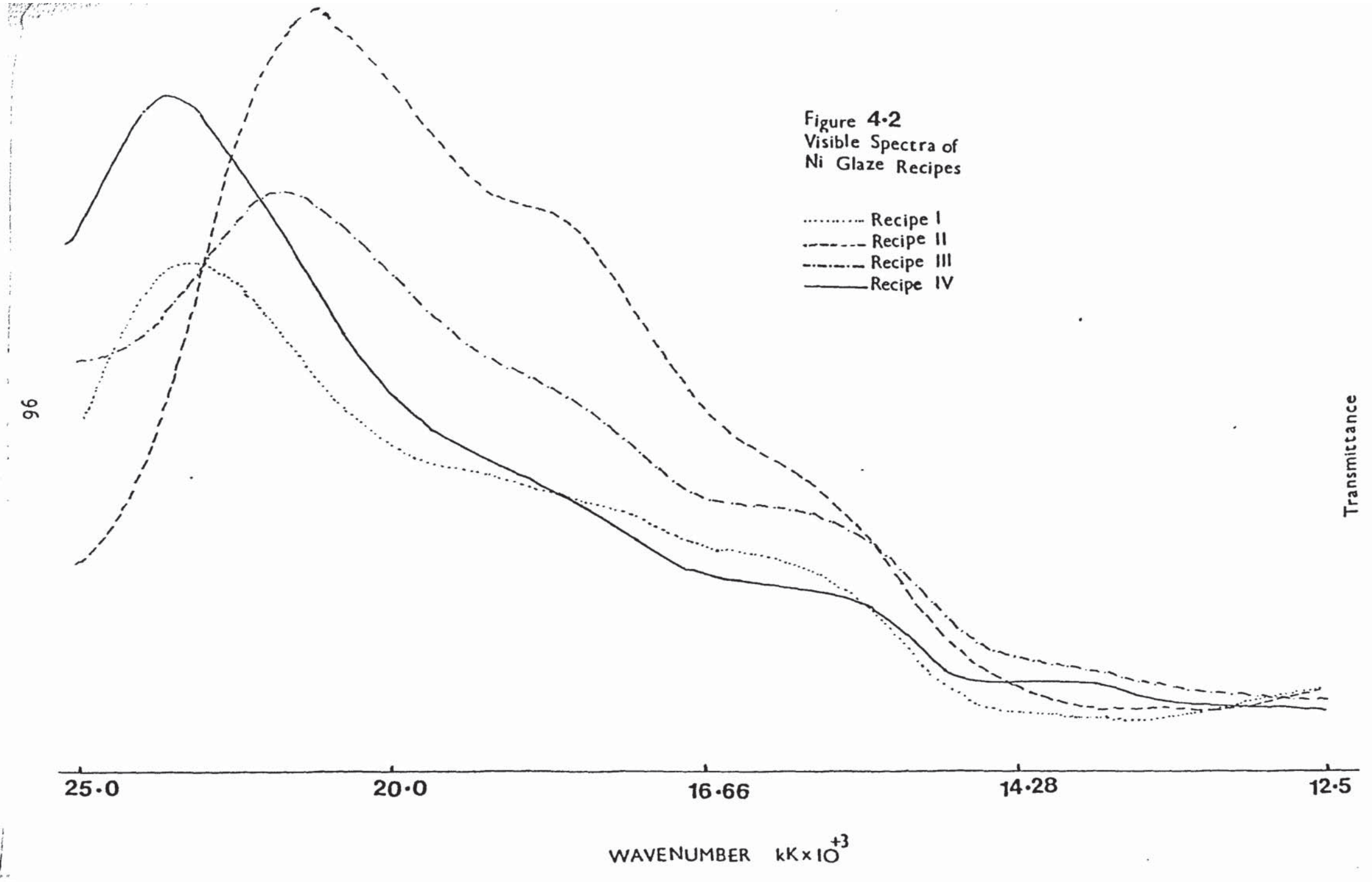

Figure 4·2
Visible Spectra of
Ni Glaze Recipes

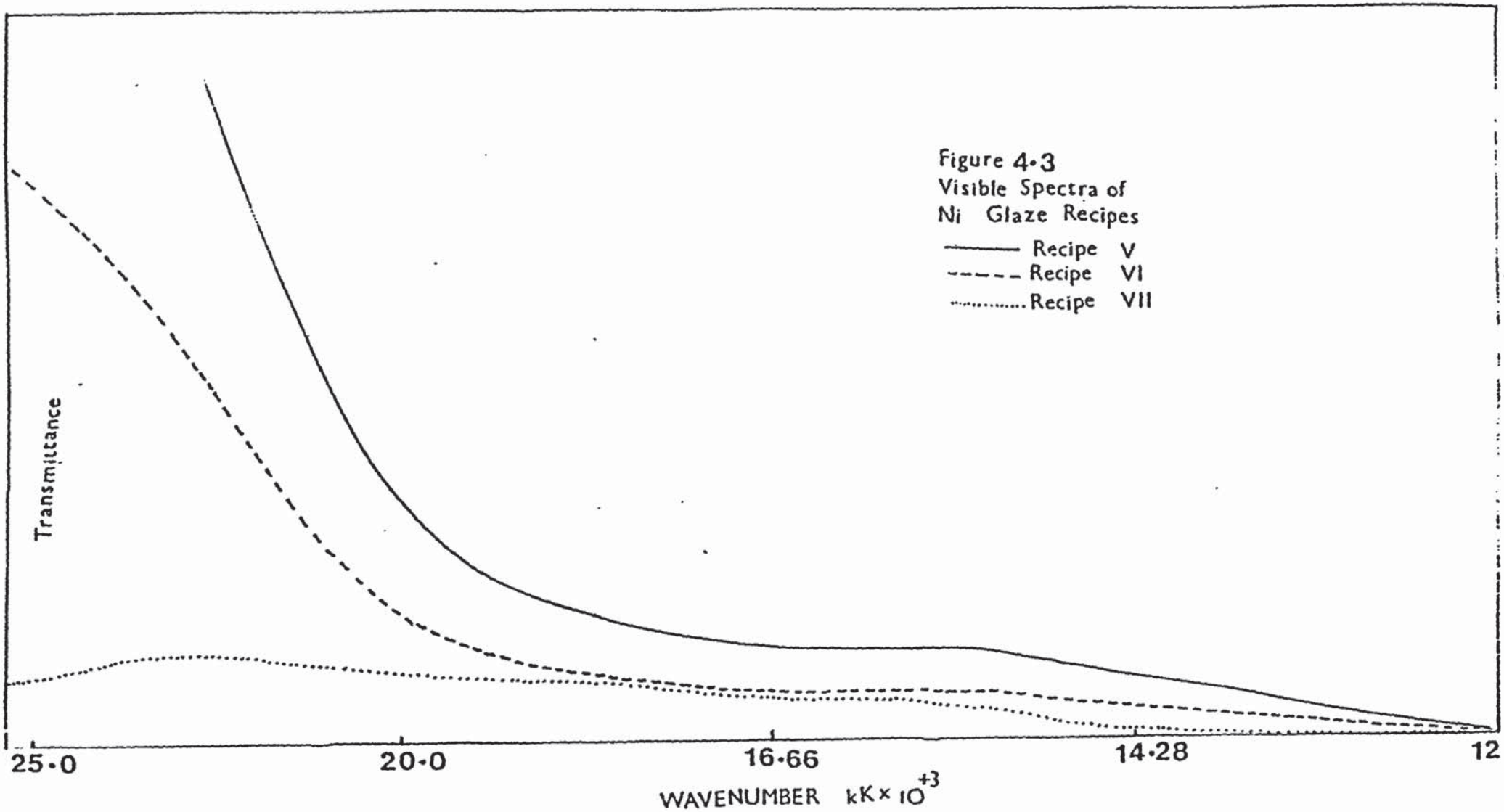

Figure 4·3
Visible Spectra of
Ni Glaze Recipes

because the transition $^3A_2 \rightarrow {}^1E(D)$ [59] arising in an octahedral ligand field occurs in the same region of the other band, 15.50 kK, which was supposed to be one of the two diagnostic bands for the tetrahedral coordination.

The decrease in the intensity of the persistent band in the absorption spectra of recipes V and VI, in which octahedral is the most predominant, compared with its intensity in the absorption spectra of recipes I - IV, in which both the octahedral and tetrahedral coordination were predominant, might be regarded as a support for the latter conclusion.

The band at the region of 12.5-13.986 kK which appears in the absorption spectra of most recipes may be attributed to the $^3A_{2g} \rightarrow {}^3T_{1g}(F)$ transition arising from octahedral ligand field[77,78].

Turner and Turner[59] suggested, depending on the intensity data, the possibility of a cubic 8-coordinated site occupied by Ni^{2+}. In the present work it is difficult to quantify the intensity data for Ni^{2+} in all recipes, and the small differences in the intensity which were observed in the spectra of some recipes may be attributed to an increase in the number of Ni^{2+} ions in an octahedral rather than tetrahedral coordination or vice versa. So the explanation of 4- or 8-coordinated species cannot

be deduced directly from the spectral data, but in this part of the discussion we will try to use the Dietzel idea as an indirect way for the elucidation of size of the coordination site around Ni^{2+}.

In the visible spectra of the glazes which have high barium and calcium oxide content, recipes II and III, the band responsible for the transition $^3A_{2g} \longrightarrow {}^3T_{1g}(P)$ appears at 21.459 kK and 21.645 kK, while it appears at higher frequency for the recipes which contain less barium (recipes I and IV) and that with TiO_2 or SnO_2 instead of ZnO (recipes V, VI and VII), Table 4.13. These data indicate that the ligand field is low at high barium and calcium oxide content i.e., exerting low electrostatic ionic field, and high at recipes which contain TiO_2 or SnO_2 instead of ZnO i.e., exerting high electrostatic ionic field. The latter results were in accordance with Dietzel's[9] predictions, who chose the ratio Ze/a^2 as a measure for the electrostatic cation field (Chapter One).

Table 4.14

Cation	Ionic Radius	Ze/a^2 $x10^8 cm^{-1}$
Ti^{4+}	0.68	8.65
Sn^{4+}	0.71	7.934
Zn^{2+}	0.74	3.652
Ca^{2+}	0.99	2.04
Ba^{2+}	1.34	1.11

According to the Dietzel idea, the small cations with a strong electrostatic field form small coordination polyhedra (4 or 6) i.e., SnO_2 and TiO_2 containing recipes, and the larger cations with weak electrostatic field form large coordination polyhedra (8) i.e., BaO and CaO containing glazes.

When the ratio $\frac{\text{Radius of Cation } (R_c)}{\text{Radius of Anion } (R_a)}$ has a suitable value the ions may alter slightly their coordination number, and consequently, the intensity of the electrostatic field changes and so does the behaviour of the corresponding oxides in the glaze.

Thus, it is concluded that it is primarily the stereochemical restrictions involved in packing the oxygen polyhedra of various oxides around Ni^{2+} that limit the site to an octahedral or a larger 8-coordinated one. So, the data in Table 4.14 indicate that the 8-coordinated site appears to be preferred when the larger oxide cations, like Ba^{2+} or Ca^{2+}, surround the Ni^{2+}, while the 6-coordinated site is the predominant one when these cations are replaced by smaller cations such as Ti^{4+} or Sn^{4+}. According to the above indirect conclusion, the possibility of 8-coordinated species in recipes II and III cannot be excluded.

The role of Ti^{4+} as an absorbing species in the spectra of titanium containing recipes was investigated by recording the visible spectra of these recipes but without Ni^{2+}. The absorption spectra of these recipes gave no bands and this can be explained as follows.

Titanium in glass may be present as tetravalent or trivalent ions. The tetravalent state corresponds to the d^{o}configuration, so it will give no absorption band. The trivalent state has the d^{1} configuration and should give a single band (i.e., near 20.4 kK)[79]. In the present recipes, it is clear that the titanium is predominantly in the colourless tetravalent state, d^{o}.

CHAPTER FIVE

CHEMISTRY OF IRON CONTAINING GLAZES

5.1 Introduction

The importance of getting knowledge about the behaviour of iron in glasses and glazes comes from two reasons, firstly, its use as a colouring agent for glasses and glazes, and secondly, its common occurrence as a troublesome impurity. The beautiful colours of the attractive Chinese glazes on stoneware such as Celadon* and Chün are due to the presence of dissolved iron oxide in its several forms of oxidation. Such aesthetic considerations make iron a commonly used colouring oxide in craft pottery. It seems likely that the inorganic chemistry involved may be complex, but interesting.

Although the behaviour of iron in glass has been the subject of numerous studies by many researchers using optical[80-83], electron spin resonance[84,85] and Mossbauer spectroscopy[86-97], its structural role is still a matter of confusion. Generally the complexity of the picture of iron in glass may be attributed to

---

* There is historical contradiction about the origin of the word 'Celadon'. Some historians referred it to a corruption of the word 'Saladin' (the Sultan) of Egypt, who sent a batch of this pottery to Damascus in 1171, and another historian suggests that the word comes from a character named Celadon, in a 17th century French play, the colour of whose costume was greyish-green[8].

the following:

(i) The unpredictable behaviour of iron in the glass system. It may be present as vitrifier or it may appear as modifier or it may precipitate as colloidal iron oxides.

(ii) The different variable coordination numbers of both di and trivalent iron in glass.

There have been considerable arguments about the appropriate tool for the determining of the coordination number of iron in glasses. Earlier workers considered primarily the behaviour of the U.V. cut-off and the visible colour of the glass as an indication of coordination. Although Bamford has applied the ligand field theory to Fe^{3+}, disagreements still exist[65,98] because of the similarity of the spectra to be expected for $3d^5$ ion in octahedral and tetrahedral sites. The application of E.S.R. would seem to be a more useful tool, but, since the initial work of Sands[84] and Castner[85] little information has been given from E.S.R.[99].

Compared to the amount of work done on the spectroscopy of iron containing glasses, not much work has been reported on glazes, especially Mössbauer work which has

mostly been used for the elucidation of archaeological problems[100-102]. To the best knowledge of the author, there has been no Mössbauer work on glazes and glasses containing iron with other transition metals except by Nolet[103] who worked on reduced synthetic Fe, Ti silicate glasses at elevated temperature.

Since the Mössbauer technique is the main spectroscopic tool used in this work to enlighten the role of iron in glazes and to review its results in terms of Shteinberg's theory of glass structure, it is useful to present here a brief treatment of the technique.

5.1.1 Mössbauer Spectroscopy

Mössbauer spectroscopy involves the recoilless emission and absorption of gamma radiation by nuclei embedded in a solid. Co^{57} is usually the embedded material which decays by electron capture with a half-life of 270 days to the second excited state of radioactive Fe^{57} (Fig 5.1). The second excited state of Fe^{57} decays to the first excited state with a mean time of 9×10^{-9} seconds, by emission of a 123 KeV gamma-ray. The transition of interest is from the first excited state to the ground state of Fe^{57} which occurs by the emission of a 14.4 KeV gamma-ray with a half-life of 1.1×10^{-7} seconds. Absorption of this gamma-ray is by the stable isotope

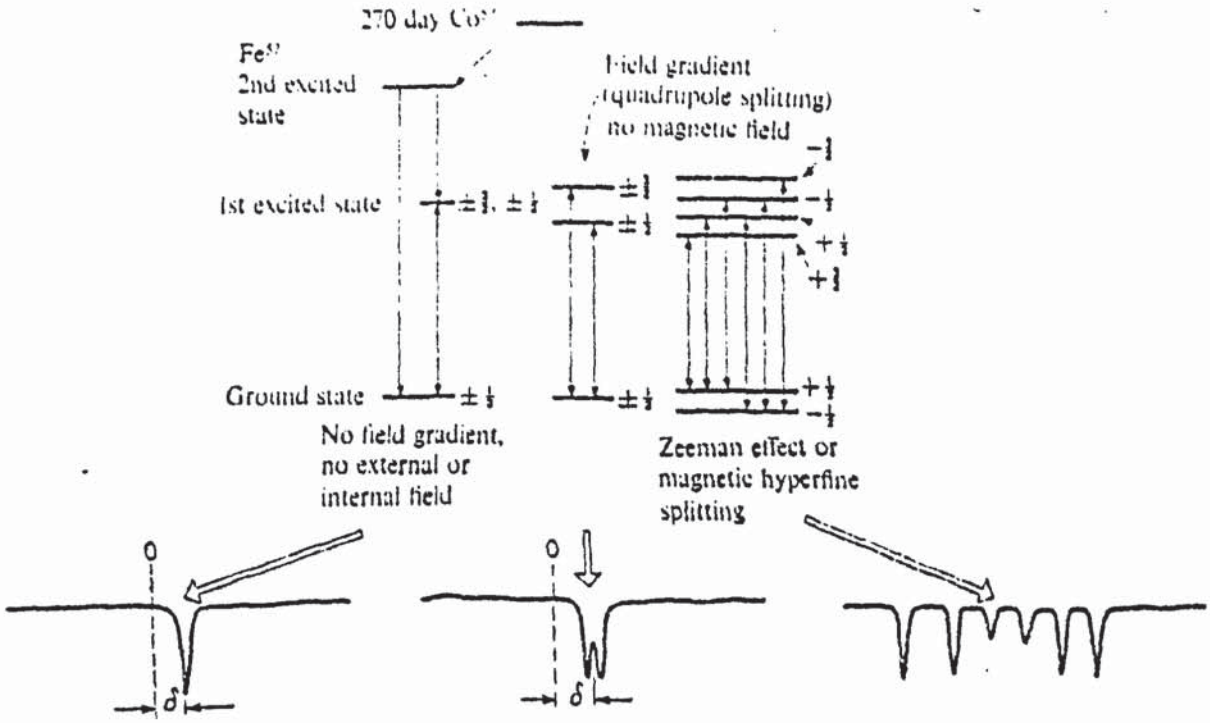

Figure 5.1 The changes in the nuclear levels and the resulting Mössbauer spectra

Fe^{57} and thus depends on the amount of Fe^{57} in the absorber. The natural abundance of Fe^{57} is only 2.14% and the use of iron enriched in this isotope is often necessary.

A range of energies for the incident γ-photons are obtained by taking advantage of the Doppler Shift which occurs when the source or absorber is moving. The absorption spectrum is plotted against this relative velocity, usually expressed in mms^{-1}. This is equivalent to scale of the energy of the incident γ-rays.

The basic parameters of interest in this technique are;

Chemical Shift (Isomer Shift), electric quadrupole interaction, magnetic hyperfine splitting and line width. The Chemical Shift is the result of a difference in s electron density at the nuclei of the source and of the absorber. The difference in density will result in a difference in energy for the two electronic configurations and a displacement of the absorption from the zero velocity position. The interaction of the nuclear quadrupole moment with a local electric field gradient (caused by the electrons in the Mössbauer isotope or from surrounding ions) splits the single line transition of the Fe^{57} into a two-peak (doublet) spectrum. The quadrupole splitting is sensitive to local symmetry and coordinating ligands about the iron. Since the surroundings of individual iron atoms in glasses are expected to vary from point to point, the line width is used as a measure of the similarity of the sites.

Values of the isomer shifts from the literature for crystalline[87-90] and vitreous materials [87-89,93-95] are shown in Figure 5.2. From these values and the literature values[87-89,93-95] of the quadrupole splitting and line width, the following general conclusions can be drawn:

1) The chemical shifts for iron (II) and iron (III) may be summarised as δ(divalent) > δ(trivalent) and

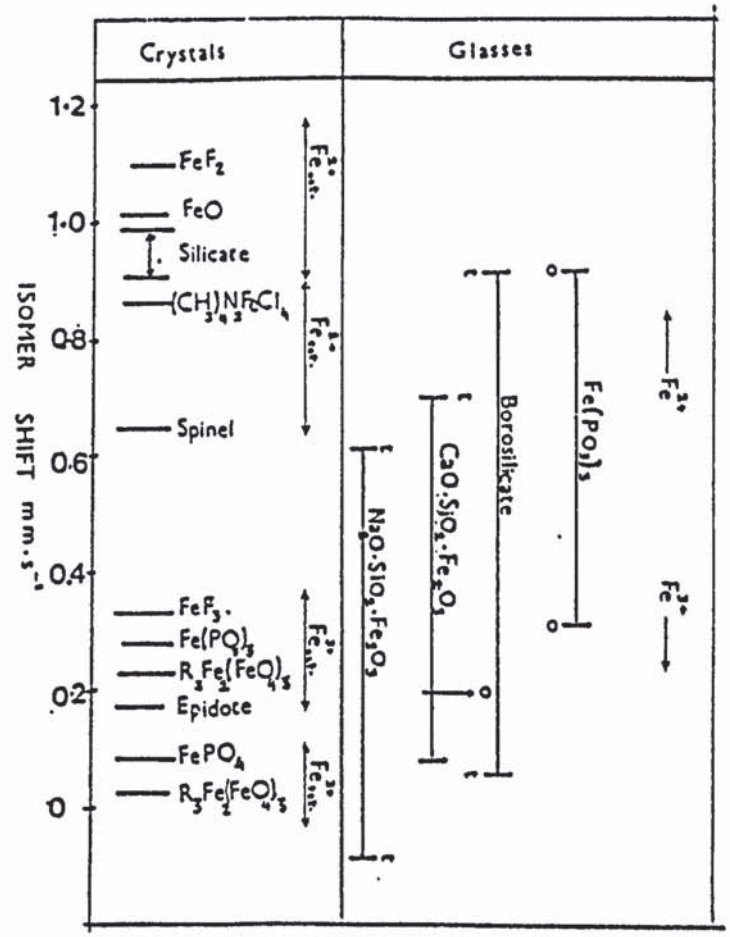

Figure 5.2 Values of the isomer shifts from literature for crystalline[87-90] and vitreous materials[87-89,93-95]

δ(octahedral) > δ(tetrahedral) for iron in the same valence state. The former results are explained by the fact that the iron (II) cation has one more d-electron than the iron (III) cation, its s-electrons are more screened from the nucleus than those of the iron (III) cation, which results in a lower electron density at the nucleus and hence in a more positive value of the isomer shift (since $\Delta r/r$ is negative for Fe^{57}). The most likely explanation[104] for the latter results is that the degree of overlap of electronic orbitals between the iron (III) cations and the oxygen anions depends on the distance between the iron atom

and oxygen. In a close packed array of spheres, the tetrahedral holes are considerably smaller than the octahedral holes so that the degree of overlap of the orbitals is greater in the tetrahedral case, consequently the s electron density at the iron nucleus is greater in the tetrahedral case due to a greater contribution from the 4s orbital than in octahedral case.

2) The quadrupole splitting for the high spin iron (II) cation is larger than for the high spin iron (III) cation. Kurkjian[87,90] attributed that to the axial or rhombic symmetry distortions generated by the electrons outside the half-filled spherical shell. The splitting in trivalent salts is mainly due to the crystal field effects because the charge distribution of iron (III) ($3d^5$) is spherically symmetrical.

3) The calculated value of the line width, on the basis of the known lifetime of Fe^{57}, is 0.1 mms^{-1} and due to the folding of the source and absorber lines, the observed linewidth should thus be 0.2 mms^{-1}. Line widths from literature are greater than this, which indicates that the iron in glass is present in a range of different sites.

5.2 Results and Discussion

5.2.1 Mössbauer Results of Calcium-, Strontium- and Barium-Iron Silicate Glasses

Mössbauer spectra were obtained for samples of the alkaline earth-iron silicate glasses fired in air at ∿1280°C and the results are given in Table 5.1. The glass systems I_a (iron silicate) and II_a (Ca-Fe silicate) show a (Figure 5.3) magnetic sextet with hyperfine field of ∿525 KOe. This sextet can be attributed to iron oxide in the form of hematite (compared to the quoted value in the literature of 515 KOe[105]). This result was supported by the X-ray results, Table 5.2, which also indicate the formation of calcium silicate in glass II_a.

The precipitation of Fe_2O_3 in the glass I_a and its unreactivity toward quartz may be due to the absence of the modifying oxides which weaken the bonds within the SiO_2 network. The insufficient heat treatment may be another reason for the presence of Fe_2O_3 in glass system I_a. The appearance of Fe_2O_3 in glass system II_a can be attributed to the formation of stable $CaSiO_3$, which needs high temperatures for reaction with iron oxide (∿1600°C[97]). The firing product of the latter glass system was a powder, so very little or no vitrification occurs at 1280°C.

Table 5.1 Compositions and Mössbauer data of the alkaline earth-iron silicate glasses

Glass systems	Mole %					Isomer shift(δ) $mm\ s^{-1}$	Quadrupole splitting(Δ) $mm\ s^{-1}$	Line width(Γ) $mm\ s^{-1}$
	Quartz	Fe_2O_3	Whiting (CaO)	SrO	BaO			
I_a	91	9				-8.253 +0.538 -4.431 +5.382 -0.853 +8.714 +1.821	H_{eff}=525KOe	0.275 0.262 0.245
II_a	74	8	18			-8.230 +5.360 -4.445 +8.727 -8.615 +1.807	H_{eff}=524KOe	0.300 0.276 0.278
III_a	74	8		18		0.285	1.178	0.613
IV_a	74	8			18	0.200	0.875	0.451

δ with reference to natural Iron Metal
Error in δ and Δ = ± 0.003 $mm\ s^{-1}$
Error in Γ = 0.004 $mm\ s^{-1}$

Table 5.2 XRD analysis of the alkaline earth-iron silicate glasses

	SiO_2	Hematite	CaO	BaO	SrO	Others
Iron-silicate I_a	√	√				
Ca-Fe-silicate II_a	√	√	√			$CaSiO_3$
Sr-Fe-silicate III_a	√	x	-		x	Amorphous
Ba-Fe-silicate IV_a	√	x		x		Amorphous

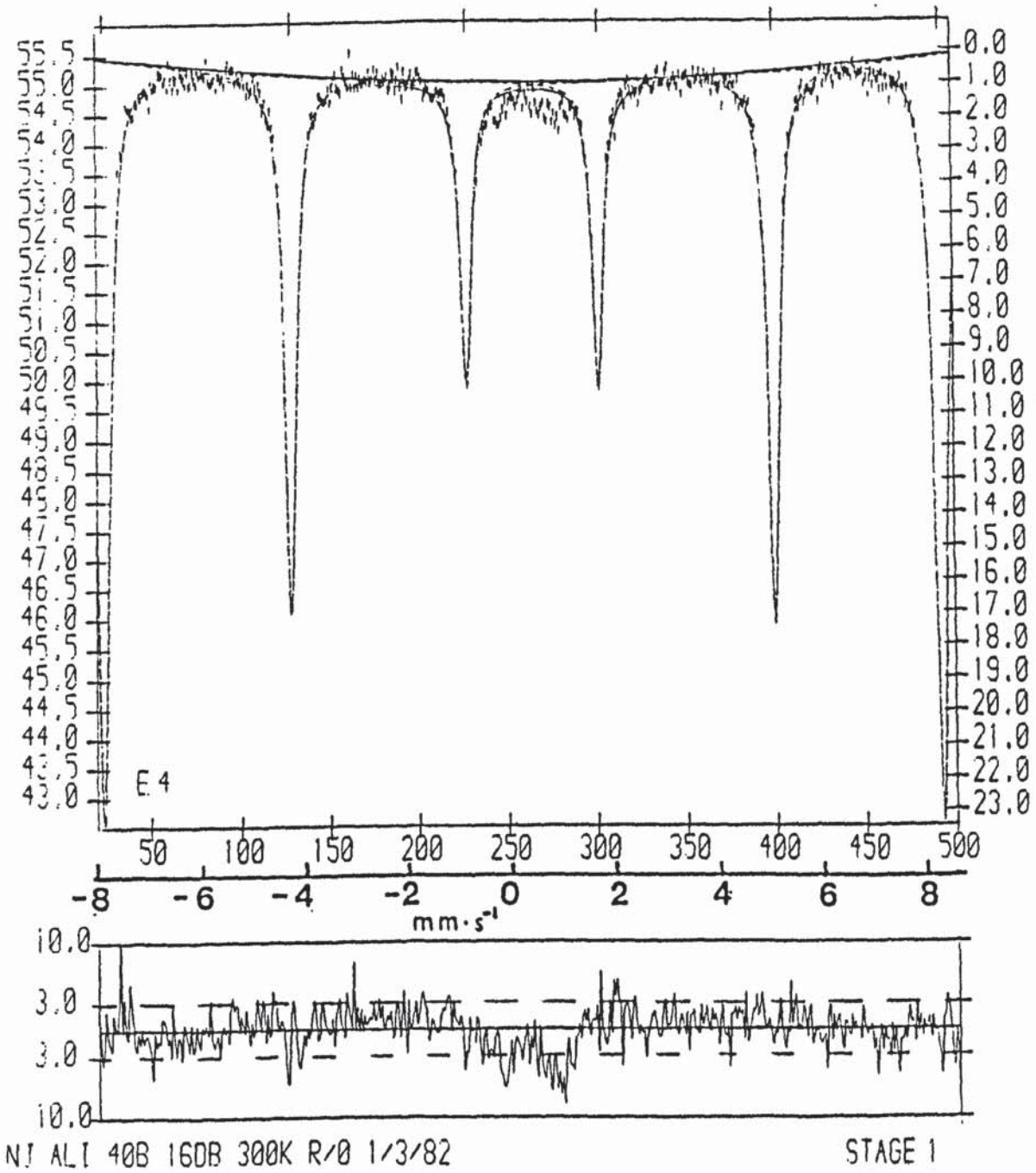

Figure 5.3 ^{57}Fe Mössbauer spectrum of glass system II_a

The Mössbauer spectra of strontium- and barium-iron silicate glasses (III_a and IV_a in Table 5.1) each show one doublet with isomer shifts of 0.285 mm s^{-1}, 0.200 mm s^{-1} and quadrupole splitting of 1.178 mm s^{-1} and 0.875 mm s^{-1} respectively. Comparison with the isomer shifts and quadrupole splittings from the literature for crystalline[87-90] and glassy materials[87-89,93-95] indicates that the separated lines are attributed to octahedrally coordinated ferric ion.

The XRD patterns of glass systems III_a and IV_a show small diffractions which were identified as being due to the presence of a small amount of quartz (Table 5.2). This broad XRD pattern assumes more vitrification in these glasses than in Ca-iron silicate glasses.

It was reported that generally the site of the iron (III) ion in silicate glasses is tetrahedral[87-89], but later on Iwamoto et al[97] found that calcium silicate glasses containing ten mole per cent of Fe_2O_3, fired in air at 1600°C have both octahedral and tetrahedral iron (III) sites. In this study, it was found that strontium and barium silicate glasses containing eight mole per cent Fe_2O_3 have predominantly octahedral iron (III) sites, Figure 5.4.

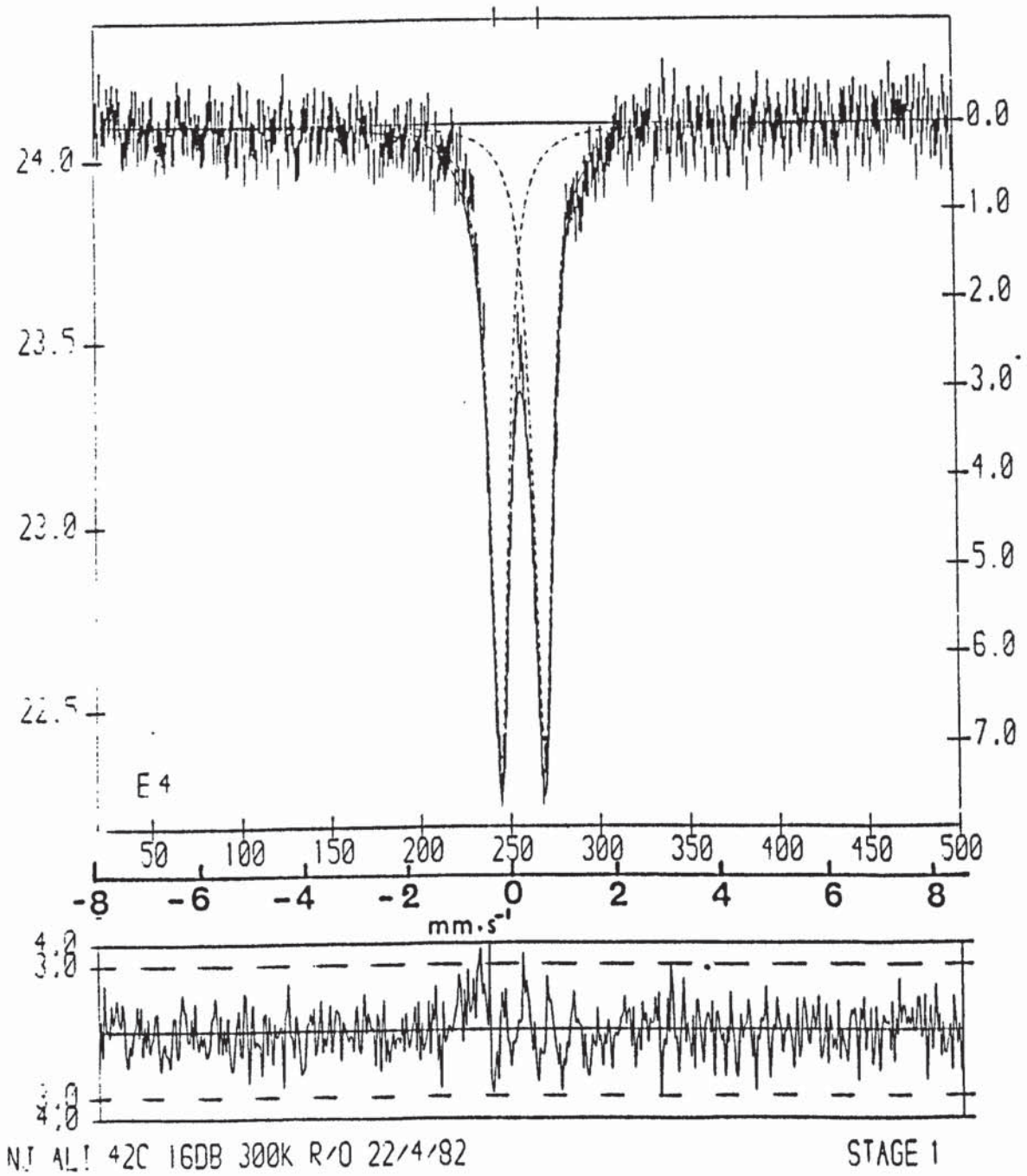

Figure 5.4 ^{57}Fe Mössbauer spectrum of glass system IV_a

The slight increase in the isomer shift values going from Ba^{2+}, Sr^{2+} (0.200 mm s^{-1} and 0.285 mm s^{-1} respectively, Table 5.1) and Ca^{2+} (0.340 mm s^{-1}[97]) is thought to be caused by the increasing field strength (Chapter One, Pg 15) of the cation M in the series M = $Ba^{2+}<Sr^{2+}<Ca^{2+}$. This leads to an increase in the field at the O^{2-} sites and hence to a decreased expansion of the oxygen electronic wave function onto the iron (III) ions, which in turn causes a decrease in the covalency of the Fe-O bond.

The large quadrupole splitting and line width observed in the Mössbauer spectra of these glasses is attributed to the large number of non-identical sites with a substantial departure from cubic symmetry as compared to the situation existing in crystals.

The quadrupole splitting for glasses III and IV decreases in the order of decreasing field strength of alkali earth cation, from Ca^{2+} to Ba^{2+}, which leads to a decrease in the covalency of the Fe-O bond.

5.2.2 Optical Absorption Spectra of Ca-, Sr-, and Ba-Iron Silicate Glasses

Although the ligand field theory has been successfully applied in the correlation of optical absorption spectra of transition metal ions in glasses[65,98], a difficulty

has been found in interpretation for iron (III) in glasses. This is due to the fact that the same Tanabe and Sugano[106] energy level diagram holds for $3d^5$ ions in both octahedral and tetrahedral coordination. The differences in the spectra will be due to, firstly, the differences in ligand field strength (i.e. $\Delta_{tet} = -(4/9)\Delta_{oct}$), and secondly to the differences in Racah parameters B and C, and to differences in molar absorptivety.

A comparison between the absorption spectra of iron (III) ion in phosphate glasses[90,107], in which iron (III) was octahedrally coordinated, and the absorption spectra of our alkali earth iron silicate glasses (Table 5.3) suggests that the iron (III) ions are present in predominantly octahedral sites.

The very long tail band at 20.00-25.00 kK for glasses I_a and II_a made the resolution of any spin-forbidden transitions very difficult. These results are in accordance with the Mössbauer data which suggested that iron (III) ions are present in predominantly octahedral sites.

5.2.3 Electron Spin Resonance of the Alkali Earth-Iron Silicate Glasses

The E.S.R. spectra of an ion with S = 5/2 spin state, like iron (III), can be described by the usual spin Hamiltonian[108]

Table 5.3 Visible absorption and E.S.R. data of the alkali earth-iron silicate glasses

Glass	Visible absorption bands kK	g-values
Fe-silicate I_a	18.86, 15.15, 12.57	2.08, 3.55, 4.37
Ca-Fe-silicate II_a	18.18, 15.38, 12.34	2.04, 3.47, 4.33
Sr-Fe-silicate III_a	22.12, 15.38, 13.07	2.01, 3.45, 4.29
Ba-Fe-silicate IV_a	22.47, 15.29, 13.05	2.01, 4.30
Phosphate Glasses Ref. (90)	Bands kK	Assignment
	23.800	$^6A_1 \rightarrow {}^4E_1, {}^4A_1$
	18.350	$^6A_1 \rightarrow {}^4T_2$
	13.350	$^6A_1 \rightarrow {}^4T_1$

$$\mathcal{H} = B.H.g.S + D[S_z^2 - \tfrac{1}{3}S(S+1)] + E(S_x^2 - S_y^2)$$

where the crystal field terms D and E, with axial and rhombic symmetry respectively, determine the resonance positions, B is a constant, the Bohr magneton, and H is the field strength. The resonance at g = 4.3 arises due to the transition within the middle doublet among the three Kramers doublets, the other resonances at 6 and 2 arise due to the transitions in the lowest doublet. The resonance at g = 4.3 and g = 2.0 was attributed to iron (III) in tetrahedral and octahedral sites respectively[85]. This attribution has been sharply disputed by Kurkjian and Sigety[90], and they suggested that the g = 4.3 resonance can be produced by low symmetry (rhombic) sites of either tetrahedral or octahedral coordination and the g = 2.0 resonance is the result of spin-spin interactions at either site. A number of papers have tended to support this idea[109 and references therein].

The E.S.R. spectra of our alkali-earth-iron silicate glasses are shown in Figures 5.5 - 5.8 (Table 5.3). In all the glasses there are two resonance observed at g $\sim$ 4.3 and $\sim$ 2.01. The analysis of the Mössbauer data (Section 5.2.1) and optical absorption results (Section 5.2.2), which suggested the predominancy of the octahedral site in these alkali earth-iron silicate glasses, indicates that the origin of these resonance absorptions,

Figure 5.5 E.S.R. spectrum of glass system I_a

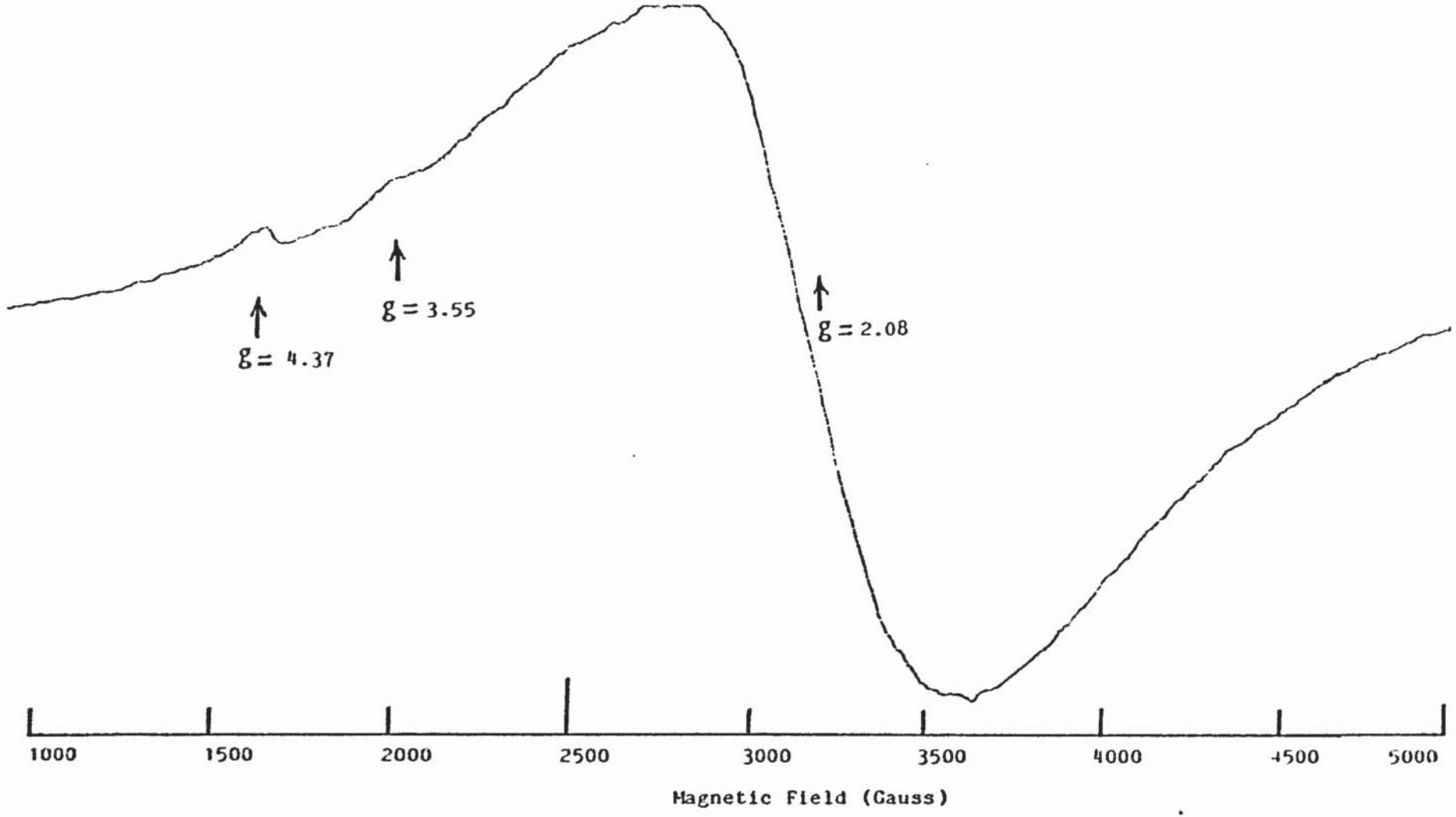

Figure 5.6 E.S.R. spectrum of glass system II_a

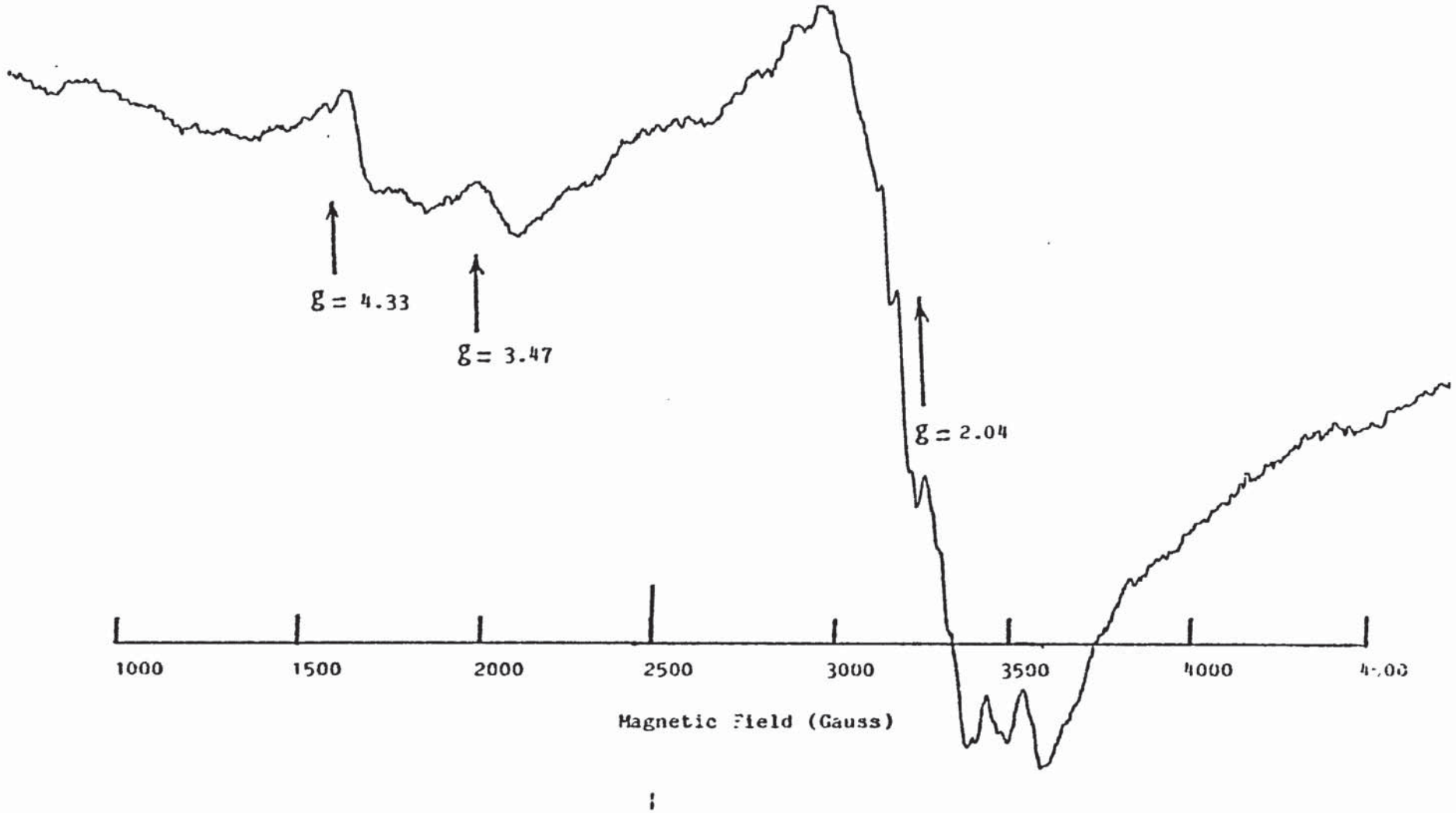

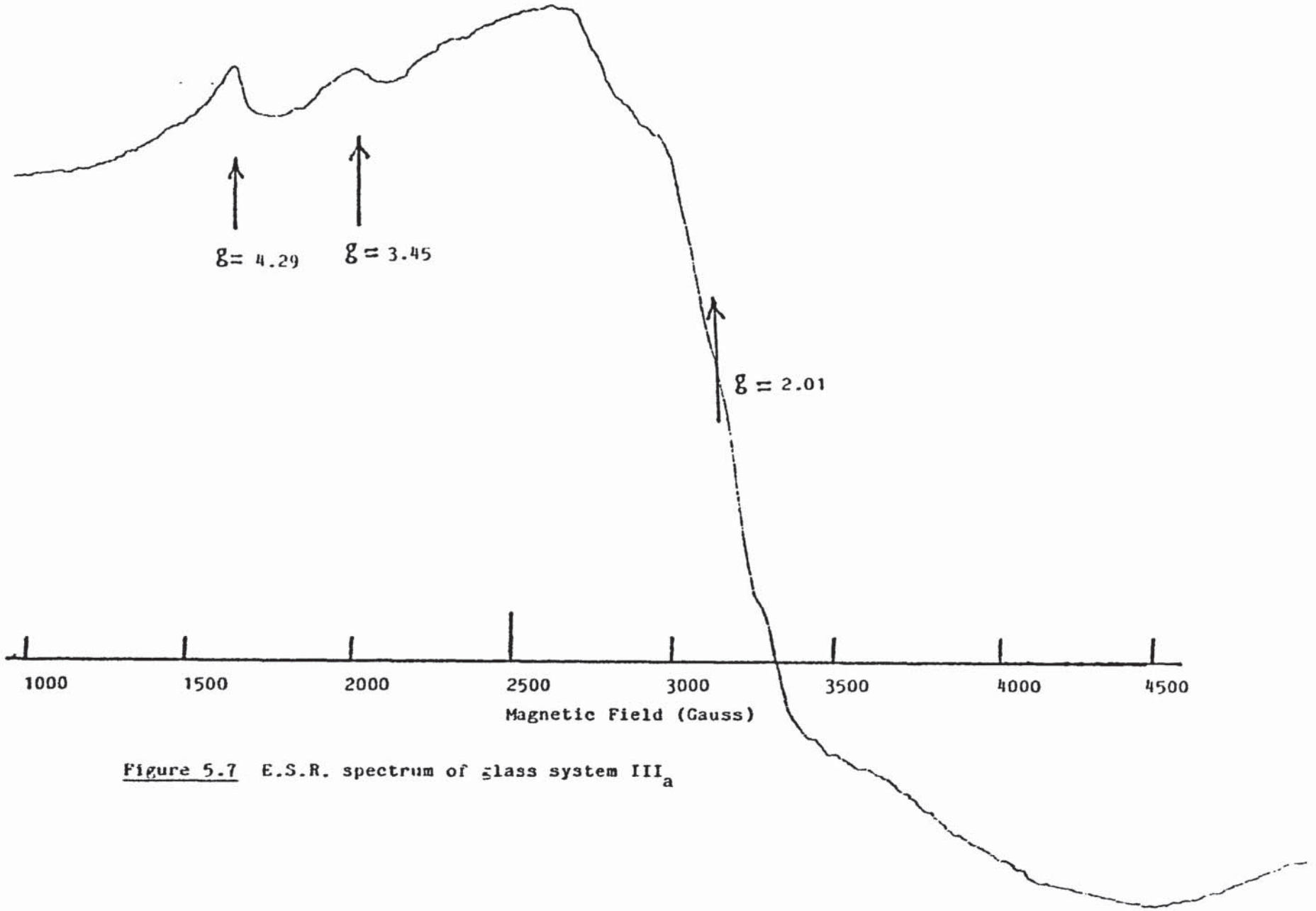

Figure 5.7 E.S.R. spectrum of glass system III_a

Figure 5.8 E.S.R. spectrum of glass system IV_a

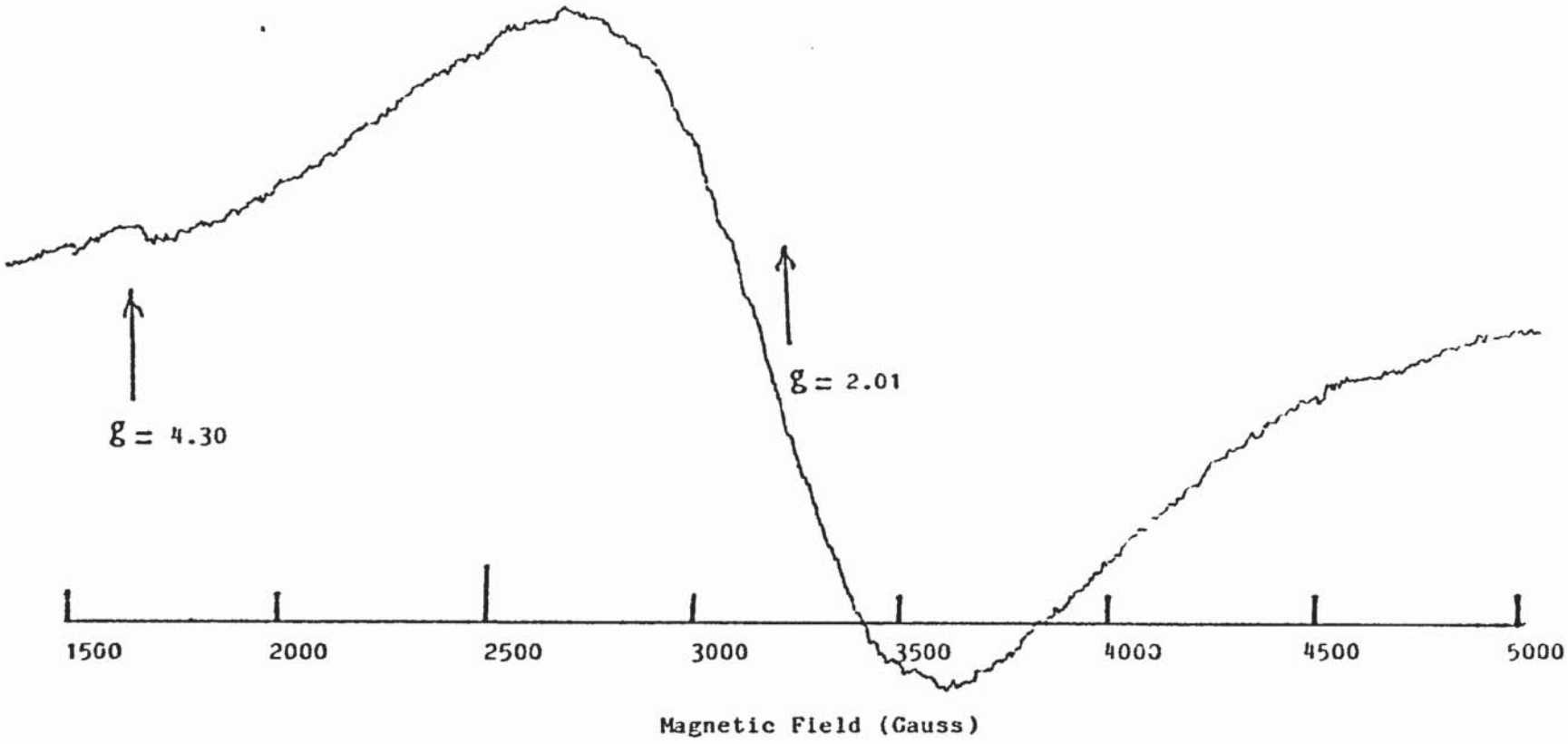

i.e., at g ≃ 4.3 and g ≃ 2, may not be related to the coordination numbers. This result is in agreement with Kurkjian and Sigety's conclusions[90].

In E.S.R. spectra of calcium- and strontium-iron silicate glasses, Table 5.3, there is a resonance absorption at approximately g = 3.3 in the calcium glass which is absent in the spectrum of barium-iron silicate glass. The origin of this resonance absorption can be explained as follows. In glass there are a large number of non-identical sites and large departures from cubic symmetry, as indicated by the large value for line width and quadrupole splitting in the Mössbauer results in Table 5.1 (Section 5.2.1), this means that the iron (III) ions in glass are present at various crystal fields, so this resonance may result from one distorted site. The Mössbauer spectrum of the barium-iron silicate glass shows the lowest value for the line width and quadrupole splitting, compared to that for glasses II and III. This means that there are a smaller number of the non-identical sites and little departure from cubic symmetry in this glass. This result may explain the disappearance of resonance absorption at ∿ 3.3 in the E.S.R. spectrum of barium-iron silicate glass in which iron (III) is present in more similar and symmetrical sites.

The electron spin resonance spectrum of calcium-iron silicate system II_a shows a six-line resonance centred at $g \sim 2$, Figure 5.6. Gillespie[26] observed such multi-line resonance in the E.S.R. spectra of samples of a mineral glaze system fired up to 700°C, he also observed a multiline resonance in the E.S.R. spectra of whiting (shown by XRD to be 100% calcite), and reagent grade calcium carbonate (a mixture of calcite and aragonite) He attributed this multiline electron spin resonance to the presence of manganese (II) which substitutes for some of the calcium cations in the calcite crystal lattice. He supported his prediction by atomic absorption analysis which indicated the presence of manganese (II) in whiting and in calcium carbonate. Gillespie related the disappearance of the multiline resonance in the spectra of samples fired above 700°C to the absence of CaO which interacted with the other component of the glaze system above this temperature. In our calcium-iron silicate, calcium oxide persists at the firing temperature, 1280°C, as indicated by the X-ray diffraction analysis, Table 5.2, so the six-lines resonance does not disappear in the spectrum of this system. This result supports Gillespie's interpretation. The absence of the multiline resonance in the electron spin resonance spectrum of the iron silicate system I_a is also good support for this interpretation which considers the persistance of the manganese multiline spin resonance to be related to the presence of CaO in the system.

5.2.4 Mössbauer Results of Iron Glaze Systems Fired In Air

Mössbauer spectroscopy is useful in the elucidation of states of iron in a glaze because various forms of iron will all have different Mössbauer spectra.

One possible form of iron in a glaze is as Fe_2O_3, another is as alkaline ferrites. In these cases the Mössbauer spectrum is a six peak magnetic hyperfine spectrum. The magnetic field for Fe_2O_3 hyperfine structure (H_{eff}) is around 515 KOe while the values for the alkaline ferrites are much smaller than that (420 - 480 KOe)[17].

The second possible situation for iron is by way of interaction with the silica network of quartz and potash feldspar. In fact, potash feldspar has the same structure as silica but some silicon is replaced by aluminium and the resultant negative charge is satisfied by potassium ions which fill the interstitial site between the ring structures in six coordinated positions. Iron (III) in the fully matured glaze may replace the potassium cation in the six coordination positions without breakdown of the strong silicate structure. Thus, the Mössbauer spectra should be a one doublet with an isomer shift of 0.15 - 0.35 mm s^{-1} and quadrupole splitting in the range of 1 - 1.3 mm s^{-1}.

A third form for iron (III) can be expected by assuming that iron (III) replaces Al^{3+} or Si^{4+} in the basic tetrahedral units of the feldspar or quartz. In this form iron (III) behaves as a vitrifier with coordination number four, and should exhibit a doublet in the Mössbauer spectrum with low isomer shift ($\sim$ -0.07 - 0.1 mm s^{-1}) and higher quadrupole splitting ($\sim$ 1.05 - 1.65 mm s^{-1}).

The compositions of the four iron glaze recipes as studied with their room temperature Mössbauer results are given in Table 5.4. The compositions of the recipes differ from each other by the type of the modifying oxide contained i.e., each of the recipes contains one of the alkaline earth oxides; CaO (Recipe I), SrO (Recipe II), BaO (Recipe III). Recipe IV contains TiO_2. All four recipes show a Mössbauer spectrum (Figure 5.9) composed of an iron (III) doublet and low intensity iron (III) hyperfine pattern. The isomer shift of these doublets, which form the major part of the spectrum, are in the range 0.16 - 0.23 mm s^{-1}, with quadrupole splitting of 0.29 - 1.15 mm s^{-1}. These values are interpreted as being due to iron (III) in an octahedral environment. The magnetic field of the low intensity hyperfine pattern is around H_{eff} = 520 KOe, which can be attributed to the presence of α-Fe_2O_3.

Table 5.4 Compositions and Mössbauer results of the glaze systems

Recipes	Weight per cent							Isomer shift$_1$ mm s^{-1} (δ)	Quadrupole splitting mm s^{-1} (Δ)	Line width$_1$ mm s^{-1} (Γ)
	Potash Feldspar	Quartz	Whiting	Ferrous oxalate	Strontium carbonate	Barium carbonate	TiO_2			
I	54.40	19.1	10.3	16.2				0.224	1.151	0.79
II	55.00	18.8	3.6	15.2	7.2			0.216	1.117	0.69
III	55.00	18.8	3.6	15.4		7.2		0.187	1.070	0.74
IV	56.8	19.1	10.1	4.0			10.0	0.162	0.296	0.23

δ with respect to iron metal
Error in δ and Δ = ± 0.006 mm s^{-1}
Error in Γ = ± 0.01 mm s^{-1}

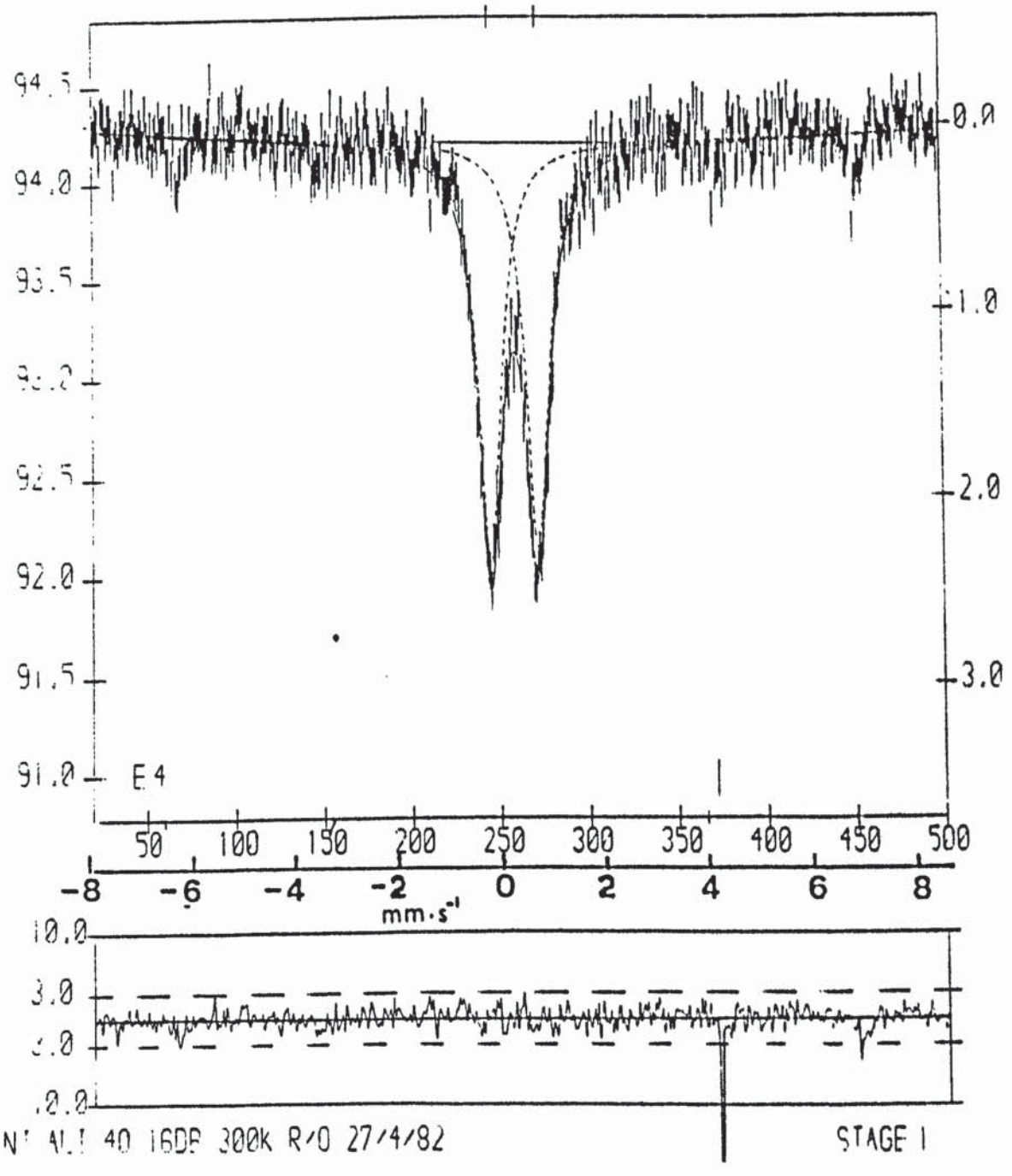

Figure 5.9 ^{57}Fe Mössbauer spectrum of glaze recipe I

A comparison between these latter results and the former discussion, suggests that the major part of iron (III) in the fully matured glazes obtained on firing to 1280°C occupies an octahedral position, while a small quantity of iron (III) is precipitated as Fe_2O_3. There is no Mössbauer evidence for the presence of iron (III) in a tetrahedral site, which means that iron (III) does not replace Al^{3+} or Si^{4+} in the tetrahedral units of the silica structure and feldspar contained in these recipes.

The effect of the nature of the group (II) cations on the state of iron (III) in the first three recipes is reflected by the slight increase in the isomer shift values going from recipe III to recipe I (i.e., from Ba^{2+}, Sr^{2+} to Ca^{2+}). The reason for this was mentioned in Section 5.2.1. However, the nature of the group (II) cation does not affect the coordination number of iron (III) in these recipes. This result is not in complete harmony with the Shteinberg theory, which placed emphasis on the role of the alkaline earth ion in determining the structure of the glass.

The values of the quadrupole splitting observed for the first three glaze recipes are in the range of 1.07 - 1.15 mm s^{-1}, but in the case of high spin iron (III) ($3d^5$, $^6S_{5/2}$) the electron distribution is spherically symmetrical and therefore should not give rise to any quadrupole splitting. Thus if the normal octahedral

coordination is undistorted, no quadrupole splitting should be observed. Kurkjian and Sigety[90] have indicated that there are a large number of non-identical sites with a substantial departure from cubic symmetry in glasses as compared with the situation existing in crystals. This will explain the large values of line width and quadrupole splittings for these glaze recipes.

The Mössbauer spectrum of the fourth recipe, which contains TiO_2 as a modifying oxide, is characterised by a low value for the isomer shift, quadrupole splitting and line width. The low isomer shift for this glaze recipe may be explained as follows; the smaller ionic radius of Ti^{4+} causes a high degree of overlap of site oxygen orbitals, and consequently high s-electron density will occur at the iron nucleus. A greater electron density in iron Mössbauer spectroscopy is reflected in lower isomer shift.

The low values quoted for quadrupole splitting and line width in the Mössbauer spectrum of this recipe mean that iron is present in more symmetrical and less numerous non-identical octahedral sites. This reduction in the site distortions of iron (III) ion and the reduction of randomness in environment of iron (III) ion may be due to the formation of microcrystalline iron titanate. The X-ray diffraction pattern of this recipe gave no evidence for such specific compounds due to its amorphous character.

The temperature dependence of the isomer shift and the quadrupole splitting between 77 ^{o}K and 300^{o}K was determined for the first three recipes and is shown in Table 5.5. Although there is a theoretical expression for the temperature dependence of the quadrupole splitting in the case of octahedrally coordinated iron (II)[110a,110b], no such analysis exists for the temperature dependence of the iron (III) quadrupole splitting.

The results in Table 5.5 indicate that the isomer shift decreases with increasing temperature. This result is in agreement with Gosselin et al[89]. Gosselin et al attributed the decrease to several mechanisms of which the most important are the temperature effect[111] and the change in the s electron density at the nucleus $|\Psi_{(o)}|^2$. They considered that the shift is perhaps due to the softening of glass as the temperature is raised, but this softening should result in the variation of the quadrupole splitting, and consequently the shielding effects will vary. In this work the quadrupole splitting are nearly constant at different temperatures (Table 5.5), as will be discussed in the next paragraph. Thus, there is no noticable change in symmetry with the change in temperature and therefore the shielding effect may not be the reason for the decrease in the isomer shift. This decrease in the isomer shift with increase in temperature may be explained as follows; as the glaze softens at higher temperatures,

Table 5.5 Mössbauer results of glaze systems at different temperatures

Glaze Recipes	mm s^{-1}	300°K	210°K	140°K	77°K
I	I.S. (δ)	0.224	0.27	0.32	0.67
	Q.S. (Δ)	1.151	1.22	1.23	1.27
	Line width (Γ)	0.79	0.88	0.64	0.80
II	I.S.	0.216	0.27	0.33	0.42
	Q.S.	1.117	1.05	1.05	0.97
	Line width	0.76	0.77	0.66	0.64
III	I.S.	0.1875		0.33	0.56
	Q.S.	1.070		1.12	1.17
	Line width	0.74		0.70	0.96

δ with respect to iron metal
Error in δ and Δ = $\pm$ 0.02 mm s^{-1}
Error in Γ = $\pm$ 0.05 mm s^{-1}

the oxygen atoms become more free to move towards the iron, causing an increase in the covalency of the Fe-O bond i.e., a decrease in the isomer shift.

As previously mentioned (Section 5.1.1) the quadrupole splitting arises from the interaction of the nuclear quadrupole moment with the gradient of the electric field at the nucleus. The origins of the field gradient are the electrostatic field produced by neighbouring ions and the non-spherically symmetric charge distribution in the iron ion itself. The direct contribution of the crystal field to the quadrupole splitting is nearly independent of temperature[93]. The type of orbitals which are occupied affect the contribution of the electron on the iron ion. Since the high spin iron (III) ion is spherically symmetric, the only contribution to the quadrupole splitting comes from the crystal field and the splitting should be independent of temperature. The values of quadrupole splittings at different temperatures for these glaze recipes are nearly constant within experimental error, Table 5.5. These Mössbauer data may be a support for the above conclusion.

The Mössbauer doublets obtained for the three glaze recipes at low temperature have lower intensity than that obtained at room temperature, while the reverse occurred for the magnetic hyperfine lines in the same spectra, but the doublets still form the major part of the spectra. This means

that a small part of the room temperature doublets belongs to the magnetic hyperfine spectrum and not the whole doublet.

The effect of firing conditions on the state of iron in the glaze system is reflected in the Mössbauer spectrum of glaze recipe III, which was fired under a nitrogen atmosphere. The Mössbauer data show one doublet (I.S. = 1.404, Q.S. = 1.095 mm s^{-1}) and one singlet (I.S. = -0.024 mm s^{-1}). These Mössbauer parameters are predicted as being due to iron in two sites, the site with the larger isomer shift and quadrupole splitting being octahedral iron (II) and the other being tetrahedral iron (III). Gillespie[26] obtained Mössbauer data for glaze recipes similar in composition to our glaze recipe III and fired under nitrogen, but his recipes contain either SrO or CaO instead of BaO which was present in recipe III. He interpreted his data as being due to the presence of both octahedral iron (II) and octahedral iron (III) in all his recipes. Accordingly, he concluded that the exact nature of the glass forming matrix is unimportant and the iron cation is determined by the nature of the iron oxide. He based his conclusion on the agreement of his data with data obtained for old Chinese glazes fired under nitrogen[112], but changing CaO or SrO (in Gillespie's recipe) with BaO (recipe III in this work) gave a different coordination site for iron (III). This comparison emphasises the effect of the nature of the modifying oxide beside the effect of firing temperature on the state of iron in glazes.

5.2.5 Mixed Iron-Vanadium Glazes

The compositions, E.S.R. and Mössbauer results for these glaze recipes, fired in air at 1280°C, are given in Table 5.6. Recipe V has a white creamy fired colour while the other two recipes, VI and VII have a blue-violet and brown colour respectively. Optical spectra of the glazes were recorded at room temperature between 12.5 kK - 2.5 kK, no absorption band of the ions were observed for the first two glaze recipes. The third recipe (VII) shows three absorption bands at 13.513 kK, 15.38 kK, 19.41 kK and a cut off at 23.255 kK. In order to obtain a clearer picture of the state of the iron and vanadium in the mixed iron-vanadium glaze, it is useful to analyse the E.S.R. spectral data of the vanadium-only glaze (recipe V).

5.2.6 E.S.R. Results of Vanadium Containing Glaze

The determination of the oxidation state of vanadium in various glasses have been the subject of contradiction. Vanadium has been predicted by Bamford[98] to exist in the V^{3+} and V^{5+} state, while others[65,80] have considered the presence of three valence states V^{3+}, V^{4+} and V^{5+}. Hecht and Johnson[113] suggested, by using E.S.R. data, that vanadium was present as the VO^{2+} ion in borate glasses.

Table 5.6 Mixed iron-vanadium glazes (compositions, E.S.R. and Mössbauer data)

Recipe	Potash Feldspar	Quartz	Whiting	V_2O_5	Iron	E.S.R. Results	Mössbauer Results
V	57	23	14	6	0	g_{11}: 1.959; $g_{\perp}$: 1.986; A: 163.09; B: 78.56	-
VI	58	23	15.2	3	0.8	Three absorption peaks with g-values: 6.3, 4.15 and 1.995	No signal observed
VII	50	20	10	14	6	Three absorption peaks with g-values: 6.4, 4.20 and 1.98	Two doublets: I.S.=0.13, -0.59 Q.S.=1.31, 4.10mms^{-1} Error in I.S. & Q.S. = ± 0.04 mm s^{-1}

The E.S.R. spectrum of the glaze recipe V shows a well resolved hyperfine structure, Figure 5.10. Fortunately, it is possible to obtain information concerning the valence state of vanadium without applying fully rigorous mathematical analysis used by some workers, this is because there is a body of theoretical and experimental information previously established, upon which we may draw for comparison with the result of our E.S.R. spectrum. For this purpose, a number of compounds with their spin Hamiltonian parameters are listed in Table 5.7.

A comparison of E.S.R. data of glaze recipe V with the data in the above table suggests that this kind of spectrum characterised by $g_{11} < g_{\perp}$ and $A > B$ belongs to the vanadium (IV) ion in an octahedral site with a strong tetragonal compression, i.e., VO^{2+}.

It is possible to suppose that vanadium (IV) works as a modifier cation and does not enter in the silica network because it exists as VO^{2+} and not as V^{4+}. In order to include the vanadyl ion in the silica network, it should be in a tetrahedral site, and hence the main distortion should be trigonal because the V-O bond in VO^{2+} is shorter than all of the others. In this case, as has been shown[113] the g-values should be very different from those g-values obtained for glaze recipe V. The large difference between these spin Hamiltonian parameters and those for tetrahe-

Figure 5·10
E·S·R Spectrum of
Glaze Recipe V

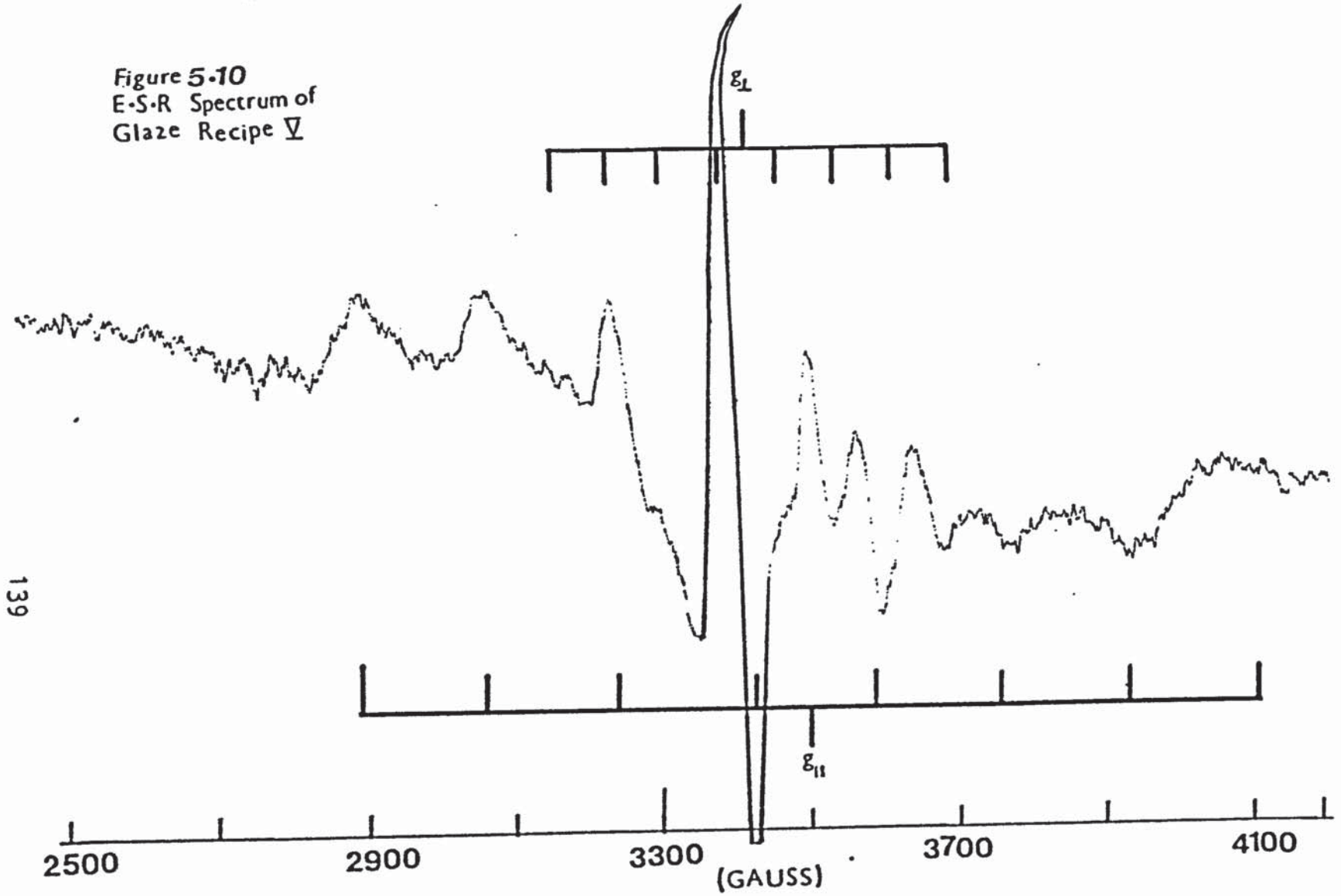

Table 5.7 Spin Hamiltonian parameters of some vanadium containing compounds and glasses

Ion	g_{11}	$g_{\perp}$	A*	B*	Ref	Interpretation
V^{4+} in tridimite	1.968	2.00	58	22	114	Tetrahedral
V^{4+} in TiO_2	1.957	1.915	142	37	115	Octahedral sites with weak tetragonal distortion
VO^{2+} in boro-silicate glasses	1.931	1.967	165.8	58.4	116	Octahedral sites with strong tetragonal distortion (vanadyl ion)
VO^{2+} in lead-silicate glasses	1.906	1.969	170	60	117	
VO^{2+} in glaze recipe V	1.959	1.986	163.09	78.5	present work	

*A and B are the hyperfine coupling constants

dral symmetry, Table 5.7, and the values from our recipe give support for the presence of vanadium in sites with a strong tetragonal distortion.

5.2.7 E.S.R. of Mixed Fe-V Glazes

The E.S.R. spectra of the Fe-V glazes, VI and VII, are shown in Figures 5.11 and 5.12. It is seen that these two glaze recipes show the resonance absorptions due to iron (III) at g = ∿6.4, ∿4.1 and ∿2.00, but no hyperfine structure due to a vanadium (IV) species was clearly observed. A broadening of the resonance absorption at g ∿ 2 occurred in the spectrum of glaze recipe VII.

During the course of this work Bandyopadhyag[116] published optical and E.S.R. results of a study of Fe-V boro-silicate glasses. He observed the same phenomenon of disappearance of the hyperfine structure in the spectra of those glasses with high concentration of Fe_2O_3. He suggested that there is a considerable interaction between iron (III) and vanadium (IV) ions which obscures the hyperfine structure in the E.S.R. spectra of his glasses. He also observed the disappearance of the E.S.R. resonance absorption at g ∿ 2. In the spectra of our glaze system the disappearance of the hyperfine structure was observed even with low concentrations of iron oxide, but the resonance absorption at g ∿ 2 was still present in the spectra of both

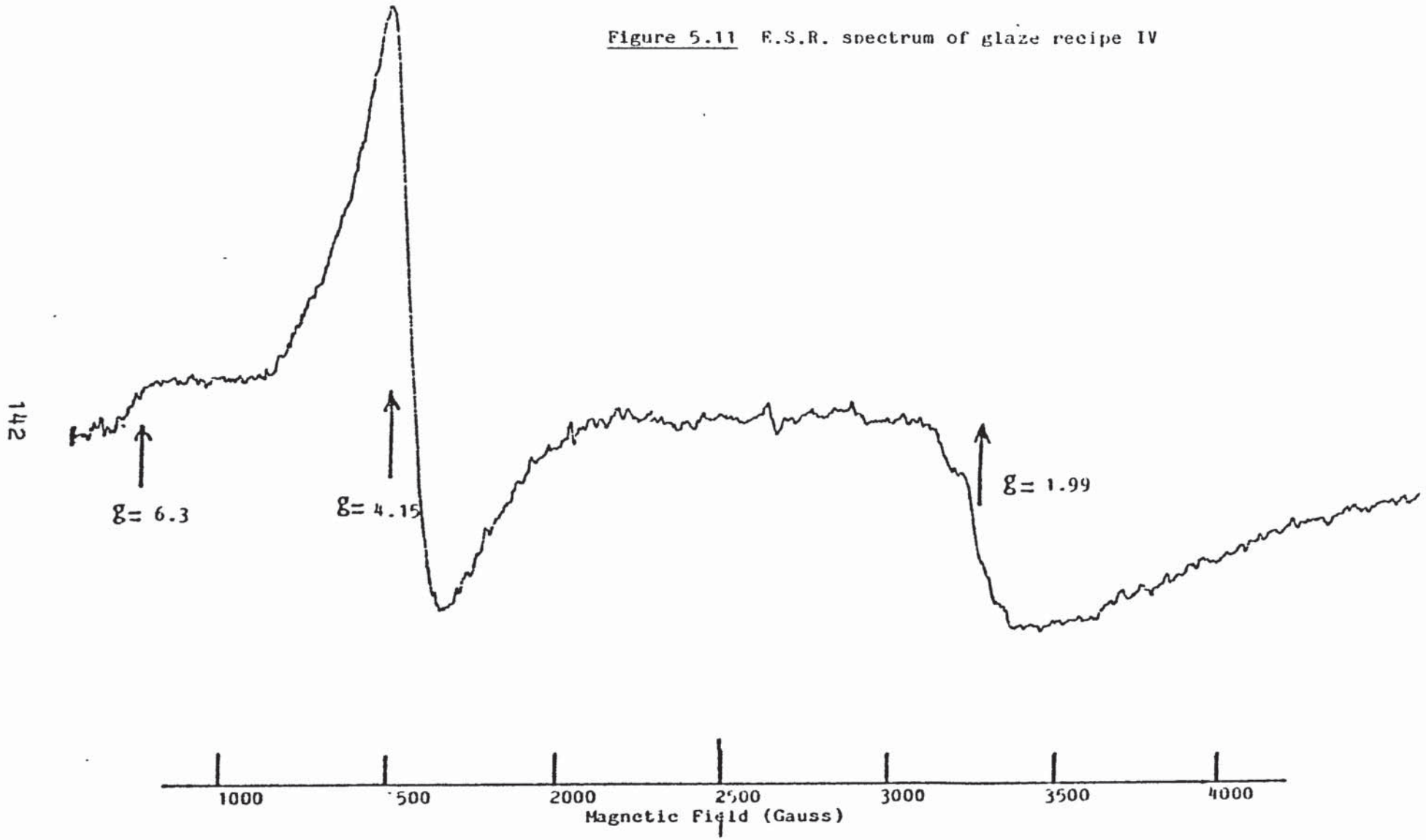

Figure 5.11 E.S.R. spectrum of glaze recipe IV

Figure 5.12 E.S.R. spectrum of glaze recipe VII

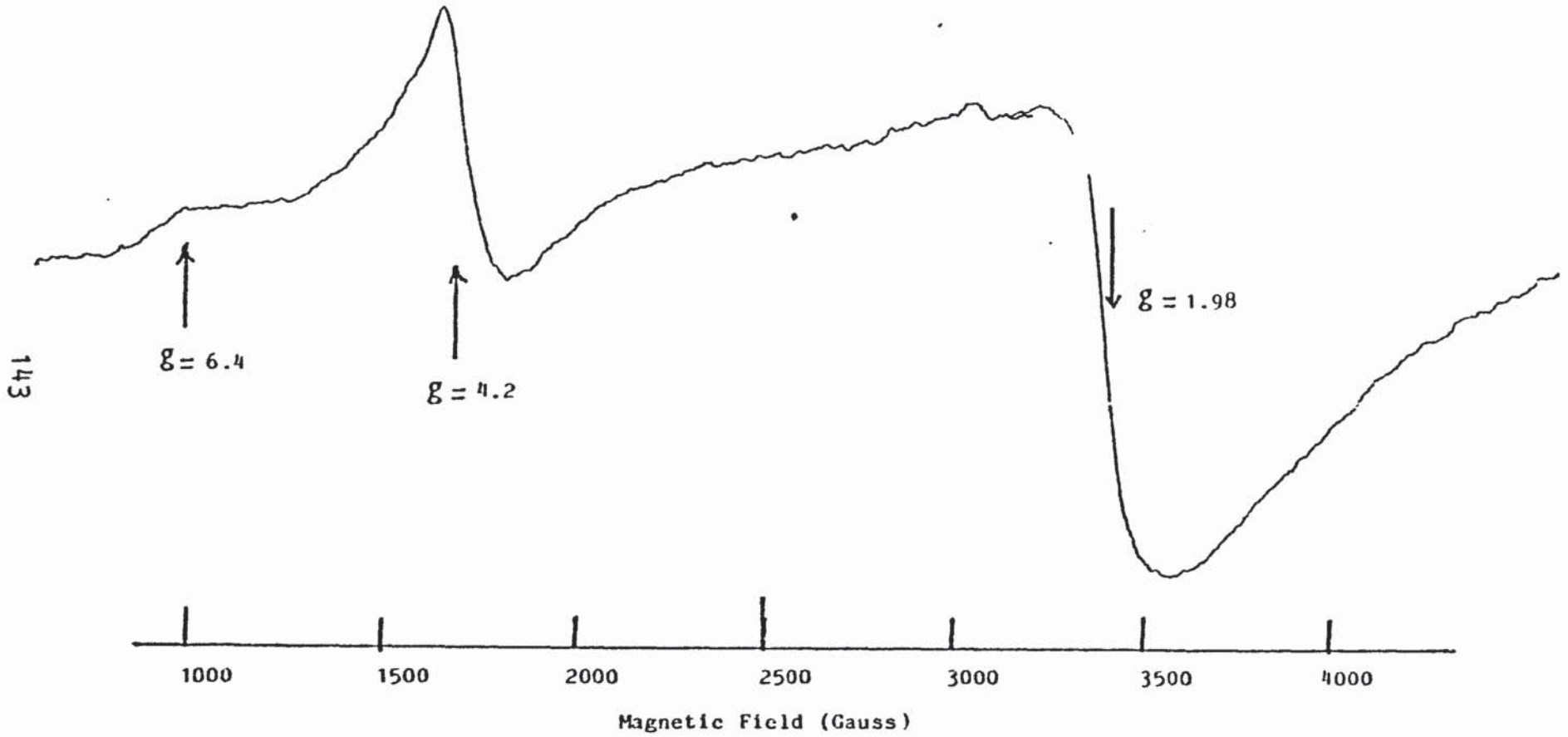

recipes. In fact, from this type of spectrum it is difficult to predict the valence state of both vanadium and iron because an ion from each element may contribute to the observed bands. However, the use of a piece of glaze VI rather than its powder, in recording its E.S.R. spectrum enhances the resolution of the hyperfine structure. This suggested the presence of V^{4+} in this glaze, Figure 5.13. The blue-violet colour of this glaze, which is the common colour of most vanadyl complexes, may be considered as a support for this prediction. The analysis of the Mössbauer data for the glaze recipe VII in the next part of the discussion may give more insight into the valence state and coordination of iron.

5.2.8 Mössbauer Results of the Mixed Fe-V Glazes

The glasses containing single transition metal ions have been extensively studied by Mössbauer spectroscopy, but very little work has been done on the Mössbauer spectra of glasses and glazes containing mixed transition metals, and no Mössbauer work has been done on mixed Fe-V glasses or glazes.

The glaze recipe VI, Table 5.6, shows no Mössbauer absorption even at liquid nitrogen temperature. This may be due to the low concentration of iron in this recipe. This small amount of iron may be distributed onto many different

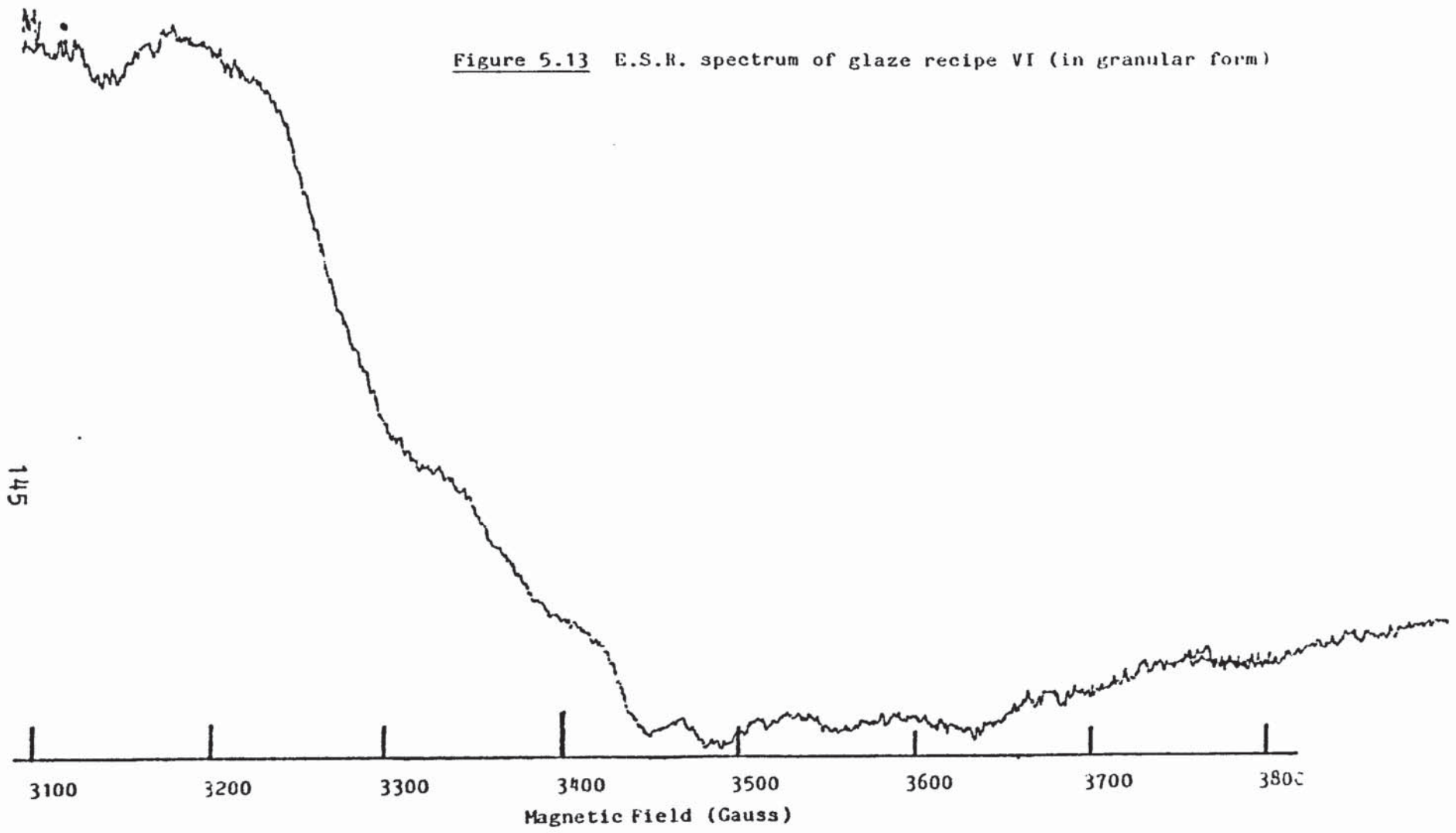

Figure 5.13 E.S.R. spectrum of glaze recipe VI (in granular form)

sites with different coordinations, and consequently, the amount of iron in each site is below the concentration detectable by Mössbauer spectroscopy.

The glaze recipe VII gives a Mössbauer spectrum which consists of two doublets at the positions, 0.13 and (Fig 5.14) -0.593 mm s^{-1} with quadrupole splittings of 1.31 and 4.10 mm s^{-1} respectively (Table 5.6). A comparison of these Mössbauer parameters with those reported in literature[87-89,93-95] suggests that iron may be present in this recipe as iron (III) (I.S. = 0.13 mm s^{-1}) and as iron (IV) (I.S. = -0.593 mm s^{-1}). The values of the isomer shift indicate that the coordination number of both iron (III) and iron (IV) is four.

Iron in oxidation state four has been identified, by using Mössbauer spectroscopy, as an intermediate during the decomposition of the barium and strontium-trioxalatoferrate (III)[118], which was calcined at 700°C and cooled slowly. The interesting observation in the work of Gallagher and Kurkjian[118] is that the Mössbauer spectra of the quenched samples did not have any portions which can be attributed to iron (IV), but if the same samples are allowed to cool slowly in air from 700°C, an iron (IV) portion in the Mössbauer spectrum can be readily distinguished. A similar case occurred for glaze systems VI and VII. When these glazes are quenched from 1280°C black

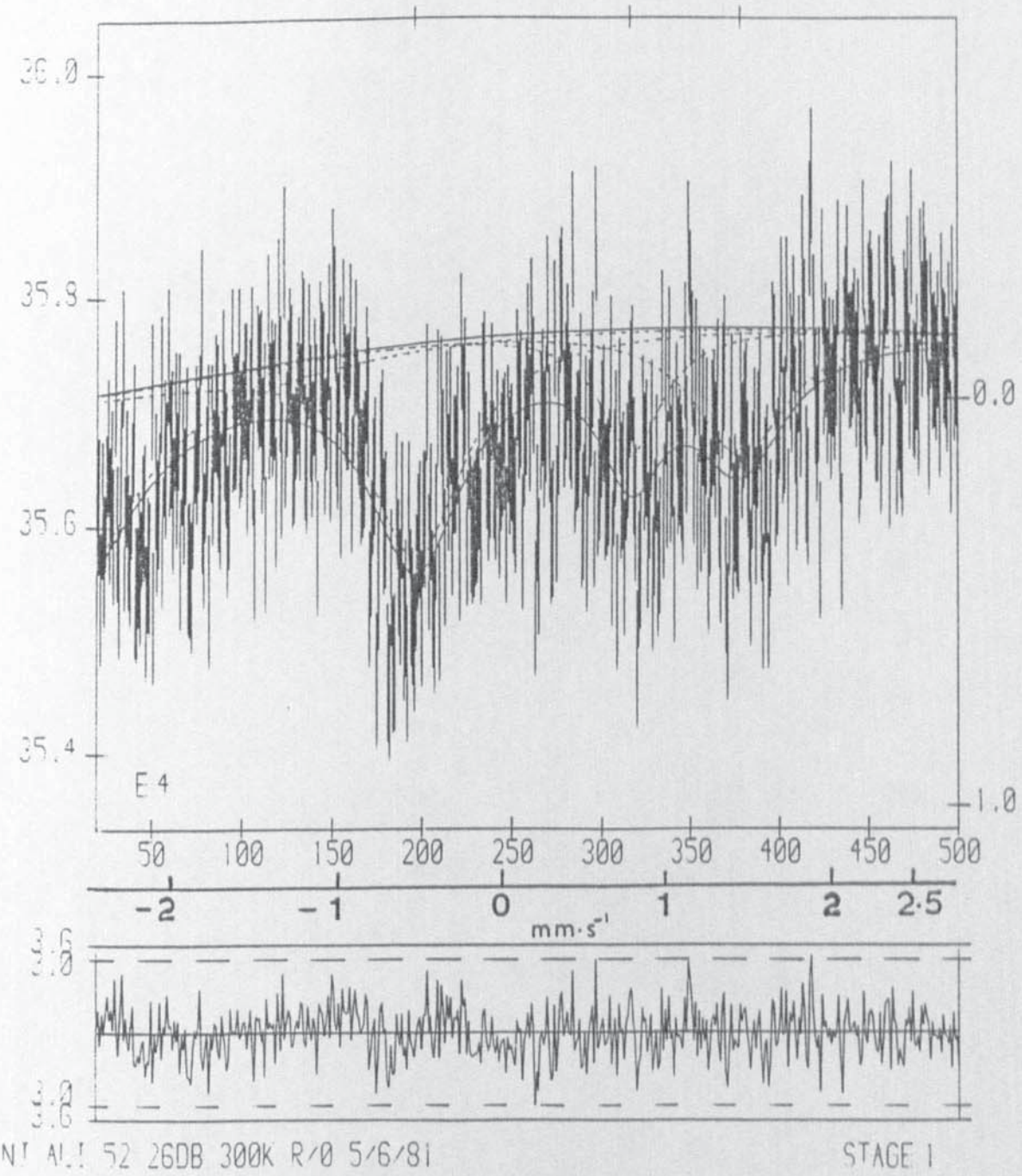

Figure 5.14 ^{57}Fe Mössbauer spectrum of glaze recipe VII

coloured glazes are obtained similar to those containing iron only. When these glaze recipes were left to cool slowly, glaze VI gave an attractive blue-violet opal colour and glaze VII gave a lustrous brown colour. Gallagher and Kurkjian attributed this behaviour to the kinetics of oxygen uptake, which may differ from one system to another, so rapid cooling is effective in preventing an uptake of oxygen. Thus it seems that there is a common factor between these results and Gallagher and Kurkjian's work, which is responsible for the appearance of iron (IV). This factor may be the rate of cooling.

This unusual oxidation state for iron has not been identified in glasses and glazes containing iron only. The presence of iron (IV) in this glaze recipe may be attributed as well to a redox reaction between iron and vanadium. Since the optical and E.S.R. measurements do not facilitate the elucidation of valence state of vanadium in these recipes, it is difficult to explain precisely the way by which Fe(IV) was formed. However, this point needs more clarification by using more specific tools which identify the valence state of vanadium and iron e.g., E.S.C.A. etc.

Because of the presence of iron (III) and iron (IV) in tetrahedral sites in these glaze recipes, it is possible to presume that it has entered the silica network.

APPENDIX

Example of Input and Output Data

In the following example, use is made of the DATA parameter and the VASPECTRUM macro to permit the instructions and spectra to be read from a filestore file.

The Control cards, the input listing, monitoring and accounting and programme output appear on the following pages:

JOB :SCS7111,NJ40A,JDCJT 400,MZ 40K)

UASPECTRUM

FULL

DATA

NJ ALI 40A 160B 300K R/0 24/3/82

0 510 0 5

(5F7.0)

6

892900.

24.0	8.0	710652.
150.0	7.0	451059.
229.0	6.0	216640.
303.0	6.0	226456.
401.0	7.0	452231.
494.0	8.0	705420.

534974	550059	549295	546337	549587
543911	547588	543679	545797	547039
545543	543433	539473	537248	537438
534847	527390	522819	510493	498319
462985	451345	440538	437057	423223
435274	453313	472836	492337	504729
514593	523383	53[illegible]	532243	538461
538032	539815	543205	545788	548903
544541	544886	547144	543389	548310
547729	548744	549201	548719	548236
543039	550290	549280	549918	549790
551998	551934	551579	550153	550237
549139	553305	550843	549358	551076
550944	549865	552157	551433	550816
549787	552155	549813	550187	552352
550723	550035	551873	551211	551891
551423	550985	553941	550549	549875
550441	550910	548931	551045	551505
550719	551228	549805	552323	553532
552295	552717	552479	550233	551519
550383	549399	551579	549032	548279
550003	548511	549153	551151	549524
547785	549947	546774	545132	543933
544194	543104	545433	542317	540939
535330	532390	522151	521112	512392
493359	481330	471384	462901	452883
471952	485153	498747	511374	521223
533383	532521	534983	539373	541477
544343	544747	543193	544376	547937
548012	547391	547053	545934	547442
548929	543773	549472	550473	551314
549330	548793	548373	552191	551319
550197	549234	555175	549357	551335
549179	551137	549371	550755	549827

550189	550554	[illegible]	[illegible]	[illegible]
550588	552201	[illegible]	551504	549739
549831	550733	550252	551023	548537
549399	551549	551455	548540	550453
552554	549183	547938	551708	549243
549434	550433	551393	549309	550158
551548	551835	550716	550033	547439
548314	549020	548534	547532	547293
547392	548285	548505	547931	548255
548198	547315	543592	545028	542357
539894	537011	534477	529071	519207
513043	504509	500854	498823	504539
511393	521505	527783	530508	532889
538234	540554	539542	541543	542510
542948	544927	545941	545737	543329
543284	542550	542735	543930	545453
546951	544259	545690	547493	547272
546818	545771	546974	548022	548957
545591	543921	545534	549330	[illegible]
544531	545891	545456	545090	544304
545520	545451	543715	543291	545353
545757	543301	544557	542540	544054
541535	543904	545780	544403	544137
543429	545837	545590	545133	544193
545273	543049	542589	542557	538285
535839	533534	528514	523511	511721
505908	499385	498515	504082	513265
524172	527707	537015	539152	543252
543543	544592	540501	543075	547341
548075	547593	545858	549171	550345
548580	547353	548495	547972	548323
546155	546882	548604	549355	550137
550448	549794	548557	548455	549151
551244	551861	549598	549739	549855
551593	552472	549514	548958	550124
550827	550054	549002	551037	547530
550593	550822	551215	549590	549331
549229	551713	549905	550505	551518
550134	549355	551271	550151	550773
549925	547984	550007	551362	548831
548430	549411	545780	550238	549975
550518	549208	550220	549247	548525
545528	550385	545685	545539	545271
545911	545915	545357	543270	542731
541932	537597	533257	529023	523984
515025	503392	490924	475209	453179
450959	453522	480102	494501	509051
518162	529515	531200	535805	540524
540074	542151	543098	545295	545751
545334	548273	549372	545412	547742
548543	548577	548329	548071	548591
549337	545457	551458	552227	549254
551531	550245	551382	551858	550114
549018	551430	551588	550535	550525
552305	550974	551807	551135	551309
550270	553223	551577	550737	551204
551145	551392	549427	550430	547293
550275	551515	549291	551183	549948
550085	548414	551201	548391	550515
548547	545443	549150	548815	549574
548358	549331	550535	548550	548395
545915	548730	545180	545729	542561
542584	540033	538032	535895	530482
527354	520158	512309	500353	465437
453143	450448	433830	428012	434099
449942	[illegible]	[illegible]	501454	510783
521773	529140	535350	537514	541044
541390	543944	544252	545791	545525
545529	548908			

```
PLOT    20 500
FIX 7
  2
AREA  1.    0.    0.    0.    0.   -1.
WDTH  1.    0.    0.    0.    0.   -1.
AREA  0.    1.    0.    0.   -1.    0.
WDTH  0.    1.    0.    0.   -1.    0.
AREA  0.    0.    1.   -1.    0.    0.
WDTH  0.    0.    1.   -1.    0.    0.
PLOT    20 500
STOP
****
```

```
SCS7111                              :SCS7111.NJ40B

#LISTING OF :SCS7111.NJ40B(1/81B0)  PRODUCED ON  2MAR82 AT 18.24.34

#68.65D AT ASTON     IN ':SCS7111.NJ40B' ON  2MAR82 AT 16.24.48 USING  U15

DOCUMENT     :SCS7111.NJ40B(1/81B0)

STARTED :SCS7111,NJ40B, 2MAR82 17.42.55 TYPE: BACK  IO ; STREAM C ; PRIORITY 2 ; ENTERED WELL  2MAR82 17.26.28
17.42.56+ JOB :SCS7111,NJ40B,JD(JT 400,MZ 40K)
17.42.56 JOB IS NOW FULLY STARTED
17.42.56+ NJ40B
17.42.57+ UASPECTRUM
ENTERING :MACROS.UASPECTRUM(1/)
17.42.59+          TA AB,CM,JL
17.44.35 0.02 CORE GIVEN 38656
ALLOT       *LPO     N
0.02: MONITOR
ALLOT       *CRO     N
0.03: MONITOR
0.05 :HALTED : 93
DISPLAY: UAFORTRAN: GRAPHICAL OUTPUT FILE IS UACALN73828
DISPLAY : GINO-F MK 2.5
18.24.19 FREE *CRO ,127 TRANSFERS
18.24.21 FREE *LPO ,243 TRANSFERS
DISPLAY : MFILM OK
3.04 :DELETED : 00
18.24.24 FREE *FH7 ,603 TRANSFERS
18.24.24 3.04 DELETED,CLOCKED 2.58
DISPLAY: UAFORTRAN: NORMAL EXIT
18.24.30 3.05 FINISHED : 2 LISTFILES
18.24.30 JOBTIME USED 185 ; MAXIMUM CORE USED 38656
18.24.30 JOB UNITS 407

*IIIIIIIIIIIIIIIIIIIIIIIIIIIIIIIIIIIIIIIIIIIIIIIIIIIIIIIIIIIIIIIIIIIIIII*
*IIIIIII                                IIIIIIIIIIIIIIIIIIIIIIIIIIIIIIII*
*IIIIIII        NUMBER OF PAGES     1   IIIIIIIIIIIIIIIIIIIIIIIIIIIIIIII*
*IIIIIII                                IIIIIIIIIIIIIIIIIIIIIIIIIIIIIIII*
*IIIIIIIIIIIIIIIIIIIIIIIIIIIIIIIIIIIIIIIIIIIIIIIIIIIIIIIIIIIIIIIIIIIIIII*
```

NJ ALI 406 16DB 300K R/O 1/3/82

STAGE 1

ITERATION 1

CHI SQUARED = 1.38091647E 05 TEST VALUE = 1.38627216E 05 DAMPING FACTOR = 1.0000

PARAMETER	VALUE	CORRECTION	PARAMETER	VALUE	CORRECTION	PARAMETER	VALUE	CORRECTION
1	551000.000	5091.819						
2	0.000000	0.000000	3	0.000000	-0.010842	4	0.0000	-0.9553
5	25.000000	-1.997054	6	8.000000	1.761274	7	998192.	760600.
8	130.000000	-2.124466	9	7.000000	2.548026	10	616798.	526590.
11	229.000000	-1.647458	12	6.000000	3.838665	13	313062.	308674.
14	303.000000	-1.892940	15	6.000000	3.838665	16	314310.	308674.
17	401.000000	-1.687494	18	7.000000	2.548026	19	630350.	526590.
20	494.000000	-1.472727	21	8.000000	1.761274	22	983904.	760600.

ITERATION 2

CHI SQUARED = 1.88418527E 04 TEST VALUE = 1.61603398E 04 DAMPING FACTOR = 1.0000

PARAMETER	VALUE	CORRECTION	PARAMETER	VALUE	CORRECTION	PARAMETER	VALUE	CORRECTION
1	556091.819	-1036.311						
2	0.000000	0.000000	3	-0.010842	0.001654	4	-0.9553	-0.2168
5	23.002946	0.871909	6	9.761274	-1.526669	7	1758792.	-75864.
8	127.875534	0.742342	9	9.548026	-2.329021	10	1143388.	-59597.
11	227.352542	0.470935	12	9.838665	-2.656397	13	621736.	-10667.
14	301.107060	0.474314	15	9.838665	-2.656397	16	622984.	-10667.
17	399.312506	0.676530	18	9.548026	-2.329021	19	1156940.	-59597.
20	492.527273	0.580139	21	9.761274	-1.526669	22	1744504.	-75864.

ITERATION 3

CHI SQUARED = 4.44522901E 03 TEST VALUE = 1.21780202E 03 DAMPING FACTOR = 1.0000

PARAMETER	VALUE	CORRECTION	PARAMETER	VALUE	CORRECTION	PARAMETER	VALUE	CORRECTION
1	555055.509	315.993						
2	0.000000	0.000000	3	-0.009188	-0.000268	4	-1.1721	0.0491
5	23.874855	-0.173426	6	8.234605	0.110697	7	1682929.	20406.
8	128.617876	-0.157791	9	7.219005	0.473637	10	1083792.	31069.
11	227.823477	-0.179696	12	7.182268	0.513240	13	611069.	12587.
14	301.581374	-0.073207	15	7.182268	0.513240	16	612317.	12587.
17	399.989036	-0.148234	18	7.219005	0.473637	19	1097344.	31069.
20	493.107412	-0.087734	21	8.234605	0.110697	22	1668641.	20406.

ITERATION 4

CHI SQUARED = 3.64769024E 03 TEST VALUE = 6.30290505E 00 DAMPING FACTOR = 1.0000

PARAMETER	VALUE	CORRECTION	PARAMETER	VALUE	CORRECTION	PARAMETER	VALUE	CORRECTION
1	555371.501	-41.033						
2	0.000000	0.000000	3	-0.009456	0.000081	4	-1.1230	-0.0137
5	23.701429	0.001633	6	8.345302	-0.021570	7	1703335.	-2588.
8	128.460085	-0.018622	9	7.692642	-0.030041	10	1114861.	-2252.
11	227.643761	-0.011121	12	7.695507	0.016503	13	623655.	592.
14	301.508167	-0.018695	15	7.695507	0.016503	16	624903.	592.
17	399.840803	-0.014436	18	7.692642	-0.030041	19	1128413.	-2252.
20	493.019678	-0.003961	21	8.345302	-0.021570	22	1689047.	-2588.

ITERATION 5

CHI SQUARED = 3.64385163E 03 TEST VALUE = 2.18134194E-02 DAMPING FACTOR = 1.0000

PARAMETER	VALUE	CORRECTION	PARAMETER	VALUE	CORRECTION	PARAMETER	VALUE	CORRECTION
1	555330.468	2.105						
2	0.000000	0.000000	3	-0.009375	-0.000001	4	-1.1367	0.0004
5	23.703063	-0.000106	6	8.323732	0.000904	7	1700747.	144.
8	128.441463	-0.000866	9	7.662601	0.002224	10	1112609.	211.
11	227.632659	0.000112	12	7.712010	0.001842	13	624247.	108.
14	301.489471	0.000068	15	7.712010	0.001842	16	625495.	108.
17	399.826366	-0.000142	18	7.662601	0.002224	19	1126161.	211.
20	493.015717	-0.000178	21	8.323732	0.000904	22	1686459.	144.

ITERATION 6

CHI SQUARED = 3.64384398E 03 TEST VALUE = 9.74619599E-05 DAMPING FACTOR = 1.0000

PARAMETER	VALUE	CORRECTION	PARAMETER	VALUE	CORRECTION	PARAMETER	VALUE	CORRECTION
1	555332.574	-0.152						
2	0.000000	0.000000	3	-0.009377	0.000000	4	-1.1363	-0.0000
5	23.702957	0.000005	6	8.324636	-0.000050	7	1700891.	-9.
8	128.440598	-0.000035	9	7.664825	-0.000176	10	1112820.	-15.
11	227.632771	0.000041	12	7.713852	0.000000	13	624355.	-1.
14	301.489539	-0.000052	15	7.713852	0.000000	16	625603.	-1.
17	399.826225	-0.000006	18	7.664825	-0.000176	19	1126372.	-15.
20	493.015540	-0.000006	21	8.324636	-0.000050	22	1686603.	-9.

ITERATION 7

CHI SQUARED = 3.64384395E 03 TEST VALUE = 6.45939765E-07 DAMPING FACTOR = 1.0000

PARAMETER	VALUE	CORRECTION	PARAMETER	VALUE	CORRECTION	PARAMETER	VALUE	CORRECTION
1	555332.421	0.005						
2	0.000000	0.000000	3	-0.009377	0.000000	4	-1.1363	0.0000
5	23.702962	-0.000000	6	8.324587	0.000002	7	1700882.	0.
8	128.440562	-0.000002	9	7.664648	0.000014	10	1112804.	1.
11	227.632812	0.000001	12	7.713853	0.000014	13	624354.	1.
14	301.489487	0.000002	15	7.713853	0.000014	16	625602.	1.
17	399.826219	0.000000	18	7.664648	0.000014	19	1126356.	1.
20	493.015534	-0.000000	21	8.324587	0.000002	22	1686594.	0.

NJ ALI 40P 1606 300K R/U 1/3/62

STAGE 1

PROCESS HAS CONVERGED
AFTER 7 ITERATIONS WITH 7 CONSTRAINTS

BASELINE = 555332. S.D. 127.81

SCAN REVERSES AT CHANNEL 0.000 S.D. 0.000

BASELINE SINE-WAVE COMPONENT =-0.938 PER CENT S.D. 0.029

BASELINE DRIFT = -1.14 P.P.M. PER CHANNEL S.D. 0.41

LINE	POSITION	S.D.	WIDTH	S.D.	INTENSITY	S.D.	XI
1	23.703	0.012	8.325	0.030	1700883.	5481.	503.61
2	128.441	0.017	7.665	0.036	1112806.	4067.	343.38
3	227.633	0.031	7.714	0.071	624355.	4528.	192.04
4	301.489	0.031	7.714	0.071	625603.	4528.	192.43
5	399.826	0.017	7.665	0.036	1126358.	4067.	347.56
6	493.016	0.012	8.325	0.030	1686595.	5481.	499.38

TEST VALUE =6.4594E-07

CHI SQUARED = 3643.84 WITH 496 DEGREES OF FREEDOM
5, 1 AND 0.1 PER CENT POINTS ARE 548.7, 571.5 AND 597.5 RESPECTIVELY

SIGNAL = 7.66152E 05 +- 1.75075E 03 OR 7.66152E 05 (1 +- 2.28512E-03)
LIMITS FOR ISOLATED AND SUPERIMPOSED PEAKS ARE 3.3928E 06 AND 6.4059E 05
SIGNAL / BASELINE = 1.38467 LIMITS / BASELINE ARE 6.10940 AND 1.15353

DISTANCE = 3.13284E 03 +- 1.14203E 02 OR 3.13284E 03 (1 +- 3.64535E-02)
DISTANCE / BASELINE = 0.00567

MISFIT = 4.08906E-03 +- 1.49353E-04 OR (0.40891 +- 0.01494) PERCENT

THE FOLLOWING CHANNELS DEVIATE SIGNIFICANTLY FROM THE CURVE

0.	-22.32	14.	4.00	15.	5.94	17.	6.03	22.	-3.97
32.	9.88	34.	3.66	37.	5.35	50.	-5.68	94.	3.72
117.	4.43	125.	-5.81	126.	-6.18	131.	-3.64	132.	-4.41
158.	4.21	162.	7.74	190.	4.45	200.	3.62	201.	4.11
215.	3.78	224.	-4.76	234.	-4.13	244.	-4.75	245.	-5.19
246.	-6.51	247.	-6.56	248.	-5.13	251.	-5.18	256.	-3.62
260.	-4.05	264.	-3.67	265.	-5.55	268.	-4.76	269.	-5.69
270.	-3.67	272.	-6.50	273.	-7.02	276.	-6.91	277.	-4.81
278.	-7.47	279.	-5.36	280.	-8.51	283.	-4.06	284.	-4.07
285.	-4.71	300.	6.59	307.	5.54	308.	3.64	309.	5.62

NO CHANNELS REJECTED FOR FITTING

CORRELATION COEFFICIENT MATRIX

1.000

-0.819	0.000	1.000								
-0.441	0.000	-0.007	1.000							
-0.021	0.000	0.025	0.003	1.000						
0.503	0.000	-0.487	0.001	-0.013	1.000					
0.675	0.000	-0.650	-0.025	-0.016	0.830	1.000				
-0.021	0.000	0.021	0.007	0.001	-0.010	-0.013	1.000			
0.107	0.000	0.012	0.025	0.001	0.082	0.106	0.001	1.000		
0.201	0.000	-0.034	0.005	-0.000	0.140	0.183	-0.001	0.768	1.000	
-0.007	0.000	0.005	0.008	0.000	-0.002	-0.003	0.000	0.001	0.000	
1.000										
-0.180	0.000	0.352	0.023	0.010	-0.080	-0.113	0.007	0.105	0.131	
-0.000	1.000									
-0.209	0.000	0.438	0.016	0.012	-0.092	-0.130	0.008	0.143	0.180	
0.000	0.788	1.000								
0.003	0.000	-0.008	0.008	-0.000	0.004	0.005	-0.000	-0.000	-0.000	
0.000	0.000	-0.001	1.000							
-0.180	0.000	0.352	0.023	0.010	-0.080	-0.113	0.007	0.105	0.131	
-0.000	1.000	0.788	0.000	1.000						
-0.209	0.000	0.438	0.016	0.012	-0.092	-0.130	0.008	0.143	0.180	
0.000	0.788	1.000	-0.001	0.788	1.000					
0.015	0.000	-0.023	0.007	-0.001	0.010	0.014	-0.000	-0.000	0.001	
-0.000	-0.007	-0.009	0.000	-0.007	-0.009	1.000				
0.107	0.000	0.012	0.025	0.001	0.082	0.106	0.001	1.000	0.768	
0.001	0.105	0.143	-0.000	0.105	0.143	-0.000	1.000			
0.201	0.000	-0.034	0.005	-0.000	0.140	0.183	-0.001	0.768	1.000	
0.000	0.131	0.180	-0.000	0.131	0.180	0.001	0.768	1.000		
0.014	0.000	-0.019	-0.001	-0.000	0.009	0.012	-0.000	-0.001	-0.001	
-0.000	-0.008	-0.010	0.000	-0.008	-0.010	0.001	-0.001	-0.001	1.000	
0.503	0.000	-0.487	0.001	-0.013	1.000	0.830	-0.010	0.082	0.140	
-0.002	-0.080	-0.092	0.004	-0.080	-0.092	0.010	0.082	0.140	0.009	
1.000										
0.675	0.000	-0.650	-0.025	-0.016	0.830	1.000	-0.013	0.106	0.183	
-0.003	-0.113	-0.130	0.005	-0.113	-0.130	0.014	0.106	0.183	0.012	
0.830	1.000									

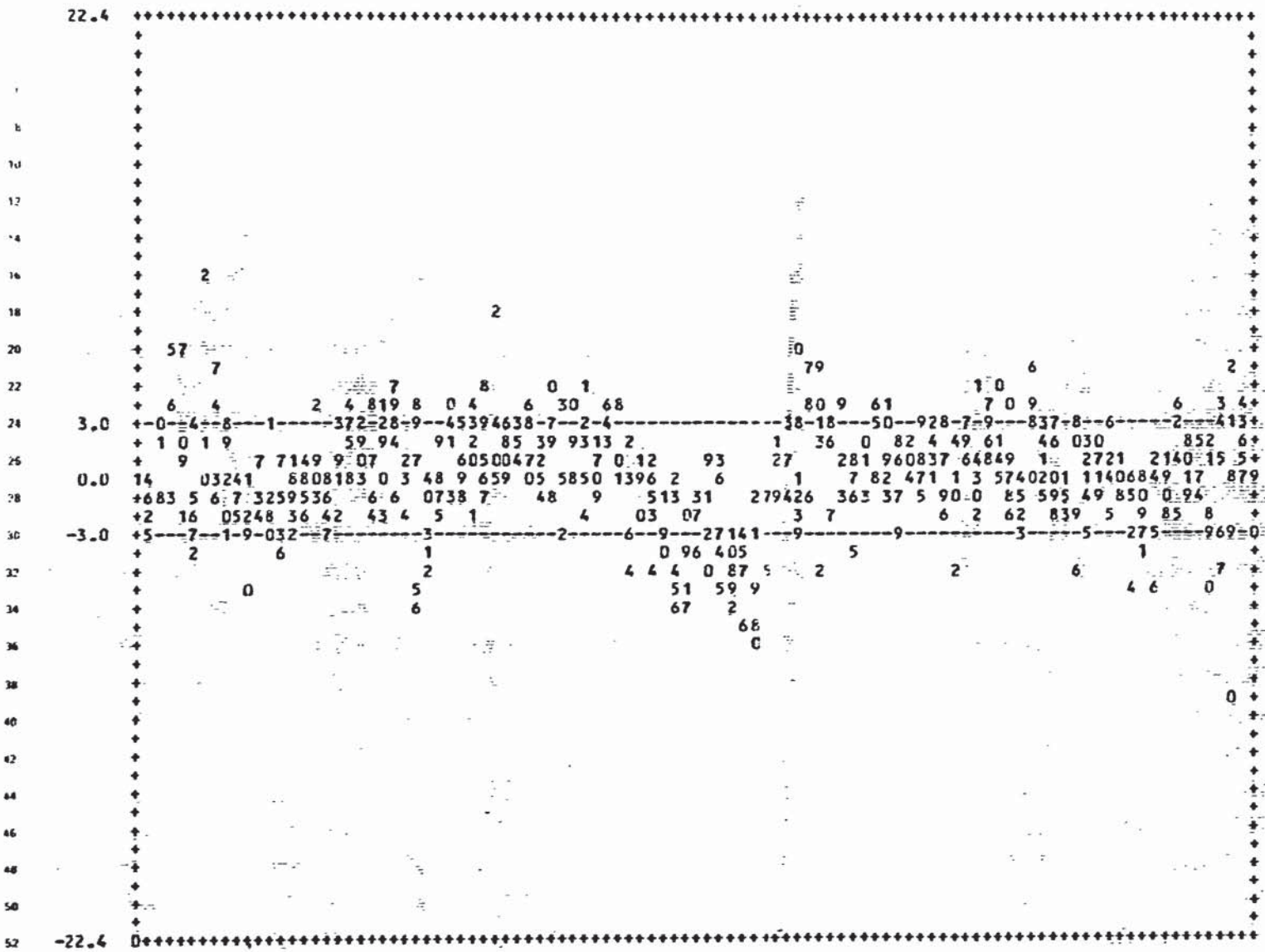

PLOT OF RESIDUAL DEVIATION (IN STANDARD DEVIATION UNITS) VS. CHANNEL NUMBER
ALL BUT ONE OR TWO POINTS SHOULD LIE BETWEEN THE HORIZONTAL LINES

PLOTTED AT THIS STAGE 2 AT INTERVAL OF 1 CHANNELS

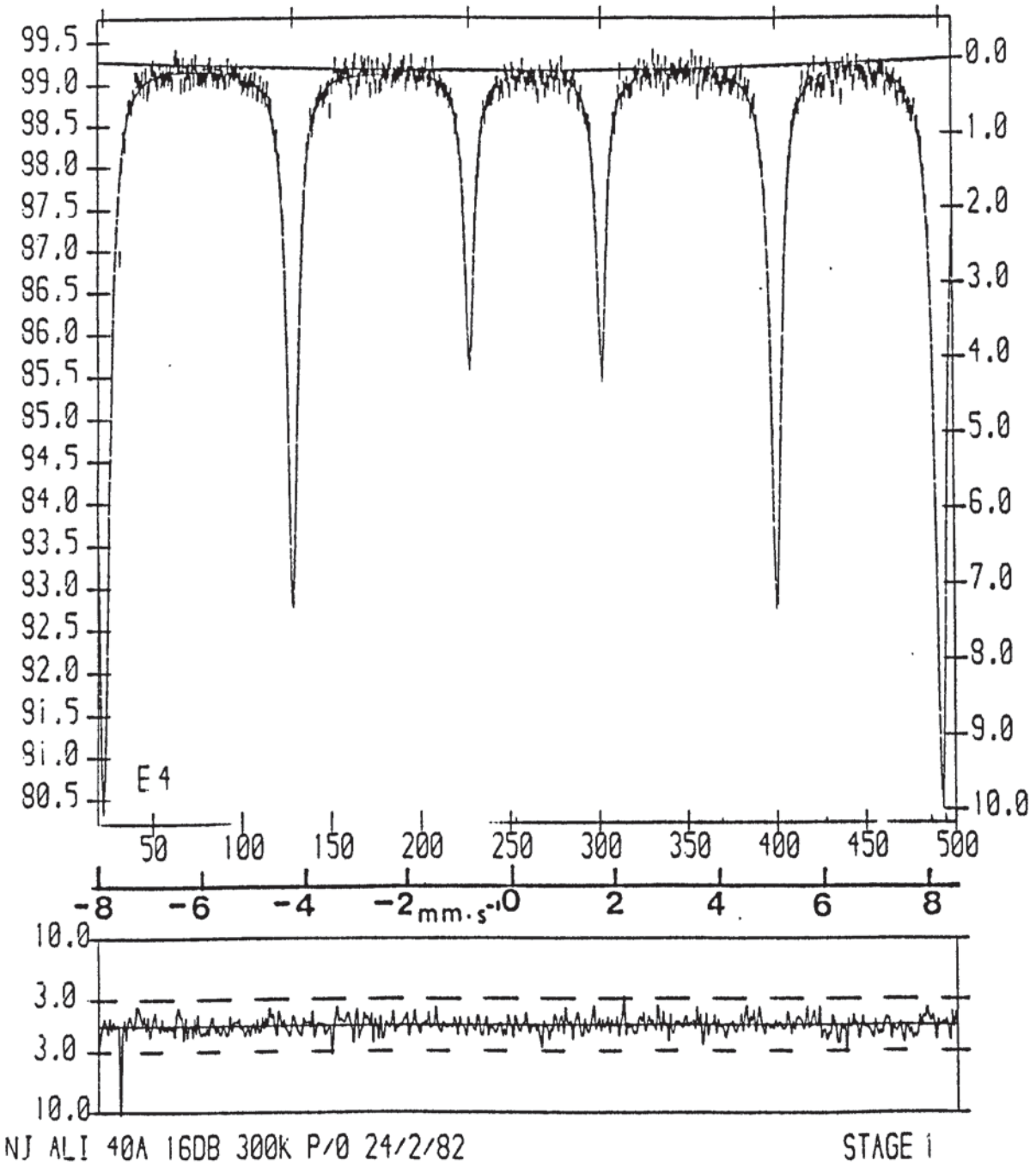
99.5
99.0
98.5
98.0
97.5
97.0
96.5
96.0
95.5
95.0
94.5
94.0
93.5
93.0
92.5
92.0
91.5
91.0
90.5
0.0
1.0
2.0
3.0
4.0
5.0
6.0
7.0
8.0
9.0
10.0
E 4
50
100
150
200
250
300
350
400
450
500
-8
-6
-4
-2
mm.s⁻¹
0
2
4
6
8
10.0
3.0
3.0
10.0
NJ ALI 40A 16DB 300k P/0 24/2/82
STAGE 1

REFERENCES

References

1. P W McMillan, "Glass Ceramics", (1979), Academic Press.
2. H Rawson, "Properties and Application of Glass", (1980), Elsevier Publishing Co Ltd.
3. M A Bezborodov, "Synthesis and Structure of Silicate Glasses", (1968), Nauka, Tekhnika, Minsk. Pg 398.
4. J F Randall, H R Rooksby and B S Cooper, J.Soc.Glass Technol., 14, 219, (1930).
5. B E Warren and J Biscoe, J.Am.Ceram.Soc., 21, 49,(1938)
6. Yu G Shteinberg, Strontium Glazes, (1967), 2nd Edn., Stroiizdat, Leningrad, Moscow, Pg 5-12.
7. N V Belov, Collection, Structure of Glass, (1955), Academy of Sciences, USSR, Pg 344.
8. K Shaw, "Ceramic Glazes", (1971),Elsevier Publishing Co Ltd.
9. A Dietzel, Z Elektrochem, 48, 9, (1942).
10. P Balta and E Balta, Introduction to the Physical Chemistry of the Vitreous State, (1976), Abacus Press.
11. J E Stanworth, J.Soc.Glass Technol., 30, 54-64T (1946); 32, 154-172T (1948); 32, 366-372T (1948).
12. W H Zachariasen, J.Am.Chem.Soc., 54, 3841, (1932).
13. K H Sun, J.Am.Ceram.Soc., 30, 277-281, (1947).
14. H Rawson, Inorganic Glass Forming Systems, (1967), Academic Press, New York, Pg 11-12, 31-43 and 108.
15. F Singer and W L German,"Ceramic Glazes", (1966), Borax Consolidated Ltd, London.

16. G A Kirkendale, "Analytical Methods for Materials Investigation", (1971), Gordon and Breach Science Publishers.

17. C R Kurkjian, J.Non-Cryst.Solids, 3, 157, (1970).

18. C Boubacor, Ber.Dtch.Keram.Ger., 56(9), GW17-GW20, (1979), C.A.;80988r.

19. E L Abdrushitova, R Y Khodakovskya, Phys.Non-Cryst. Solids, Int. Conf. 4th, 1976, (Pub.1977), 160-5 C.A.87;140028m.

20. D L Griscom, Electron Spin Resonance In Glasses, J.Non-Cryst. Solids, 40, 211-272, (1980).

21. J D Mackenzie, "Modern Aspects of the Vitreous State", (1962), Butterworth, Pg 195.

22. C R Bamford, "Colour Generation and Control in Glasses", (1977), Elsevier Scientific Publishing Company.

23. W Ryan, "Properties of Ceramic Raw Materials", (1978), Pergamon Press Ltd.

24. R J Angelici, "Synthesis and Technique in Inorganic Chemistry", 2nd Edition, (1977), W B Saunders Co.

25. G M Bancroft, A G Maddock, W K Ong, R H Prince and A J Stone, J.Chem.Soc. (A), 1976A, 1966-1971, (1967).

26. P A Gillespie, "A Study of the Chemistry of Some Transition Metal Ions in Ceramic Glazes", Ph.D. Thesis, University of Aston in Birmingham (1979).

27. W R WcWhinnie, Co-ordination Chem.Rev., 5,293 (1970).

28. W L Johnson and J F Geldard, Inorg.Chem., 18,3 , (1979).

29. G P McQuillon and S E Pritchard, Inorganica Chimica Acta, 53, L141-L142, (1981).

30. B J Brisdon and G F Griffith, J.Chem.Soc., Dalton, 1999, (1975).

31. N J Ray and B J Hathaway, Acta Cryst., B34, 3224, (1978).

32. J B Wibaut and G L C La Bastide, Versl.Kon.Akad.Wetensch. Amsterdam, 36, 514, (1927).

33. J C Lancaster, Ph.D. Thesis, Chemistry Dept. University of Aston in Birmingham (1971).

34. J Selbin, J Chem. Educ., 41, 86, (1964).

35. J Selbin, H R Manning and G Cessac, J.Inorg.Nucl.Chem., 25, 1253, (1963).

36. J Selbin, Chem.Rev., 65, 2, 153, (1965).

37. J Selbin, Coord.Chem.Rev., 1, 293-314, (1966).

38. J B Wibaut and G L C La Bastide, Rec.Trav.Chim., 52, 493, (1933).

39. J C Lancaster and W R McWhinnie, J.Chem.Soc., (C),2435, (1970).

40. G C Kulasingam, Ph.D. Thesis, University of London, (1967).

41. J E Johnson and R A Jacobson, Acta Crystallogr., Sec B, 29, 1669, (1973).

42. G C Kulasingam and W R McWhinnie, J.Chem.Soc., 1317, 7145-7148, (1965).

43. W R McWhinnie, J.Inorg.Nucl.Chem., 27, 763, (1965).

44. C G Barraclough, J Lewis and R S Nyholm, J.Chem.Soc., 3552, (1959).

45. J Selbin, L H Holmes Jr and S P McGlynn, J.Inorg. Nucl.Chem., 25, 1354, (1963).

46. P J Lucchesi and W A Classon, J.Am.Chem.Soc., 48, 1347, (1956).

47. R J H Clark, J.Chem.Soc., 1377, (1963).

48. V V Zelentsov, Russ.J.Inorg.Chem., 7, 6,(1962).

49. D J Phillips and S Y Tyree, J.Am.Chem.Soc., 83, 1809, (1961).

50. K Nakamoto, J Fujita, S Tanaka and M Kobayashi, J.Am. Chem.Soc., 79, 4904, (1957).

51. C J Ballhausen and H B Gray, Inorg.Chem., 1, 111,(1962).

52. T R Ortolano, J Selbin and S P McGlynn, J.Chem.Phys., 41, 262, (1964).

53. G Basu, W Yeranos and R L Belford, Inorg.Chem., 3, 929, (1964).

54. R A D Wentworth and T S Piper, J.Chem.Phys., 41, 3884, (1964).

55. D Kivelson and S K Lee, J.Chem.Phys., 41, 1896, (1964).

56. K Wuthrich, Helv.Chim.Acta, 48, 779, (1965).

57. I Bernal and P H Rieger, Inorg.Chem., 2, 256, (1963).

58. W Kerstan, Keram.Z., 25(12), 668-70, (1973).

59. W H Turner and J A Turner, J.Am.Cer.Soc., 55, 4,(1972).

60. R Zsigmoney, Ann.Phys.(Leipzig), 4, 60, (1901).

61. P P Fedotiev and A A Lebedeve, Z.Anorg.Chem., 134, 87, (1924).

62. W A Weyl and E Thuemen, Glass Tech.Ber., 11(4), 113-20, (1933).

63. W A Weyl, Coloured Glasses, (1959), Dawsons of Pall Mall (London).

64. H Moore and H Winkelmann, J.Soc.Glass Technol., 39, 215-249, "I" (1955); "II" ibid, pp 250-286, "III" ibid, pp 287-313.

65. T Bates, Modern Aspects of the Vitreous State, (1952), Butterworth (London).

66. C R Bamford, Phys.and Chem.Glasses, 3, 189, (1962).

67. T Bates and R W Douglus, J.Soc.Glass Technol., 43, 289, (1959).

68. S Kumer, Cetr.Glass Ceram.Res.Inst.Bull., 6, 99, (1959).

69. R Juza and K H Shulz, Z.Anorg-Allg.Chem., 316, (1-2), 89-104, (1962).

70. M Gitter and W Vogel, Wiss.Z.Friedrich-Schillar University Jene, Math-Naturwiss, Reibe, 28(2-3), 307, (1979).

71. M Gitter and W Vogel, Silikattechnik, 29(2), 36-41, (1978).

72. The International Rubber Handbook, The Rubber Co Ltd, (1972).

73. J P Gha and D Kolar, J.Am.Cerm.Soc., 55(1), 55, (1972).

74. W Lagua, E W Schulz and B Reuter, Z.Anorg-Alleg. Chem, 433, 167, (1977); C.A. 87;157761t.

75. W D J Evans, Trans.Br.Ceram.Soc., 67, 397, (1968).

76. W Low, Phys.Rev., 109, 247, (1958).

77. M Berretz and S L Holt, J.Am.Cerm.Soc., 61, 3, 136,(1979).

78. R S Drago "Physical Methods in Chemistry", (1977), W B Saunders Co.

79. H Hartmann and H L Schlafer, Z.Phys.Chem., 197, 116, (1951).

80. W A Weyl, Coloured Glasses, Society of Glass Technology, (1951), Sheffield.

81. H Cole, J.Soc.Glass Technol., 35, 6, (1951).

82. H Moore and S N Prasad, J.Soc.Glass Technol., 33, (1949); 34, 173, (1950).

83. A E M Abou-el-Azm, J.Soc.Glass Technol, 38, 101,(1954).

84. R H Sands, Phys.Rev. 99, 1222, (1955).

85. T Castner Jr, G S Newell, W C Holton and C P Slichter, J.Chem.Phys., 32, 668, (1960).

86. H Pollak, M De Coster and S Amelinex, Proc. 2nd Int. Conf. on the Mossbauer Effect, Saclay, (1961), ed. D M Compton and A H Schoen, (Wiley, New York, 1962), Pg 298.

87. C R Kurkjian and D N E Buchanan, Phys.Chem.Glasses, 5, 63, (1964).

88. A A Belyustin, Yu M Ostanevich, A H Pisarevskii, S B Tomilov, U Bai-shi and L Cher, Soviet Physics - solid state, 7, 1163, (1965).

89. J P Gosselin, U Shimony, L Grodzins and A R Cooper, Phys.Chem.Glasses, 8, 56, (1967).

90. C R Kurkjian and E A Sigety, Phys.Chem.Glasses, 9, 73, (1968).

91. C K Lewis Jr and H G Drickamer, J.Chem.Phys., 49, 3785, ((1968).

92. G H Frischat and G Tomandl, Glastech.Ber., 42,182,(1969).

93. (a) M F Taragin and J C Eisentein, J.Non-Cryst.Solids, 3, 311, (1970).

(b) M F Taragin and J C Eisentein, Phys.Chem.Glasses, 8, 2, (1967).

94. L Pargamin, C H P Lupis and P A Flinn, Met.Trans., 3, 2093, (1972).

95. Ch Labar and P Gielen, J.Non-Cryst.Solids, 13, 107, (1973).

96. R A Levy, C H P Lupis and P A Flinn, Phys.Chem.Glasses, 17, 94, (1976).

97. N Iwamoto, Y Tsunawaki, H Nakagawa, T Yoshimura and N Wakabayashi, J.Non-Cryst.Solids, 29, 347-356, (1978).

98. C R Bamford, Phys.Chem.Glasses, 1, 159,(1960); 2, 163, (1964); 3, 54, (1962).

99. D L Griscom, J.Non-Cryst.Solids, 40, 211-270, (1980).

100. N H Gangas, A Kostikas and A Simopoulos, Nature, 229, 485, (1971); 5th International Conference on the Applications of the Mossbauer Effect, Bratislava, Sept. 3-7, 1973.

101. Ch Janot and P Delcroix, J.Physique, Colloque C6, Suppliment au No 12, Tome 35, C6-557, (1974).

102. R Bouchez, J M D Coey, R Coussement, K P Schmidt, M Van Rossum, J Aprahamian and J Deshayes, J.Physique, Collque C6, au No 12, Tome 35, C6-541, (1974).

103. D A Nolet, J Non-Cryst.Solids, 37, 99-110, (1980).

104. J J Van Loef, Physica, 32, 2102, (1966).

105. O C Kistner and A W Sunyar, Phys.Rev.Letters, 44, 412, (1960).

106. Y Tanabe and S Sugano, J.Phys.Soc.Japan, 9, 753,(1954).

107. R J Edwards, A Paul and R W Douglus, Phys.Chem.Glasses, 13, 5, 137, (1972).

108. B Bleaney, K W Stevens, Rep.Prog.Phys. 16, 108-159, (1967).

109. T Komatsu and N Soga, J.Chem.Phys, 72, (3), 1, (1980).

110. (a) R Ingall, Phys.Rev, 133,A787-A795, (1964).
(b) P R Edwards, C E Johnson and R J William, J.Chem.Phys., 47, 2074-2082, (1967).

111. B D Josephin, Phys.Rev.Lett. 4, 342, (1960).

112. R E M Hedges, Nature, Vol 254, April 10th, Pg 501, (1975).

113. H G Hecht and T S Johnston, J.Chem.Phys., 46,(1), 23-34, (1967).

114. V S Grumin, V A Loffe and Z N Zonn, J.Non-Cryst.Solids, 11, (4), 341-49, (1973).

115. H J Gerritsen and H R Lewis, Phys.Rev., 119, (3), 1010-12, (1960).

116. A K Bandyopadhyay, J.Materials Science, 16, 189,(1981).

117. L D Bogomolova, V A Zhachkin, V N Lazukin and V A Shmucher, J.Non-Cryst.Solids, 27,(3), 427-35, (1978).

118. P K Gallagher and C R Kurkjian, Inorg.Chem., 4,965,(1965).